EARLY IDENTIFICATION AND CLASSIFICATION OF THYROID NODULE IN MEDICAL ULTRASOUND IMAGES

Thesis submitted in fulfilment of the requirements for the Degree of

DOCTOR OF PHILOSOPHY

By

RAJSHREE SRIVASTAVA

Enrolment No. 196204

Department of Computer Science & Engineering and Information Technology

JAYPEE UNIVERSITY OF INFORMATION TECHNOLOGY

Waknaghat, Solan-173234, Himachal Pradesh, INDIA

January, 2024

SUPERVISOR'S CERTIFICATE

This is to certify that the work in the thesis entitled **"Early identification and classification of thyroid nodule in medical ultrasound images"** submitted by **Rajshree Srivastava at Jaypee University of Information Technology, Waknaghat, India,** is a bonafide record of her original work carried out under my supervision. This work has not been submitted elsewhere for any other degree or diploma.

(Signature of Supervisor)

Dr. Pardeep Kumar

Associate Professor

Department of Computer Science & Engineering and Information

Technology,Jaypee University of Information Technology,

Waknaghat, Solan, India

Date:

DECLARATION BY THE SCHOLAR

I hereby declare that the work reported in the Ph.D. thesis entitled **"Early identification and classification of thyroid nodule in medical ultrasound images"** submitted at **Jaypee University of Information Technology, Waknaghat, India,** is an authentic record of my work carried out under the supervision of **Dr. Pardeep Kumar**. I have not submitted this work elsewhere for any other degree or diploma. I am fully responsible for the contents of my Ph.D. thesis.

Rajshree Srivastava

Department of Computer Science & Engineering and Information

Technology, Jaypee University of Information Technology,

Waknaghat, Solan, India

Date:

ACKNOWLEDGEMENT

With the divine grace of "Almighty God", the journey of Ph.D comes to end. I would like take this opportunity to thanks each and every person who has helped me to complete this journey.

It is an immense pleasure to express my profound gratitude towards my supervisor **Dr. Pardeep Kumar**, Associate Professor, Department of Computer Science & Engineering and Information Technology who graciously gave me the opportunity to work under his guidance. I am thankful for his patience, continuous support, optimistic approach and time to time guidance throughout this course. His valuable motivation, help, suggestion, affirmative vision, magnificent supervision and enormous confidence in my abilities made me face tough circumstances during the progress of the research work. It is a great honour to work under his supervision.

I would like to express my gratitude to our Honorable Vice Chancellor Prof. (Dr.) Rajendra Kumar Sharma, Dean (Academics and Research) Prof. (Dr.) Ashok Kumar Gupta and Head Department of CSE/IT Prof. (Dr.) Vivek Kumar Sehgal to promote the research and facilitate resources in the institution. I would also like to thank my doctoral committee members for their valuable feedback and critical reviews during presentations and time to time help.

I am also grateful for the support received from JUIT, Waknaghat. In particular, I thank, all staff members at the Department of Computer Science and Engineering and Information Technology, JUIT, Waknaghat who has been extremely helpful at numerous occasions. I would like to thank my parents for supporting me spiritually throughout my life. Last but not the least, I thank my fellow Ph.D. friends for their consistent help and valuable discussion.

Date: (Rajshree Srivastava)

iii

ABSTRACT

In medical imaging, machine learning (ML) and deep learning (DL) play a significant role to predict symptoms of early diseases. DL is one of the growing trends in general data analysis since 2013. It is an improvement of artificial neural networks (ANN) as it consists of many hidden layers to permit high level of abstraction from data. In particular, convolutional neural networks (CNNs) have proven to be a potential tool for computer vision tasks. Deep CNNs have a capability to automatically learn raw data especially images.

The accurate assessment or identification of disease depends on image interpretation as well as acquisition. Due to the improvement in last decade in image acquisition, devices acquire data at high rate with increased resolution. However, the interpretation of images has recently begun to benefit from computer technology. Mostly these are made by the radiologist, physicians and senior doctors but limited due to its subjectivity and high skilled physicians/ doctors. Computerized tools in the medical imaging field are the key enablers to improve diagnosis by facilitating the findings.

Analysis of thyroid ultrasonography (USG) images via visual inspection and manual examination for early identification and classification of thyroid nodule has always been cumbersome. This manual examination of thyroid USG images in order to identify benign and malignant thyroid nodule can be tedious and time-consuming. Various deep learning models have emerged in medical field especially in thyroid nodule classification with the rapid advancement in technology and increase in computational resources. Early identification of such nodules can improve the effectiveness of clinical interventions and treatments. Therefore, many researchers now advocate the use of computer diagnostic system (CDS) to objectively and quantitatively analyze the USG images of thyroid nodules. This helps the radiologists to solve the differences in interpretation of results.

Incidents of thyroid tumor have dramatically increased in recent years. However, early ultrasound diagnosis can reduce morbidity and mortality. The work in clinical situations relies heavily on the subjective experience of the sonographer. Thus, developing of a reliable thyroid nodule identification model based on ultrasound images is needed to ensure the accuracy and efficiency of thyroid nodule diagnosis. The key motive of this thesis is to develop efficient models using ML and DL techniques for thyroid nodule identification and classification. The first phase of this thesis proposes two hybrid models namely ANN-SVM and CNN-SVM. These models work in four stages namely data collection, preprocessing, classification using

hybridization of ML and DL classifiers andanalysis of results. The second phase of this thesis proposes an optimized CNN based model using segmentation and boundary detection techniques. In this work, Alex-Net, visual geometry group (VGG-16), deep neural network (DNN) and Res-Net-50 models are optimized using grid search optimization (GSO) technique. The third phase of this thesis proposes a deep-generative adversial network (Deep-GAN) model to improve the accuracy of the VGG and Alex-Net models. VGG-GAN and Alex-GAN. The proposed model will be useful to physicians, researchers, practitioner and small hospitals having limited resources can benefit from using this model to assist with thyroid ultrasound examination diagnosis.

TABLE OF CONTENTS

LIST OF TABLES

LIST OF FIGURES

xiii

LIST OF ACRONYMS & ABBREVIATIONS

AI	Artificial Intelligence
ACWE	Active Contour Without Edges
AC	Active Contour
ANN	Artificial Neural Network
AFUD-SVM	Artificial Fish Coupled with Uniform Design – Support Vector Machine
Ab-LSTM	Attention-based Bi-Directional LSTM
ATA	American Thyroid association
BTND	Benign Thyroid Nodule
CT	Computed Tomography
CMR	Closest-matching CAD system
CAD	Computer-aided Diagnostic System
CNN	Convolutional Neural Network
CPU	Central Processing Unit
DCNN	Deep Convolutional Neural Network
Deep-GAN	Deep- Generative Adversarial Network
D	Discriminator
DL	Deep Learning
DT	Decision Tree
DA	Data Augmentation
DNN	Deep Neural Network
DRLSE	Distance-Regularized-Level-Set-Evolution
EGFS	Ensemble Gain Ratio Feature Selection
EHR	Electronic Health Record

ELM	Extreme Learning Machine
FP	False Positive
FN	False Negative
FE	Feature Engineering
FD-SMOTE	Farthest-Distance-Based-Synthetic-Minority-Oversampling Technique
FFNN	Feed Forward Neural Network
GAN	Generative Adversial Network
GSO	Grid Search Optimization
GB	Giga bytes
G	Generator
GM	Generative Models
GPU	Graphical Processing Unit
GLCM	Grey Level Co-Occurrence Matrix
GC-ACWE	Graph Cut- Active Contour without edges
GLRLM	Gray Level Run Length Matrix
GAN	Generative Adversarial Network
GLCM	Grey Level Co-occurrence Matrix
hyp	Hyperparameter
IOT	Internet of Things
IDMIE	Instituto de Diagnostico Medico
LDA	Linear Discriminant Analysis
LR	Logistic Regression
LRN	Local Response Normalization
MTN	Malignant Thyroid Nodules
MHz	Megahertz

ML	Machine Learning
MLP	Multi-Level Perceptron
MKSVM	Multi-Kernel-Based Support Vector Machine
MTND	Malignant Thyroid Nodules
MPR	Maximum Retention of Inter-Pixel Relations
MCDLM	Multi-Task Cascade DL
NABH	National Accreditation Board for Hospitals
NN	Neural Network
NLP	Natural Language Processing
P	Probability
RF	Random Forest
RAM	Random Access Memory
Res-GAN	Resnet-Generative Adversial Neural Network
Re-Rx	Recursive Rule Extraction Algorithm
RIFO	Ranked Improved F-Score ordering
RTE	Real-Time Elastography
SMOTE	Synthetic-Minority-Oversampling Technique
SSD	Solid State Drives
SVM	Support Vector Machine
SVM-L	SVM Linear
SVM-Q	SVM Quadratic
SFTA	Segmentation-Based Fractal Texture Analysis
SIFT	Scale Invariant Feature Transform
SE	Squeeze And Excitation
SURF	Speeded Up Robust Features

TSH	Thyroid-stimulating hormone
TNDs	Thyroid nodules
T4	Thyroxine
T3	Triiodothyronine
TDID	Thyroid Digital Imaging Database
TI-RADS	Thyroid Imaging Reporting and Data system
TN	True Negative
TP	True Positive
TA	Texture Analysis
USG	Ultrasonography
U.S.A.	United States of America
UCI	University of California, Irvine
VLAD	Vector of locally Aggregated Descriptor
VGG-16	Visual Geometry Group-16

CHAPTER 1

INTRODUCTION

Disease prediction is important for medical institution as well as for the patients to make possible medical care decisions. Sometimes, incorrect decision might lead to serious consequences. Hence, early identification and classification of disease is important. According to the latest report of American Thyroid Association (ATA), more than 12 percent of the U.S. population will develop a thyroid condition during their lifetime [1]. Thyroid dysfunction is the most prevalent endocrine disorder worldwide having an epidemiology of 4.6% in the United Kingdom, 11% in India and 2% in the U.S among the overall population [2]. Thyroid gland is a small butterfly shaped endocrine gland located in neck region below Adam's apple [3]. It produces three types of hormones namely thyroxine(T4), calcitonin and triiodothyronine (T3) to maintain the metabolism of the body. The function of these hormones depends on the right amount of supply of iodine in diet [4]. The ductless gland located at the bottom of our brain sends signals to secret hormones called as Thyroid Stimulating Hormone (TSH). It informs the thyroid gland to secret the hormones as per the requirement [5]. Thyroid Nodules (TNDs) are solid or fluid filled lumps formed within the thyroid region/gland. Figure 1.1 shows an image of thyroid gland. There are various imaging processes like Ultrasonography (USG) and Computed Tomography (CT) used for the identification of diseases [6]. USG is highly recommended for the identification of TNDs as it is cost friendly, radiation free, real-time and painless.
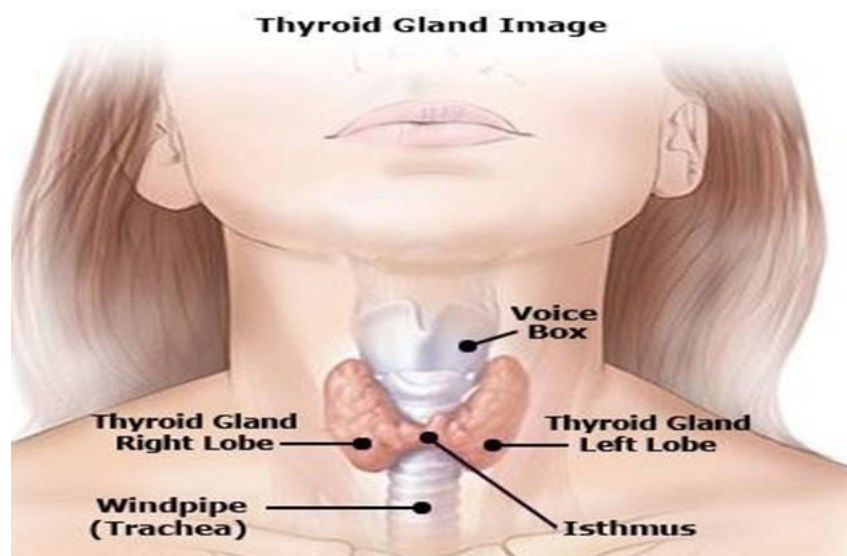
Figure 1.1: Thyroid gland [7]

When there is an excess production of TSH in the body, it is said to be hyperthyroidism. Some of the common hypothyroid signs noticed are abundance weight, dry skin, fatigue of body quality and tiredness [8]. Hypothyroid is a condition when there is less production of TSH in the body. Some of common sign noticed signs are tremors, weight loss and loose bowels. Thyroid problems are common among people as its symptoms are mild. There are twocategories of TNDs namely benign (BTND) and malignant (MTND) [9]. MTND are consideredas one of the top 10 MTND and account for 1.1% of all the malignant tumors [10]. There are certain distinctive features of TNDs which can be found in TI-RADS system [11]. Table 1.1 shows the TI-RADS score.

Table 1.1: TI-RADS Score

TI-RADS Score	Type	Category
1	Benign	BENIGN
2	Not Suspicious	
3	Mildly Suspicious	
4	Moderately suspicious	MALIGNANT
5	Highly suspicious	

In last few decades, success of Machine Learning (ML) and Deep Learning (DL) techniques in image identification/diagnosis tasks leads to solve challenges in diagnostic imaging. ML techniques have a great potential to deal problems in the field of medicine, drug discovery and decision making. Medical images are mostly analyzed by the radiologists who are highly experienced and have knowledge in the respective domain. A delayed or erroneous diagnosis causes harm to the patients [12]. In ML, learning new features are well described by the patterns in images. The sparse representation (i.e., feature extraction/selection) in ML techniques finds informative patterns from a shallow architecture but they lack in its representational power [13]. DL techniques use the feature engineering (FE) step into a learning step [14]. It works by discovering informative representation in a self-taught manner with some pre-processing steps without extracting features manually [15]. Thus, the manual feature engineering has been shifted to computers thereby allowing the non-experts of ML to use DL techniques efficiently especially in the medical diagnosis filed. Some of the popular reasons lead to success of DL techniques are: (1) development of advance algorithms [16], (2) availability of large amount of data [17], (3) easy derivation of hierarchical features from low-level to high-level [18], (4) improvement in the traditional Artificial Neural Networks (ANN) i.e., increase in multiple layer [19] and (5) advancement in high-tech processing units [20].

1.1 Thyroid Nodule Datasets

This section focuses on the datasets used for the identification and classification of TNDs in this thesis. The dataset plays significant role while conducting any experiment. It contains information that helps the model to have a high level of understanding. In this thesis, two datasets are considered:

1.1.1 Thyroid Digital Imaging Database (TDID)

This dataset is collected from Instituto de Diagnostico Medico (IDIME) ultrasound department, Colombia. The dataset has 295 thyroid USG images, having 107 BTND and 188 MTND images [21]. The images were captured with Toshiba Nemio 30, MX Ultrasound devices and Toshiba Nemio with 12MHz convex and linear transductors.

1.1.2 Collected Dataset

This dataset is collected from Kriti Scanning Center, Prayagraj, Uttar Pradesh (U.P.), India duly approved by National Accreditation Board for Hospitals (NABH) and Healthcare Providers [22]. The collected sample size was 654 images, out of which 428 and 226 were BTND and MTND images. The duration of dataset collection was from July 2020 to March 2021. The images were captured with SIEMENS Healthier, Mindray-Resona 7 and Voluson E- 10 Ultrasound devices with 3 to 11MHz convex and linear transductors. In both cases, Thyroid Imaging Reporting and Data system (TI-RADS) scores is used to pre-classify the TNDs images.

The criteria for the inclusion and exclusion of thyroid USG images are as follows:

Inclusion-
- Images having clear boundary of the nodules.
- Images having one or multiple nodules.
- Patients having age greater than 16 years.
- Patients with the confirmed thyroid nodules problem.

Exclusion –
- Excluded the images which were zoomed in or zoomed out.
- Patients having age less than 16 years.
- Patients without confirmed thyroid nodules problem.

1.2 Performance Parameters

There are four different parameters considered for evaluation of proposed models in this thesis:

- **Accuracy:** It is defined as the ratio of correctly classified TNDs to the total number of examples and computed using equation 1.1:

$$Accuracy = \frac{TP+TN}{TP+TN+FP+FN} * 100 \qquad (1.1)$$

- **Specificity:** It is defined as the percentage (%) of people who test negative for a specific disease among a group of people who do not have the disease and calculated using equation 1.2:

$$Specificity = \frac{TN}{TN+FP} * 100 \qquad (1.2)$$

- **Sensitivity:** It is defined as the percentage (%) of people who test positive for a disease that have disease and calculated using equation 1.3:

$$Sensitivity = \frac{TP}{TP+FP} * 100 \qquad (1.3)$$

- **F-measure:** It measures the test accuracy of the model and calculated using equation 1.4:

$$F - measure = \frac{2TP}{2TP+FN+FP} * 100 \qquad (1.4)$$

1.3 Research Objectives

The objectives of this thesis are highlighted below:

1. To design a hybrid model for the identification and classification of TNDs.
   a. To propose a hybrid model using hybridization of ML classifiers.
   b. To propose a hybrid model using hybridization of ML and DL classifiers.
2. To propose an optimized DL model the identification and classification of TNDs
3. To design an improved DL model for the identification and classification of TNDs.

1.4 Organization of Thesis

The thesis consists of seven chapters as per the details below:

Chapter 1: This chapter provides the introduction about thyroid nodule problem along with its types, datasets used, and performance parameters for the identification and classification of TNDs.

Chapter 2: This chapter discusses the literature review of different ML and DL techniques for identification and classification of TNDs.

Chapter 3: This chapter discusses the first part of objective one of the thesis i.e. design of a hybrid model using hybridization of ML classifiers for the identification and classification of TNDs.

Chapter 4: This chapter discusses the second part of objective one of the thesis i.e. design of a hybrid model using hybridization of ML and DL classifier for the identification and classification of TNDs.

Chapter 5: This chapter elaborates the second objective of the thesis i.e. design of an optimized DL model for the identification and classification of TNDs.

Chapter 6: This chapter focuses on the third objective of the thesis i.e. design of an improved DL model using Generative Adversial Network (GAN) for the identification and classification of TNDs.

Chapter 7: This chapter concludes the thesis and throws light on future perspectives.

CHAPTER 2

LITERATURE REVIEW

This chapter describes literature review related to thyroid disorder. The method of categorization of work is based on techniques related to identification, classification and feature selection for thyroid identification and detection. For this study, the selected articles are assorted into three categories namely simple, improved and hybrid techniques. Figure 2.1 shows the assortment of literature review.
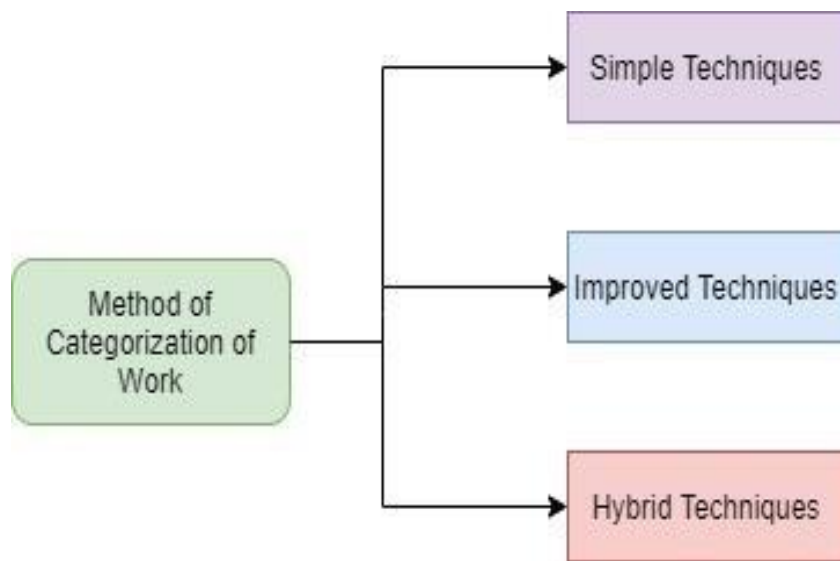
Figure 2.1: The assortment of literature review

2.1 Simple Techniques

Simple techniques are mainly ML techniques. It is a subset of Artificial Intelligence (AI) that builds a mathematical model based on sample examples to predict without itself being explicitly involved [23]. Simple techniques are widely used in medical diagnosis to detect patterns of diseases from Electronic Health Record (EHR) and inform clinicians of any acute problem [24]. It works in four phases namely (1) data collection, (2) data processing (preparation of data, model selection), (3) train the model and (4) analysis of results. Figure **2.2** shows the framework of simple techniques.
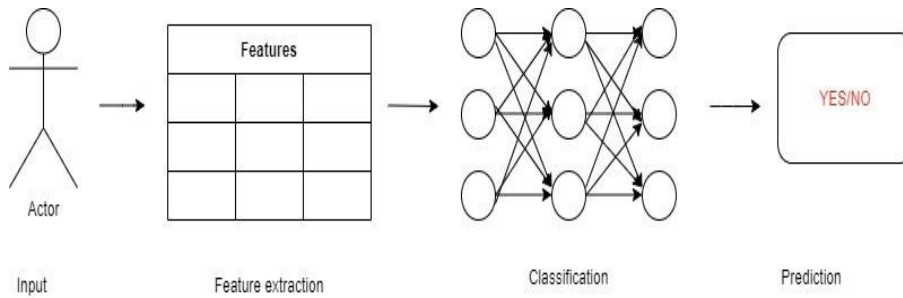
Figure 2.2: Framework of simple techniques [23]

Zhu et al. proposed ML-based CAD system [25]. Sonographic features are extracted from the USG images and ANN is used for discriminating USG images. The model has achieved specificity of 81.80%, accuracy of 83.10% and sensitivity of 83.80%.

Naryan et al. presented a multi-organ segmentation algorithm that is successful to perform volumetric analysis and US-guided interventions [26]. The model was evaluated on two datasets having 34 and 18 USG images. The model is yet to be evaluated on a large dataset.

Song et al. proposed a Grey Level Co-Occurrence Matrix (GLCM) method for feature extraction and different ML classifiers for classification [27]. The logistic regression has achieved a good result from the rest of the classifiers on 155 USG images.

Ardakani et al. evaluated the CAD system with Texture Analysis (TA), Linear Discrimant Analysis, Principal Component Analysis, (PCA+LDA) for the classification of TNDs [28].

Nugroho et al. used bilateral filters for the pre-processing step results in smoothen images and also preserves the boundaries of the object followed by Active Contour Without Edges (ACWE) for the segmentation of the thyroid nodules [29]. The result shows not only improvement in the accuracy of the segmentation of active contours (AC) but also makes localization of the TNDs clear.

Song et al. proposed a GLCM based texture feature model using different ML algorithms for classification [30]. The model was evaluated on 147 USG images. The best accuracy result is achieved by Support Vector Machine (SVM) with 76.6%, Random Forest (RF) with 74.1%, ANN with 72.8% and Decision Tree (DT) with 67.1% accuracy.

Pan et al. proposed Principal Component Analysis (PCA) ensemble method for feature

reduction and found that it performs better than Bagging and AdaBoost [31].

Alrubaidi et al. proposed an interactive segmentation method evaluated on 27 USG images of public datasets [32].

Vanithamani et al. proposed CAD system using GLCM for feature extraction, segmentation using fuzzy c- means clustering and classification using SVM on TDID dataset [33].

Nugroho et al. proposed a texture feature extraction using Gray Level Run Length Matrix (GLRLM), histogram and GLCM. Multi-Level Perceptron (MLP) classifier was considered for classification [34]. Model is evaluated on small public dataset.

Mustafa et al. proposed the Farthest-Distance--Based-Synthetic-Minority-Oversampling Technique (FD-SMOTE) system and evaluated it on University of California, Irivine (UCI) repository thyroid dataset [35].

Pasha et al. proposed Ensemble Gain Ratio Feature Selection (EGFS) model [36]. The model ensemble RF & gain ratio algorithm to find the most efficient features followed by its alignment with LR, K-Nearest Neighbor (KNN) and Naive Bayes.

Jothi et al. proposed a novel SVM linear+ SVM Quadratic+ Closest-matching CAD system i.e. (SVM-L+SVM-Q+ CMR) [37]. The proposed CAD system has achieved a good result by combining the advantages of SVM and CMR classifiers.

Jiang et al. proposed an intelligent model using ML-based techniques [38]. All ML-based classifiers have achieved 84% accuracy except DT classifier.

Shankar et al. proposed a Multi-Kernel-Based SVM (MKSVM) system for thyroid disease classification using the UCI and private datasets [39].

Ma et al. proposed a ML-based model (center clustering, deep neural network, SVM, KNN and LR) for thyroid nodule classification [40]. A total of 508 USG images are used in the experiment. The highest accuracy achieved is 87%.

Zheng et al. proposed the serum Raman spectroscopy technique combined with Artificial Fish Coupled with Uniform Design (AFUD) –SVM discriminant model capable for the detection of thyroid dysfunction [41].

Dandan et al. proposed CAD system using Wavelet Multi-Sub-Bands Co-Occurrence Matrix (WMCM) and other feature extraction techniques [42]. The model is evaluated on 180 USG images.

Poudel et al. proposed an autoregressive feature for thyroid ultrasound images without modeling the images [43].

Prochazka et al. proposed a 2-threshold binary decomposition CAD system that uses direction independent feature set [44]. Authors addressed the problem of direction-independent features problem. Model was evaluated on 40 USG images and used histogram and segmentation for classification. The results show that SVM gives good results in comparison with RF.

Wu et al. proposed texture analysis system using Local Binary Pattern (LBP) and Histogram of Oriented Gradients (HOG) feature extraction techniques [45]. The model was evaluated on 4,574 USG images.

Colakoglu et al. proposed ML-based model to differentiate between BTND and MTND via extracting 306 features from 235 USG images [46]. Among ML-based algorithms, the RF classifier gives a good result with an accuracy of 86.8%.

Zhang et al. proposed ML-based thyroid nodule detection using sonographic features and Real-Time Elastography (RTE) [47]. Nine different ML algorithms like RF, LR, SVM, Neural Net, Adaptive Boosting, Naive Bayes and Convolutional Neural Network (CNN) were considered but RF shows the best result with an accuracy of 84.1 % in comparison with other classifiers.

Kesarkar et al. proposed an ANN based CAD system [48]. The ACWE based segmentation method and MLP for the classification of TNDs images.

Zhao et al. compared various ML classifiers for thyroid nodule detection using sonographic features [49]. The model shows that the application of ML-based classifiers like DT, SVM,

KNN, RF, LR, MLP, Xgboost, Gradient Boosting Tree and Naive Bayes on sonographic features has achieved the best result. The model was evaluated on 849 USG images. Table 2.1 shows summarization of literature review using simple techniques.

Table 2.1: Summarization of literature review using simple techniques

Article [Ref.]	Proposed Model	Feature extraction/ Detection techniques	Classification	Dataset	Findings	Limitations
Zhu et al. (2013)	CAD System	Sonographic features	ANN	Public dataset	(i)It has achieved 83.10 % accuracy, 83.80% sensitivity and 81.80% specificity	(i)The result can further be improved by using hybridization of two or more classifiers.
Narayan et al. (2015)	Speckle Patch Similarity model	----		Department of Radiology, Sardjito Hospital, Yogyakart	(i)It has achieved 92.1% accuracy.	(i)The model is yet to be evaluated on large dataset.
Song et al. (2015)	Texture based thyroid detection model	GLCM	SVM, RF, DT, LR, ANN	Shandong Provincial Qianfoshan Hospital	(i)LR has achieved 84% accuracy, 78.5% specificity and 78.5% sensitivity.	(i)Other different texture feature extraction can be used to achieve better result.
Nugroho et al. (2015)	Active Contour Bilateral Filtering model			Department of Radiology, Sardjito Hospital, Yogyakart	(i)It is insensitive to noise.	(i)Manual parameter tuning and initial contour is required.
Song et al. (2015)	ML based CAD System	GLCM	SVM, RF, DT, ANN	Public dataset	(i)SVM achieved the best result among rest of the classifier.	(i)The model is evaluated on 147 thyroid USG images.
Ardakani et al. (2015)	CAD System	Statistical features	------	Radiology Department Imam Khomeini hospital, Urmia, Iran	(i) No operator dependency. (ii)It takes additional cost and time loss. (ii) It has achieved accuracy 97.14% specificity 100% and sensitivity 94.45%.	(i)Model can further be improved by using other type of feature extraction method.
Vanithamani et al. (2016)	CAD System	GLCM	Fuzzy C-means clustering, SVM	TDID	(i)It has achieved accuracy 86.6% specificity 85.7% and sensitivity 87.5%. (ii) It achieves good results in less numbers of features extracted.	(i)The size of the dataset is very less.
Nugroho et al. (2016)	CAD System	GLRM, GLCM, Histogram	MLP	------	(i)It can be used as 2nd opinion by clinicians. (ii)Model has achieved accuracy 89.74% specificity 91.67% and	(i)The size of the dataset is very less.

					sensitivity 88.89%.	
Koundal et al. (2016)	Automated delineation of thyroid nodules	----	Spatial neutrosophic distance regularized level set	Public dataset	(i) It is insensitive to nodule echogenicity. (ii) It has achieved 95.45% sensitivity.	(i) It has strong resistance to noise.
Pasha et al. (2017)	EGFS model	EGFS	LR, Naive Bayes, KNN	UCI repository and local dataset	(i) It has achieved 96.45% accuracy. (ii) The model has achieved good result with a few numbers of features.	(i) It has strong resistance to noise. (ii) Complex data pre-processing is used.
Mustafa et al. (2017)	FD-SMOTE Technique	Minimum Description Length Method, PCA	Genetic algorithm	UCI repository	(i) The model works good on less dataset. (ii) It has achieved 84.12% accuracy.	(i) Work can be extended on rough theory problem.
Jothi et al. (2017)	SVM-L+SVM-Q+CMR CAD System	PSO	SVM	Public dataset	(i) The proposed CAD system differentiate PT C and NT H&E- stained thyroid histo-pathology images. (ii) It has achieved accuracy 99.54% sensitivity 100% and specificity 98.57%.	(i) Size of dataset is less.
Jiang et al. (2017)	ML based CAD system	Sonographic features	SVM, KNN, LR, DT, RF	Public dataset	(i) The model has achieved 84% accuracy.	(i) Other feature extraction techniques can be explored. (ii) Size of the dataset is less.
Zheng et al. (2018)	AFUD System	Wavelet Multi-sub-bands Co-occurrence matrix	SVM	First Affiliated Hospital	(i) It has achieved 82.74% accuracy. (ii) The proposed technique can be used to develop a portable device for detecting TNDs function.	(i) Size of the dataset used is less.
Dandan et al. (2018)	ML based CAD system	WMCM	SVM	Public dataset	(i) he model has achieved 87% accuracy.	(i) Work can be extended on other different types of feature extraction methods. (ii) Size of the dataset is less.
Shankar et al. (2019)	MKSVM method	Auto-regressive features	SVM	Public and UCI	(i) It has achieved accuracy 97.49%, specificity 94.5%	(i) High computation time.

					and sensitivity 99.05%. (ii)The model has achieved good result with a few numbers of features.	
Ma et al. (2020)	ML based CAD System	Sonographic features	KNN, LR, SVM	Public dataset	(i)The model has achieved 87% accuracy.	(i)Work can be extended on other different types of feature extraction methods. (ii) Size of the dataset is less.
Poudel et al. (2019)	Autoregressive Feature based CAD model	Histogram features, SFTA	SVM, RF	SurgicEye GmbH, University Clinic of Magdeburg, Germany	(i)The proposed approach outperforms from DSC and had similar SE and SP. (ii)It has achieved 90% accuracy.	(i)Bi-Spectral model can be used in future work.
Prochazka et al. (2019)	CAD System	HOG, LBP	SVM, RF	Our clinic	(i)It uses direction-independent features. (ii)It has achieve-d 94.64% accuracy.	(i)Work can be extended on large dataset.
Wu et al. (2019)	CAD System	LBP, GTF, HOG, FOS, GLCM, HWF, Autoregressive model, GRLM		Second Affiliated Hospital of Fujan Medical University	(i)Can be used as 2nd opinion for diagnosis of TNDs. (ii)It has achieved 88.58% accuracy.	(i)High computation time.
Colakoglu et al. (2019)	ML based CAD system	Ultrasonography, shear wavelet texture	ML classifiers	---	(i)It has achieved accuracy 86.8%, sensitivity 85.2% and specificity 87.9%.	(i)Work can be extended on large dataset.
Zhang et al. (2019)	ML based CAD system	-----	RF, LR, SVM, Neural net, adaptive boosting, naive bayes and CNN	First Affiliated Hospital	(i)The model has achieved 84.6% accuracy, 84.2% specificity and 88.1% sensitivity.	(i)Different other feature selection techniques can be used for better result.
Kesarkar et al. (2021)	ANN model for thyroid nodule diagnosis	Sonographic features	MLP	-----	(i)It has achieved 93.84% accuracy, 97.82% sensitivity and 93.75% specificity.	(i)Size of the dataset is less.
Zhao et al. (2021)	ML based techniques for classification of thyroid USG	EGFS	DT, SVM, KNN, RF, LR, MLP, Xgboost, gradient	-------	(i)It has achieved 88.8% accuracy, 92.9% specificity and 81.7% sensitivity.	(i)Work can be extended to other feature extraction methods.

	images		boosting tree and Naive baye			

2.2 Improved Techniques

Improved techniques are the DL techniques based on ANN with representation learning. It uses various layers to progressively extract a higher level of features from the user input [50]. DL techniques applications include audio recognition, medical image analysis, speech recognition, bioinformatics and Natural Language Processing (NLP) [51]. The term "deep" means large number of features to be extracted from raw image as input. E.g., lower layers and higher layers identify edges and letters [52]. DL reduces the cost of feature engineering and retrieves a lot of information that helps the model to achieve better results [53]. One of the major differences between ML and DL is that ML cannot extract features automatically; it requires labelled parameters whereas in the case of DL, it extracts features automatically without human intervention [54]. Figure 2.3 shows the working of the improved techniques. It also works in three steps: (1) input, (2) feature extraction and classification and (3) prediction.
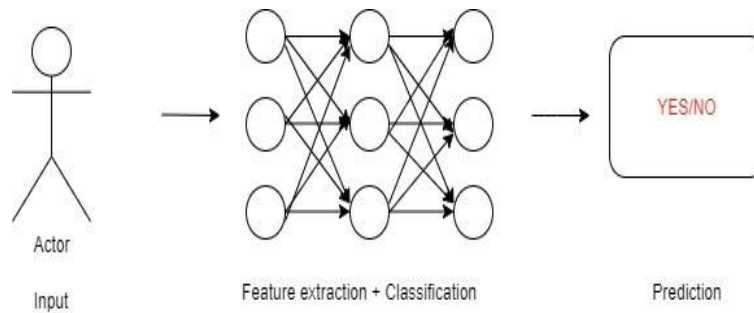
Figure 2.3: Working of improved techniques [54]

Du and Sang et al. proposed an improved Distance-Regularized-Level-Set-Evolution (DRLSE) method for the segmentation of 2D TNDs USG images [55]. It consists of three steps namely image processing, extracting boundaries and image post-processing. It does not perform well to automatically segment the TNDs USG images.

Archarya et al. proposed Gabor transform features from high-resolution TNDs images [56]. The model was evaluated on 240 USG images.

Peng et al. show the first order features selection in TNDs ultrasound image recognition as image biomarkers [57].

Zhu et al. proposed an image augmentation CAD system using transfer learning technique as Generative Adversarial Network (GAN) [58].

Song et al. proposed a multi-scale DL single-shot detection network method guided by nodule with the help of a CNN [59].

Zhang et al. proposed a multi-scale single-shot detection network guided by nodule [60]. The model was evaluated on 45 USG images.

Sundar et al. explored different DL techniques like CNN, VGG-16 model and Inception-V3 model for the diagnosis of TNDSs [61].

Wang et al. proposed a novel EM-based model to train Alex-Net for the diagnosis of the TNDs [62]. Authors addressed the problem of labeled data and evaluation was done on public and private datasets.

Chen et.al proposed 2- Level Attention-Based Bi-Directional LSTM (Ab-LSTM) for TNDs classification [63].

Li et al. proposed a Deep Convolutional Neural Network (DCNN) model for the detection of TNDs [64]. The result shows good improvement in sensitivity, accuracy and specificity in comparison with a group of skilled radiologists.

Ko et al. proposed a DCNN for TNDs diagnosis [65]. The model was evaluated on 589 USG images dully approved by the radiologist and used 3 layers of CNN for the classification of TNDs.

Wang et al. proposed a DL-based CAD system using YOLOv2 NN [66]. The proposed method achieved a real-time and synchronous diagnosis CAD system for TNDs diagnosis.

Liu et al. proposed clinical-knowledge-guided CNN model for the TNDs classification [67].

Aboudi et al. proposed a CAD system combining different attributes after optimization to achieve good accuracy [68].

Guo et al. proposed an improved DL technique for TNDs identification [69]. A new CNN

model is proposed which integrates Squeeze and Excitation (SE) and Maximum Retention of Inter-Pixel Relations Module (CNN-SE-MPR). The model was evaluated on 407 USG images.

Ajilisa et al. used various pre-trained CNN network [70]. K-means clustering is employed to deal with imbalanced datasets.

Nguyen et al. used a fusion of spatial and Fourier based methods for feature extraction and also used two CNN models together to improve the accuracy [71].

Vasile et al. proposed an intelligent diagnosis model using ensemble DL methods [72]. Model was designed with 5 CNN layers and then ensemble with pre-trained VGG-19 model. The model was evaluated on 230 USG images.

Zhu et al. proposed an automatic DCNN CAD system [73]. The model was evaluated on 719 USG images.

Yang et al. proposed a Multi-Task Cascade DL (MCDLM) model [74]. It works in three steps namely pre-processing, U-Net model for segmentation of nodules and semi-supervised method for feature extraction and classification. The model has achieved good result on small dataset. Table 2.2 shows summarization of literature review using improved techniques.

Table 2.2: Summarization of literature review using improved techniques

Article [Ref.]	Proposed Model	Feature extraction/ Detection techniques	Classification	Dataset	Findings	Limitations
Du et al. (2015)	CAD System	--	DLRSE	Wuhan Tongji Hospital, China	(i) It is insensitive to noise and nodule echogenicity. (ii) Achieved 85% sensitivity.	(i)It requires manual initial contour.
Acharya et al. (2016)	CAD System	Gabor Transform	MLP, SVM, KNN	Chiang Mai University Hospital, Thailand	(i)It has achieved 94.3%.	(i)Work can be extended to non-linear feature extraction algorithms.
Peng et al. (2017)	CAD System	FOS	SVM	Ruian People Hospital, Zhejiang, China	(i)It has achieved specificity 93.3%, accuracy 88% and sensitivity 82.1%.	(i)Work can also extend on large thyroid USG dataset.
Zhu et. al (2017)	DL based CAD system	---	CNN	TDID	(i) It can be used as a 2nd opinion by the radiologist. (ii) It has achieved 93.75% accuracy.	(i)Handcrafted and DL model can be used for better result.
Song et. al (2019)	MC-CNN Framework	----	VGG-16	TDID	(i) It has achieved accuracy 92.1%, sensitivity 94.1% and specificity 96.2%. (ii) Embedded spatial pyramid module into traditional CNNs.	(i)Sample size is less
Zhang et al. (2018)	FAFL Model	Multi-channel feature association	---	Local hospital	(i) New feature association model is proposed. (ii) It has achieved 83% accuracy.	(i) Improvement can be done by fusion of two or more classifiers. (ii) The dataset size is very small.
Sundar et al. (2018)	DL CAD System	VGG-16 and Inception-V3 model	-	Public and private	(i) Achieved good result on a smaller number of datasets. (ii) It has achieved accuracy 93% with Inception-v3 + CNN and with VGG-16 with 89%.	(i)The dataset size is very small.
Wang et al. (2018)	Semi-supervised method	VGG-16	----	TDID	(i)The model solves multi-instance problems and also improves the classification accuracy.	(i)The dataset size is very small.

					(ii) It has achieved accuracy 80.91%, sensitivity 81.82% and specificity 80%.	
Chen et al. (2018)	Ab-LSTM Memory method	--	CNN	Ruijin Hospital, Shanghai	(i) Model perform good. (ii) It has achieved 86.18% accuracy.	(i) The dataset size is very small.
Li et al. (2019)	DCNN	----	CNN	Traditional Chinese Weihai Municipal Hospital, Shandong, Tianjin Cancer Hospital and Western Medicine Hospital, Jilin	(i) It can be used as 2nd opinion for diagnosis. (ii) It has achieved sensitivity 93.4% and specificity 86.1%.	(i) The dataset size is very small.
Ko et al. (2019)	DCNN	---	CNN	-----	(i) The model has achieved 86% accuracy.	(i) Sample size is less
Wang et al. (2019)	DL- CAD System	----	CNN	Tertiary class A hospital	(i) Can be used as 2nd opinion for the diagnosis. (ii) It has achieved sensitivity 90.5% and accuracy 90.31%.	(i) Work can be extended on large database.
Liu et al. (2019)	DL- CAD System	---	CNN	Cancer Hospital ofthe Chinese Academy of Medical Sciences	(i) The pixel annotation used in this work is coarse. (ii) It has achieved accuracy on dataset-I 97.5% and accuracy on dataset-II 97.1%.	(i) Work can be extended on large database.
Aboudi et al. (2020)	CAD system	Statistical, GLCM	CNN	CIM Laboratory of the National University of Columbia	(i) Fusion of (intensity + textural features + shape) is used. (ii) It has achieved 96.13% accuracy.	(i) Work can be extended on large database.
Guo et al. (2020)	CNN-SE-MPR System	---	CNN	Co-operate hospitals	(i) With the help of MPR module, loss of inter pixel relation is solved. (ii) It has achieved accuracy 90.17%, specificity 92.35% and sensitivity 86.99%.	(i) Work can be extended on big database.
Ajilisa et al. (2020)	CAD System	----	Alexnet, DNN, Inception v-3, Googlenet, VGG-19,	TDID	(i) DNN performs best.	(i) Work can be experiment on large database. (ii) Failed to address the problem of noise.

			Xception, Resnet-10, VGG-16, Resnet-50,			
Nguyen et al. (2021)	DL based CAD system	FFT	CNN	TDID	(i) Fusion of Res-Net50 and Inception Model is considered for classification. (ii) It has achieved 92.05% accuracy.	(i)Work can be extended on large database.
Vasile et al. (2021)	Ensemble model	----	CNN	Public dataset	(i)Ensemble CNN and VGG-19. (ii)It has achieved sensitivity 95.75%, accuracy 97.35% and specificity 98.43%. (iii)It can be used as 2nd opinion by the physician.	(i)Work can be extended on large database.
Zhu et al. (2021)	DL based model	---	CNN	Ethics committee Hospital of Shanghai	(i) It has achieved 86.5% avg. accuracy, 87.1% specificity and 86.6% sensitivity. (ii) It can be used as 2nd opinion by the physician.	(i)Hand-crafted feature extraction methods can also be used to improve accuracy.
Yang et al. (2021)	DL CAD system	Sonographic features	CNN	Partner hospitals	(i)Used augmentation technique. (ii)It has achieved 90.01% accuracy, 92.15% specificity and 87.47% sensitivity.	(i)Size of the dataset is less.

2.3 Hybrid Techniques

Hybrid techniques are the combination of two or more classifiers to improve performance of model [75]. It works in three steps namely, (1) data pre-processing, (2) model selection and (3) prediction. Figure 2.4 shows the working of hybrid techniques.
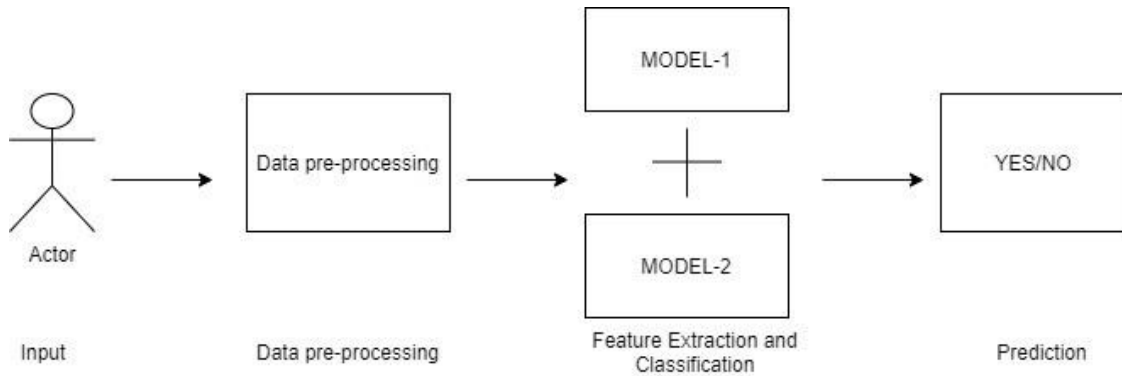
Figure 2.4: Working of hybrid techniques [75]

Liu. et al. proposed a combination of hand-crafted feature and DL feature-based extraction technique for the thyroid image classification i.e., VGG-F model with Scale Invariant Feature Transform (SIFT) + Vector of Locally Aggregated Descriptor (VLAD) and GLCM [76].

Xia et al. proposed a hybrid Extreme learning machines (ELM) based approach for TNDs diagnosis [77]. The model was evaluated on 230 USG images.

Nguyen et al. proposed a model based on fusion of spatial and frequency domain for feature extraction from USG images and achieved an accuracy of 90.88% [78].

Qin et al. proposed (conventional ultrasound+ elasticity imaging) model for the classification of TNDs [79].

Xie et al. proposed a (DL +handcrafted features) model and achieved an accuracy of 85% [80]. The model was evaluated on 623 USG images.

Sun et al. proposed a (DL-based technique + statistical) features together for classification of TNDs [81]. The model was evaluated on 490 USG images.

Hang et al. suggested a Res-GAN model [82]. In this work, authors have compared ResNet-18 with Res-GAN model and Speeded Up Robust Features (SURF) with deep features along

with RF as classifier. The proposed Resnet-Generative Adversial Neural Network (Res-GAN) model has achieved an accuracy of 95%.

Srivastava R., et al. proposed a hybrid model using ANN and SVM for the classification of TNDs [83]. The model shows that when two classifiers hybrid together, the accuracy is increased. Table 2.3 shows summarization of literature review using hybrid techniques.

Table 2.3: Summarization of literature review using hybrid techniques

Article [Ref.]	Proposed Model	Feature extraction/ Detection techniques	Classification	Dataset	Findings	Limitations
Liu et al. (2017)	Hybrid method	SIFT, HOG, VLAD, LBP	CNN	Cancer Hospital of the Chinese Academy	(i) The feature used shows that both hand-crafted features and DL features contribute to the thyroid image classification. (ii) It has achieved specificity 94.1%, accuracy 92.9% and sensitivity 90.8%.	(i)There is no comparison with the other models.
Xia et al. (2017)	Hybrid method	Relief method	SVM	Wenzhou Central Hospital	(i) It can be used as 2nd opinion for TNDs diagnosis. (ii) It has achieved accuracy 87.72%, sensitivity 78.89% and specificity 94.55%.	(i)Small dataset.
Nguyen et al. (2019)	DL-CAD System	---	CNN	TDID	(i) Used the combination of spatial and frequency domain problem. (ii) It has achieved 90.88% accuracy.	(i)Work can be extended on other different type of feature extraction method.
Qin et al. (2019)	Hybrid method	-----	VGG-16	Huiying Medical Technology (Beijing) Co.Ltd	(i)Use of end-to-end implementation leads to good efficiency result. (ii)It has achieved accuracy 94.70%, specificity 92.7% and sensitivity 97.96%.	(i)The model is yet to be evaluated on large dataset.

Xie et al. (2020)	Hybrid deep learning based feature method	LBP	CNN	Shanghai Tenth People's hospital	(i) Can be used as 2nd opinion for the diagnosis. (ii) It has achieved 85% accuracy.	(i)Different other feature methods can be explored.
Sun et al. (2020)	Hybrid method	Statistical features	CNN	First Affiliated Hospital of Nanjing Medical University	(i) A voting system is used. (ii) The model has achieved 86.5% accuracy.	(i) Different other feature methods can be explored. (ii)The model is yet to be evaluated on large dataset.
Hang et al. (2021)	Res-GAN model	Statistical features	ResNet-18, Random Forest, AdaBoost	TDID	(i) The model has performed well in less sample size. (ii) The Res-GAN model performs well in comparison with ResNet-18. (iii) In this work, fusion of SURF + deep features+ RF is used for classifier. (iv) Accuracy: 95%	(i) Different other feature methods can be explored. (ii)Different other DL techniques can be explored for the identification of TNDs.
Srivastava, R et al. (2021)	Hybrid model	GLCM	ANN, SVM, DT, KNN, RF	TDID, collected	(i) The model has performed well in less sample size. (ii) The issue of noise in images is addressed. (iii) Model shows that accuracy of the model is increased in comparison with standalone classifier when it is hybrid. (iv)The model is evaluated on 2 datasets.	(i) Different other feature methods can be explored. (ii) DL models can be explored.

2.4 Inferences Drawn from Literature Review

The literature review shows significant research carried out for the identification and classification of TNDs. However, there are many gaps which are partially unexplored and needs immediate attention. The following are the inferences drawn from the detailed review:

1. Most of the existing study relies on either ML or DL classifier for the identification and classification of TNDs. Thus, there is a scope to build hybrid model.

2. This review sheds light on the possible use of segmentation, clustering, boundary and edge detection techniques to enhance the performance of improved techniques.

3. It is inferred from that improved techniques model require continuous training and adjustment of hyper parameters. It is still an unresolved issue as it requires complete domain knowledge.

4. It is evident that less attention has been paid by the researchers for noise removal in thyroid USG images.

5. This review sheds light on the importance of TNDs disorder. Such thyroid disorder has also attracted a large number of health care experts subject to availability of USG images with advancement in medical imaging. Hence, such images are a good inspiration for the healthcare analysts to identify and detect TNDs disorder.

2.5 Summary

This chapter described the literature review conducted for TNDs identification and classification. The inferences drawn are inked from the detailed literature review carried out in this chapter. The coming chapters in the thesis will present effective and efficient models for the identification and classification of TNDs.

CHAPTER 3

ANN-SVM HYBRID MODEL FOR THE IDENTIFICATION AND CLASSIFICATION OF THYROID NODULE

ML and DL techniques have been widely used in recent years in medical imaging. USG is one of the suggested diagnostic methods for accurately differentiating BTND and MTND images. In this chapter, ANN-SVM hybrid model is proposed for the identification and classification of TNDs USG images.

3.1 Proposed Methodology

It consists of five steps namely (1) data collection phase, (2) pre-processing, (3) feature extraction phase, (4) classification and (5) result analysis. Figure 3.1 shows the framework of ANN-SVM hybrid model.
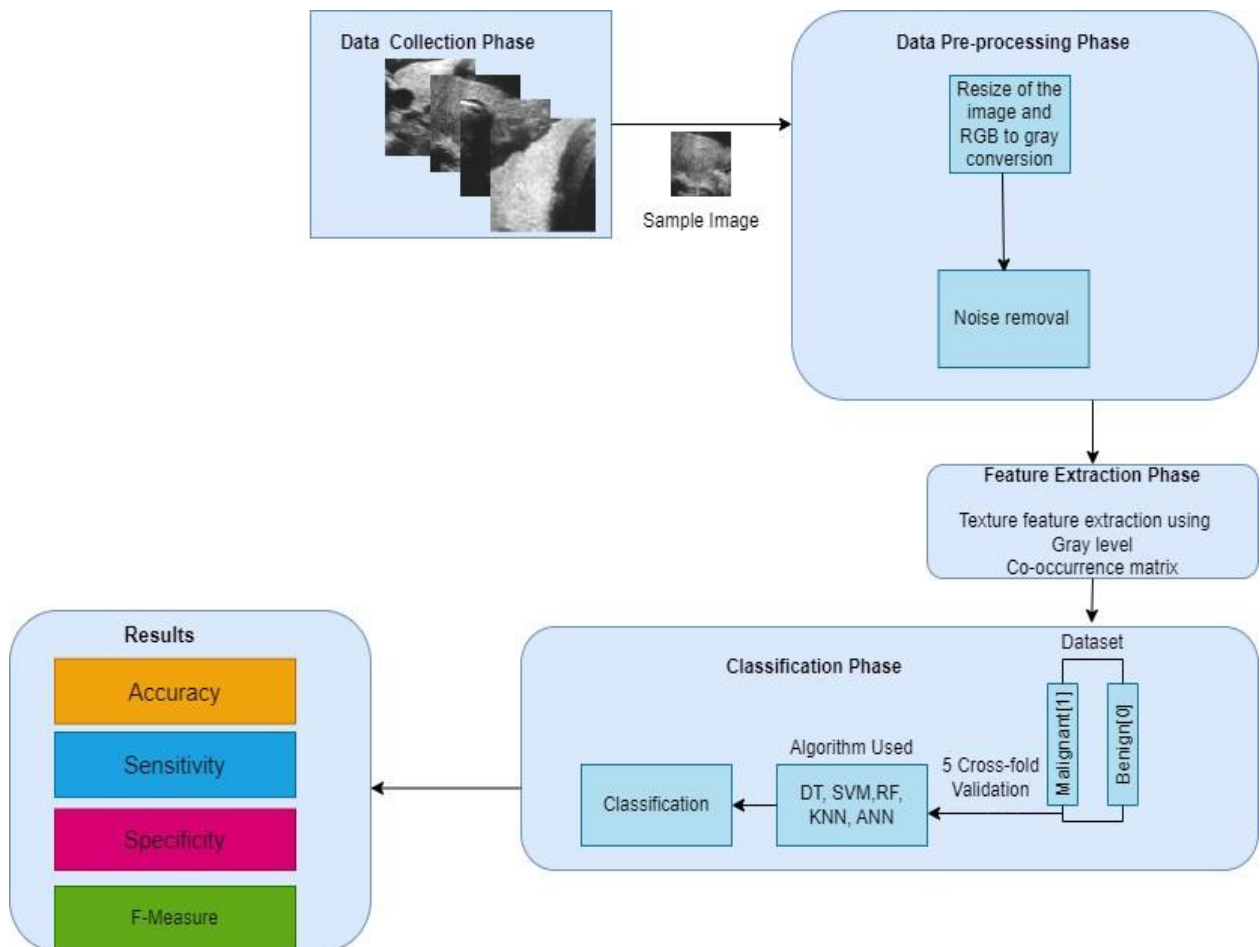
Figure 3.1: Framework of ANN-SVM hybrid model

3.1.1 Data Collection

Two datasets are considered namely public TDID and collected dataset. The public dataset has 188 malignant and 107 benign images i.e., a total of 295 USG images whereas collected dataset has 226 malignant and 428 benign i.e., a total of 654 USG images. The complete detail of dataset has given in under subsection 1.1.1.

3.1.2 Pre-processing

It is an important phase for the development of any model. In this phase, image resizing, noise removal using median filter and RGB to gray scale conversion are performed to maintain the uniformity of the dataset. All these steps are computed using equation 3.5-3.7:

$$resize = tf.keras.Sequential([layers.Resizing(IMG\_SIZE, IMG\_SIZE)]) \qquad (3.5)$$

where IMG_SIZE: size of the image

$$tf.image.grayscale\_to\_rgb(images, name = None) \qquad (3.6)$$

where images: the RGB tensor to convert the images, name: name of the operation

$$y[m, n] = median\{x|i, j|, (i, j)\epsilon\ v\} \qquad (3.7)$$

where w is a neighborhood, [m, n] pixel is location in the image

The main reason for using median filter is that it removes the noise and also preserves the edges of the images for the accurate prediction [84]. Benign images are labelled as "0" and malignant images as "1".

3.1.3 Feature extraction

GLCM texture analysis is used in this work to find underlying characteristics of textures and represent them in unique manner to have accurate classification of an image [85]. It works by calculating how often the pairs of pixels with a specific value and in a specified spatial relationship occur in input image [86]. Let there be a square matrix of size "N x N", where N is considered as the number of levels specified and f (a, b) is the pixel value at the point (a, b) of an image size N x N. A total of 4 features are extracted using GLCM technique. The description is given as:

3.1.3.1 Contrast: It measures the local variance in GLCM and can be computed by using equation 3.8:

$$Contrast = \sum_{k=0}^{N-1} k^2 \sum_{a,b=0}^{N-1} \left(f(a,b)\right) \qquad (3.8)$$

where k: is range [0 to (size (GLCM)-1))2]

3.1.3.2 Correlation: It computes the combined probability rate of the particular pixel pairs and can be computed by using equation 3.9:

$$Correlation = \sum_{a,b=1}^{N-1} (a-\mu)^2 f(a,b) \qquad (3.9)$$

where μ is mean

3.1.3.3 Homogeneity: It measures the closeness of the distribution of the elements in the GLCM to the GLCM diagonal using equation 3.10:

$$Homogeneity = \sum_{a,b=0}^{N-1} \{f(a,b)\}^2 \qquad (3.10)$$

3.1.3.4 Energy: It computes the total number of squared elements in the GLCM and can be computed by equation 3.11:

$$Energy = \sum_{a,b=0}^{N-1} f(a,b)^2 \qquad (3.11)$$

3.1.4 Classification

Four different types of ML classifiers are considered namely ANN, SVM, DT, KNN and RF. These are discussed below:

3.1.4.1 SVM

It is one of the frequently used supervised ML classifiers, widely used in image processing and pattern recognition [87]. In SVM, an optimal hyperplane decides the separation between individual classes of patterns. It must be maximum so that the problem of underfitting and overfitting can be reduced [88-89]. Figure 3.2 shows the optimal hyperplane of SVM,

C1(diamonds) and C2(circles). Here, SVM tries to fit a linear boundary known as a hyperplane between two different classes and tries to maximize the distance between the boundary and its nearest point of each class.
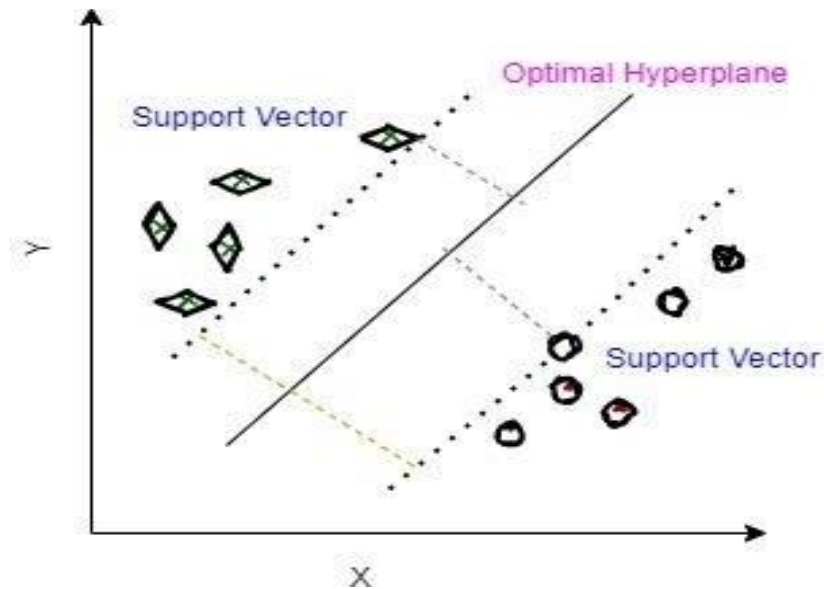
Figure 3.2: Optimal hyperplane in SVM [89]

3.1.4.2 KNN

It is one of supervised classifier that can be used for classification and regression. In both the conditions, the training part consists of k closest training examples while testing part computes the distance between the samples and then gives output based on classification or regression [90].

3.1.4.3 DT

Its structure is like a tree where the top most nodes is called as "root node", leaf node as the "class label", branches as result on the test, decision node represent the test of an attribute. One of the advantages of using DT classifier is its ability to give good classification result but it may lead to the problem of overfitting [91].

3.1.4.4 ANN

It is inspired by the "nervous system" where nodes act as an artificial neuron and the directed edges between neurons are defined by weights [92]. Figure 3.3 shows structure of ANN. In this work, we have used three layered ANN.
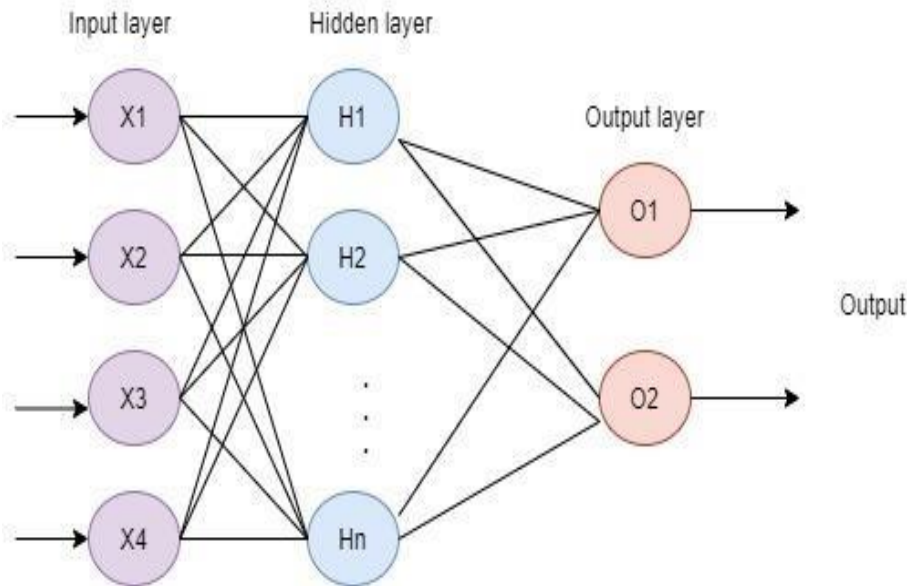
Figure 3.3: Architecture of ANN [92]

3.1.4.5 RF

It is a kind of ensemble learning technique involving a large number of individual DT. It works by first selecting the random samples from a given dataset and then constructs DT for each sample. Thereafter, it performs prediction based on maximum voting. RF does not suffer from the problem of overfitting and is used for both regression problems and classification [93].

3.1.4.6 Hybridization

An ANN- based 3-layer Feed Forward Neural Network (FFNN) is used along with hybridization of SVM classifier for the classification of TNDs. A simple ANN having one hidden layer with 4 neurons in the input layer was created. The neurons present in MLP network are trained consequently on backpropagation algorithm until an output value is obtained at each of the output neurons. ANN was trained with the extracted features and the output of the hidden layer was used to train the SVM classifier. Figure 3.4 shows the ANN-SVM hybrid model.
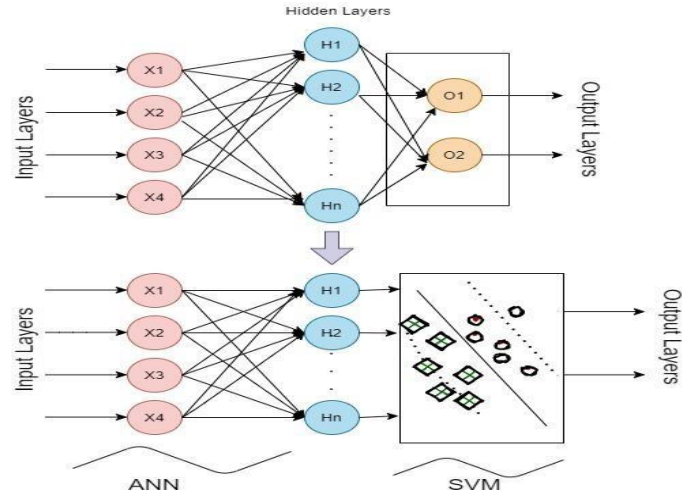
Figure 3.4 : The ANN-SVM hyrbid model

3.1.5 Result Analysis

This section summarizes the results of the ANN-SVM hybrid model for classification of TNDs. The work is done on MATLAB 2016b software using intel core i5 8th generation computer. The k-fold cross validation technique is used to validate the results of the ANN-SVM model. In this work, 5 cross validation is considered i.e., D= [c1, c2,……c5], where 4-fold is used for training and 1-fold is used for testing. Once, the pre-processing phase is over and features are extracted using GLCM method, various ML algorithms like RF, SVM, KNN, DT and ANN are employed for the classification. For better representation, public dataset is named as: Dset-1 and collected dataset is named as: Dset-2. Figure 3.5 shows the parameter setting for ANN-SVM hybrid model. The various parameters considered are batch size, optimizer, etc. Table 3.1 shows the standalone ML classifiers comparison on Dset-1. The ANN classifier has achieved an accuracy of 79.28%, specificity of82%, F-measure of 80.9% and sensitivity of 77.16% and SVM has achieved an accuracy of 78.4%, specificity of 80.4%, sensitivity of 76.3% and F-measure of 79%. Table 3.2 shows the performance of the standalone ML classifiers on Dset-2. The ANN classifier has achieved an accuracy of 84.96%, specificity of 85.88%, F-measure of 85.4% and sensitivity of 81.56% andSVM has achieved an accuracy of 82.65%, specificity of 83.50%, sensitivity of 80.12% and F-measure of 84%. From the table 3.2 and table 3.3, it can be seen that ANN performs better in comparison with the rest of the other classifiers i.e., DT, KNN, RF followed by SVM classifier. Table 3.3 show classification results of the best two classifiers and the proposed hybrid modelon Dset-1 and Dset-2. It can be analyzed from the table that when ANN and SVM classifiers are hybrid together then the performance of the model is increased.

Thus, it can be said that theproposed ANN-SVM performs better in comparison with the standalone ANN and SVM classifier. Table 3.4 shows comparison of the ANN-SVM hybrid model with existing models.An improvement of 2% to 4% is reported with ANN-SVM hybrid model in comparison with reported literature. The ANN-SVM hybrid model has achieved an accuracy of 84.12%,specificity of 82.95%, F-measure of 85.23% and sensitivity of 85.14% on Dset-1 and an accuracy of 90%, specificity of 87.5%, F-measure of 91.67% and sensitivity of 91.66% on Dset-2.

Figure 3.5: Parameter setting of ANN-SVM hybrid model [83]

Parameters	Value
Optimizer	adam
No. of epochs	80
Batch size	20
No. of neurons	4
Activation	Sigmoid
Loss function	MAE
Random state	50
Stop criteria	End of Epoch
Kernel	rbf
Tol	0.5
Degree	0
Gamma	scale
C	1.2

Table 3.1: Performance comparison of ML classifiers on Dset-1

Models	Accuracy (%)	Sensitivity (%)	F-measure (%)	Specificity (%)
DT	74.5	73.26	75	79
SVM	**78.4**	**76.3**	**79**	**80.4**
KNN	71.4	68.69	72	74.59
RF	74.5	72.60	76	77.99
ANN	**79.28**	**77.16**	**80.9**	**82**

Table 3.2: Performance comparison of ML classifiers on Dset-2

Models	Accuracy (%)	Sensitivity (%)	F-measure (%)	Specificity (%)
DT	75.90	73.55	77.1	80.68
SVM	**82.65**	**80.12**	**84**	**83.50**
KNN	70.1	68.11	71.6	75.55
RF	80.60	77.79	81.11	81.41
ANN	**84.96**	**81.56**	**85.4**	**85.88**

Table 3.3: Classification results of the best two classifiers and the proposed ANN-SVM hybrid model on Dset-1 and Dset-2

Datasets	Classifiers/ Models	Accuracy (%)	Specificity (%)	F-measure (%)	Sensitivity (%)
Dset-1	ANN	79.28	77.16	80.9	82
	SVM	78.4	76.3	79	80.4
	ANN+SVM (Hybrid model)	**84.12**	**82.95**	**85.23**	**85.14**
Dset-2	ANN	84.96	81.56	85.4	85.88
	SVM	82.65	80.12	84	83.50
	ANN+SVM (Hybrid model)	**90**	**87.5**	**91.67**	**91.66**

Table 3.4: Comparison of the ANN-SVM hybrid model with existing models

Model	Feature Extraction Technique	Classifier	Accuracy (%)	Specificity (%)	Sensitivity (%)	F-measure (%)
(Zhu et. al (2013))	Sonographic features	ANN	83.10	81.80	83.80	-
(Song et. al (2015))	GLCM	SVM, ANN, RF, LR, logistic	84	78.5	78.9	78.4
(Jiang et. al (2017))	Sonographic features	SVM, KNN, LR, DT, RF	84	-	-	-
(Dandan et. al (2018))	WMCM	SVM	87	-	-	-
(Zhang et. al (2019))	Sonographic features	RF, logistic regression, SVM, Neural net, adaptive boosting, naïve bayes, CNN	84.6	84.2	88.1	-
(Colakoglu et. al (2019))	Texture features	RF	86.8	87.95	85.2	-
(Ma et. al (2020))	Sonographic features	KNN, LR, SVM	87	-	-	-
Proposed model	**GLCM**	**Hybrid of ANN-SVM**	**Dset-1: 84.12; Dset-2: 90**	**Dset-1: 82.95; Dset-2: 87.5**	**Dset-1: 85.14; Dset-2: 91.66**	**Dset-1: 85.23; Dset-2: 91.67**

3.2 Summary

This chapter presents a hybrid model using hybridization of two ML classifiers for identification and classification of TNDs. The proposed ANN-SVM model is compared with standalone classifiers as well with hybrid model. From the experiments, it can be inferred that the performance of the proposed model is competitive when the two ML classifiers are hybrid together.

CHAPTER 4

CNN-SVM HYBRID MODEL FOR THE IDENTIFICATION AND CLASSIFICATION OF THYROID NODULE

CNN and its variants are one of the most famous and commonly employed algorithms in the field of medical imaging [94]. Some of the popular reasons include automatic identification of relevant features from the images without any human supervision. Its structure is inspired from neurons processing in human brains [95]. This chapter gives an elaborative explanation on the hybridization of CNN with SVM for the identification and classification of TNDs. The efficiency of the CNN-SVM hybrid model is tested on collected and TDID datasets.

4.1 Proposed Methodology

The working of CNN-SVM model for the identification and classification of TNDs is discussed in this section. The model works in four stages namely: (1) data collection, (2) pre-processing, (3) classification and (4) result analysis. Figure 4.1 shows the systematic flow of the CNN-SVM model.
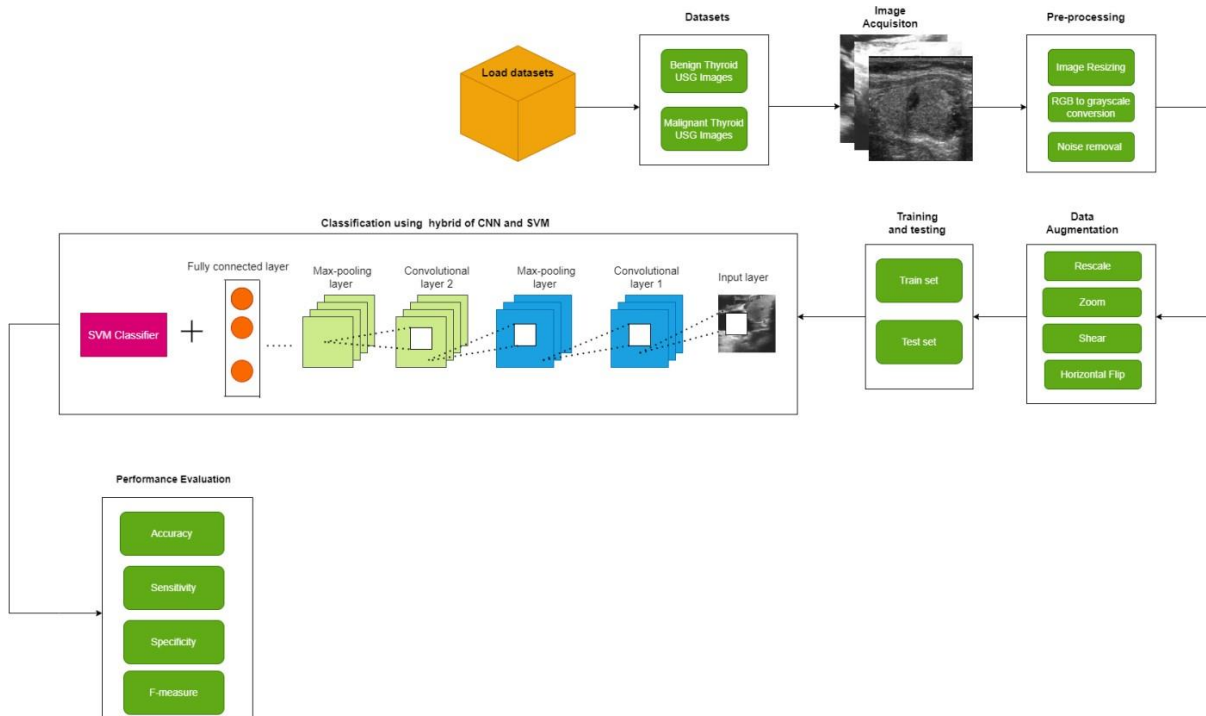
Figure 4.1: Systematic flow of CNN-SVM hybrid model

4.1.1 Data Collection Phase

In this work, public TDID dataset and collected dataset are considered. The public dataset has 188 malignant and 107 benign images i.e., a total of 295 thyroid USG images whereas collected dataset has 226 malignant and 428 benign i.e., a total of 654 thyroid USG images. Figure 4.2 shows the sample of benign and collected dataset.

Sample benign thyroid nodules

Sample malignant thyroid nodules
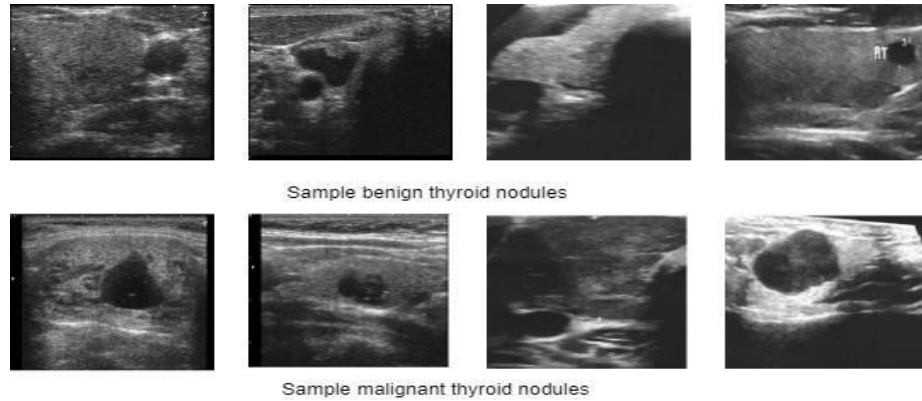
Figure 4.2: Sample of benign and malignant TNDs

4.1.2 Pre-processing

It is defined as a way of converting raw data into a desired form [96-97]. This derived information will be fed into the training model for the successful diagnosis [98]. The various steps involve in pre-processing are image resizing, noise removal using gaussian blur function, RGB to grayscale conversion and data augmentation respectively. Initially the size of image was 560 X 360 pixels, for the uniformity it's being resized to 256 X 256 pixels. In this work, four types of data augmentation techniques are used namely like rescale, zoom, shear and horizontal flip respectively. All these steps are computed using equation [4.12-4.15]:

$$resize = tf.keras.Sequential([layers.Resizing(IMG\_SIZE, IMG\_SIZE)]) \quad (4.12)$$

where IMG_SIZE: size of the image

$$tf.image.grayscale\_to\_rgb(images, name = None) \quad (4.13)$$

where images: the RGB tensor to convert the images, name: name of the operation

$$gaussian = np.random.normal(mean, sigma, image.shape) \quad (4.14)$$

where sigma: standard deviation

$$train\_datagen = ImageDataGenerator(Name, Value) \qquad (4.15)$$

where Value: values assigned to techniques, Name: name of the techniques

4.1.3 Classification using Hybridization of CNN and SVM Classifiers

4.1.3.1 CNN

The CNN architecture consists of four parts namely: (1): input layer, (2): convolutional layer, (3): max-pooling layer, (4): fully connected layer and (5): output layer [99]. Figure 4.3 shows the workflow of CNN.
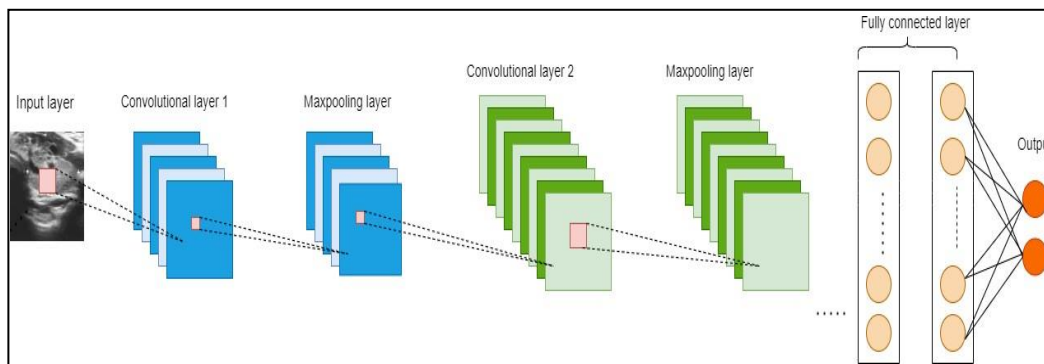
Figure 4.3: Workflow of convolutional neural network [100]

1. Input Layer

It specifies a complete description of an image (Nh x Nw x Nc) were h: height, w: width and c: channel size of an image [101].

2. Convolutional Layer

In this layer, 2-D kernels are learned during the initial phase. The coefficients(coeff.) of all these kernels encodes the important information from the input image [102]. There are some hyper-parameters like number of kernels, padding, size of kernels and stride to improve the performance [103]. Convolution works by finding the sum of the dot(.) products between the input image and the kernel [104]. The output of the convolution becomes the input of the next layer. It works as the spatial filtering [105]. Here, the size of kernel (k) is defined by equation 16:

$$W \ x \ H \qquad (4.16)$$

where W: width and W=2a+1, a and b: positive integer, H: height of the image pixel and H=2b+1

37

During the entire convolutional operation, the size of the image and the kernel are same. Padding is one of the techniques of the convolution process to introduce zeros (0s) around the border of the image to maintain the aspect ratio of the resultant image after convolution [106]. This can be computed using equation 4.17:

$$[N, N, Z] * [W, W, N_C] = ([\frac{N+2\rho-w}{s} + 1], [\frac{N+2\rho-w}{s} + 1], N_f) \tag{4.17}$$

where [N, N, Z]: Size of an image, [W, W, N_C]: Size of a kernel, p: no. of padding, s: stride length, N: filter depth, Z: image depth, Nf: filters of the kernel

Figure 4.4(a-e) explains the illustration of a convolutional operation with 3X3 kernel size. In this case, the input to the image is 5X5 matrix with stride 1. After the 9th convolution operation, 3X3 feature map is obtained. This shows the size of the input image is reduced extracting some useful global and local features.

(a) Image and kernel data

(b)First convolutional operation and its result (c) Second convolutional operation and its result

(d) Third convolutional operation and its result (e)Last convolutional operation and its result
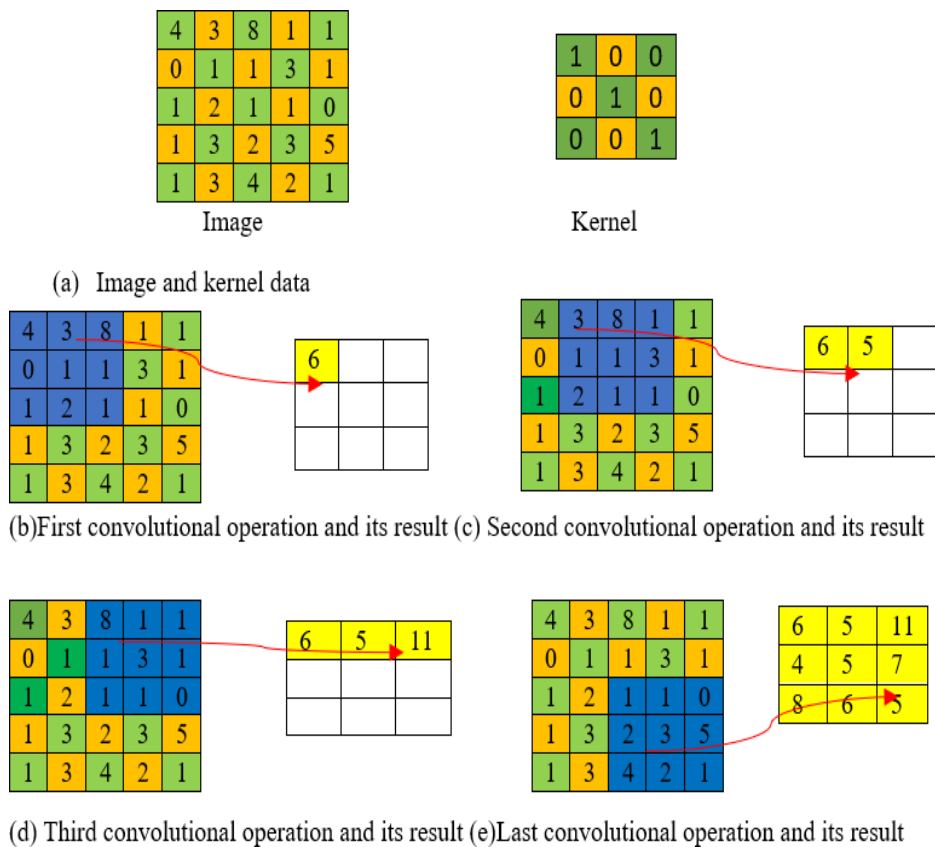
Figure 4.4(a-e): The illustration of a convolutional operation with 3X3 kernel size [106]

3. Max-pooling Layer

The output of the convolutional layer becomes the input of the max-pooling layer [107]. It

extracts the most essential features from each feature map, thereby giving the best feature output. The major benefits of using this layer are as follows: (1) it prevents overfitting, (2) feature invariance and (3) dimensionality reduction of the features [108]. It can be computed using equation 4.18 and 4.19:

$$y_i = \max Rx\ R\{y_i^{rxr}\}f(r,r) \tag{4.18}$$

$$f(r,r) = \varepsilon.\ y_i^{k-1}\ x\ v_{i,j}^k + e_j^k \tag{419}$$

where max RxR: max-pooling in RxR, y_i^{rxr}: i-th output of rxr window, ϵ: trainable variant

Figure 4.5(a-b) explains the illustration of max-pooling operation. The complete operation works from left(L) to right(R), the first picture is the input, next is the max-pooling and so on.
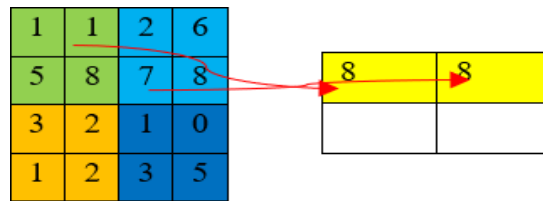
(a) First and second max-pooling function
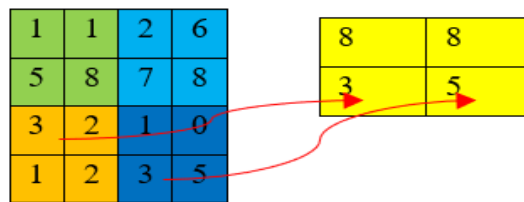
(b) Third and fourth max-pooling function

Figure 4.5(a-b): Illustration of max-pooling operation [107]

4. Fully Connected Layer

This layer combines all the features extracted from the input images learned by the previous layers to classify the images [109]. Here flattening function is performed to convert a 2D matrix to the 1D array which helps in reducing dimension and computation complexity [110]. In this, each node of neuron has some weight and bias associated with it to help the input image to gain information [111]. Figure 4.6 shows the flattening operation performed in fully connected layer.
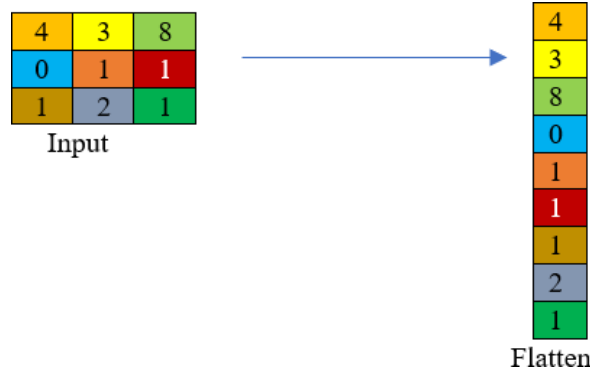
Figure 4.6: The flattening operation performed in fully connected layer [109]

5. Output Layer

In this layer we have the classified result which is mostly followed by softmax function (i.e., the normalized exponential function) which gives the output mapped into the range of [0,1] [112]. It can be computed using equation 4.20:

$$\sigma(z_i) = \frac{e^{z_i}}{\Sigma_{i=1}^{n} e^{z_i}} \tag{4.20}$$

where n: maximum no. of classes, z_i : input

4.1.3.2 SVM

It is a class of ML algorithms works by finding (n-1) dimensional hyper-plane. It finds a plane by maximizing the dist. between the data points available or given in the classes with the help of support vectors [113]. SVM employs the use of kernels like sigmoid, radial basis function (rbf), linear, polynomial and non-linear which takes the data as the input and gives output accordingly [114-115].

Let there be a sample dataset input: $\{(x_1, y_1), (x_2, y_2), \ldots \ldots (x_n, y_n)\}, x_i \in R^d$, target output: $i = 1, 2, \ldots \ldots N, y \in \{\mp 1\}$[116]. The optimal classification hyperplane is defined as given in equation 4.21:

$$v^T x_i + b = 0 \tag{4.21}$$

where b: bias, v: weight vector

Then b and v can be determined using equation 4.22:

$$y_i(w^T x_i + b) \geq 1 - x\xi_i \tag{422}$$

where ξ_i is the slack variable(var.).

According to Lagrange multiplier method, the solution to optimal classification hyperplane is converted into optimization using equation 4.23:

$$Q(a) = \sum_{i=1}^{N} a_i - \frac{1}{2} \sum_{i=1}^{N} \sum_{j=1}^{N} a_i a_j y_i y_j K(x_i, x_j) \tag{4.23}$$

where $\{a_i\}_{i=1}^{N}$ is lagrange multiplier, $K(x_i,x_j)$ is kernel function

4.1.3.3 Hybridization of CNN-SVM Model

This model works by removing the last output layer of CNN with SVM model. It can be said that the output of the last layer will become the input to SVM for better classification of TNDs. The CNN model applies different convolutional (conv.) and subsampling technique in convolutional layer [117]. These functions speed up the extraction of important data from the input given to the model. At the end, SVM trains the feature vectors obtained from fully connected layer and take decision in an effective manner. Figure 4.7 shows the CNN-SVM model.
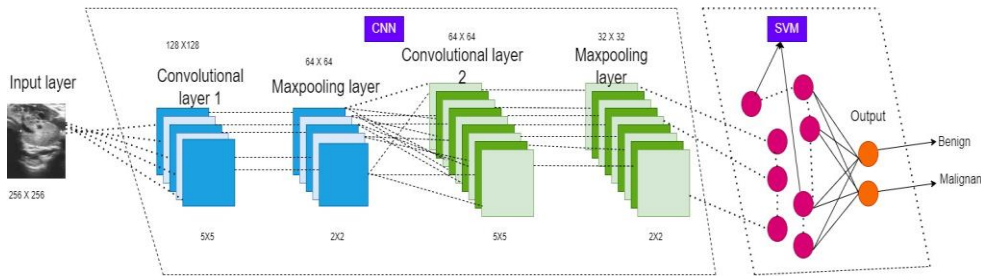
Figure 4.7: Proposed CNN-SVM hybrid model

4.1 Algorithm: Proposed CNN-SVM hybrid model

Algorithm 4.1: Proposed algorithm for CNN-SVM hybrid model
Input: Imd→ Image, AugImd →Augmented Images **Output:** Type of TNDs **BEGIN** 1. *Upload the image dataset on the google drive account* 2. *for i→row(Imd)*   *for j→column(Imd)* 3. *B= tf.keras.Sequential ([Resize(IMG_SIZE,IMG_SIZE)])* 4. *B= tf.image.rgb_to_grayscale(images,name=None)* 5. ***denoise*** *← Gaussian_blur* 6. ***Data Augmentation*** *←imageDataGenerator (Name, Value)* 7. Initialize the parameters of CNN

            - dropoutfactor
            - maxepoch
            - batchsize
            - learning rate
            - activation function
            - optimizer

8.   *Remove the last layer of CNN*
9.   *Add SVM classifier*
10.   *Set training and testing ratio*
            Train model← *Train (Net, Training data)*
            Classification result← *Train (Net, Training data, test data)*
11.   **if** *(Classification result = true)*
            Classify type of TNDs
END
END

4.1.4 Result Analysis

The proposed model is performed on Google Collaboratory, intel core i5 8th Generation, 16GB RAM, 1TB SSD, 8 GB NVIDIA GPU. The libraries used in this work are matplotlib, keras, sklearn, sys, imageio, PIL and tensorflow. For better representation, public TDID and collected datasets are re-named as Dset-1 and Dset-2. Further for comparing the proposed CNN-SVM model, those research (Rs.) papers are considered that have used the public TDID dataset. Data augmentation technique is used to increase the sample size of the datasets after applying the various pre-processing steps. The initial public and collected sample size were 295 and 654 USG images. After data augmentation, initial and collected sample size are 1180 and 2616 USG images. For both the datasets, 8:2 ratios are set for CNN-SVM model training and testing. Table 4.1 shows the various parameters set for the CNN-SVM hybrid model on Dset-1 & Dset-2. Table 4.2 shows the comparison of the CNN-SVM hybrid model on Dset-1 and Dset-2 with the existing models used for classifying TNDs. It can be analyzed that the CNN-SVM hybrid model has performed well on both the datasets. The model has achieved an accuracy of 94.57%,F-measure of 95.64%, sensitivity of 96.70% and specificity of 91.89% on Dset-1 and an accuracy of 96%, F-measure of 98.33%, sensitivity of 97.80% and specificity of 93.93% on Dset-2. Figure 4.8 shows the performance comparison of the accuracy parameter with existingmodels and proposed model on Dset-1 and 2. It can be analyzed from the figure that there is an improvement of 3% to 5% in the performance of the proposed model. Figure 4.9 shows performance comparison of specificity, F-measure and sensitivity parameters with existing and proposed model on Dset-1 and Dest-2. The proposed model has achieved sensitivity of 96.70%,

F-measure as 95.64% and specificity of 91.89% on Dset-1 and specificity of 93.93%, F-measure of 98.33% and sensitivity of 97.80% on Dset-2. An improvement of 2% to 3% is reported by proposed model in figure 4.9. Figure 4.10 shows the epoch-accuracy graph for Dset-1. Figure 4.11 shows the epoch-accuracy graph for Dset-2.

Table 4.1: Parameters set for training CNN-SVM hybrid model for Dset-1 and Dset-2

Parameter	Batch Size	Kernel Size	Activation	Stride	Pooling layer	Activation	Optimizer	Epoch	Regularizer l2
Values	32	3	Relu	2	Max-pooling layer	Linear	Adam	100	0.01

Table 4.2: The comparison of the CNN-SVM model on Dset-1 and Dset-2 with existing models used for classifying TNDs

Models	Accuracy (%)	F-measure (%)	Sensitivity (%)	Specificity (%)
(Wang et al. (2018))	80.91	-	81.82	80
(Nguyen et al. (2019))	90.88	-	-	-
(Song et al. (2019))	92.1	-	94.1	96.2
(Ajilisa et al. (2020))	89.93	89.43	92.76	-
(Nguyen et al. (2021))	92.05	-	-	-
(Proposed CNN-SVM hybrid model on Dset-1)	**94.57**	**95.64**	**96.70**	**91.89**
(Proposed CNN-SVM hybrid model on Dset-2)	**96**	**98.33**	**97.80**	**93.93**
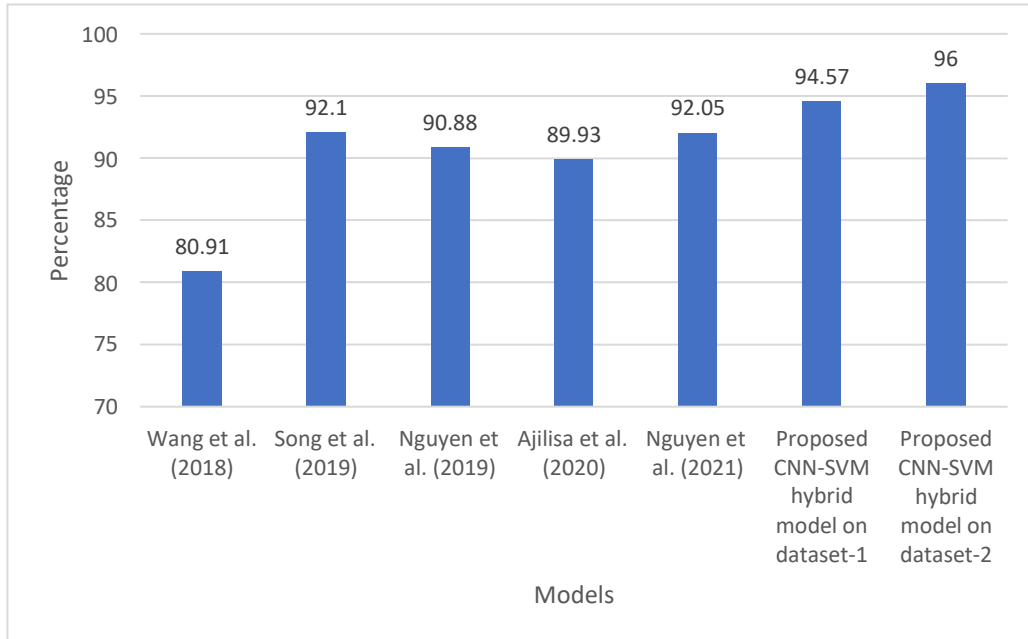
Figure 4.8: Performance comparison of the accuracy parameter with the existing and CNN-SVM model on Dset-1 and Dset- 2
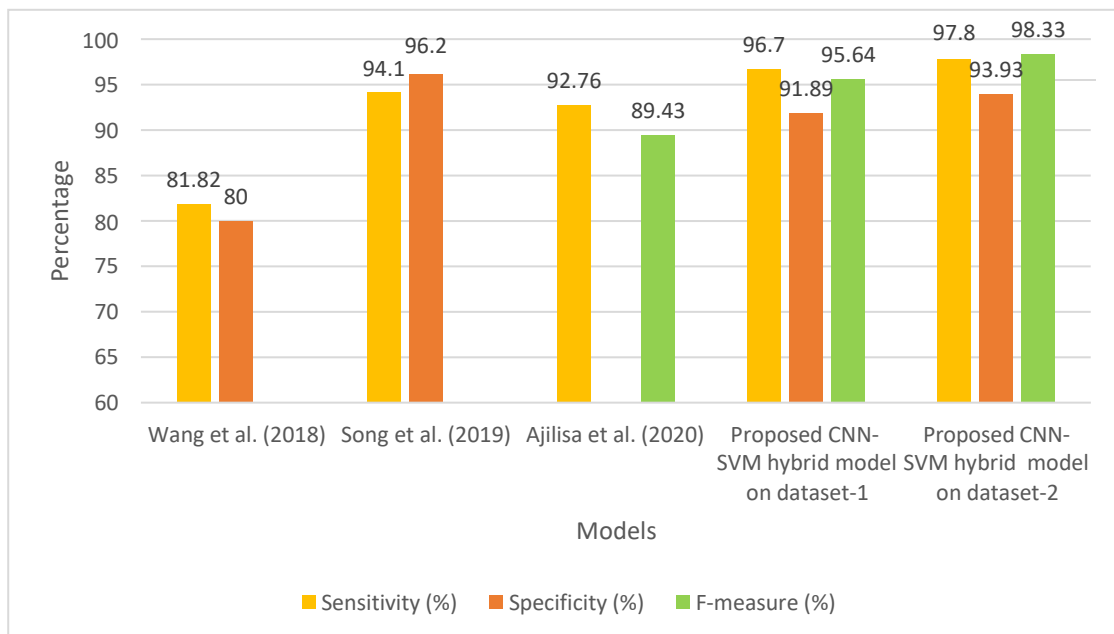
Figure 4.9: Performance comparison of specificity, f-measure and sensitivity parameters with existing and CNN-SVM model on Dset-1 and Dset-2
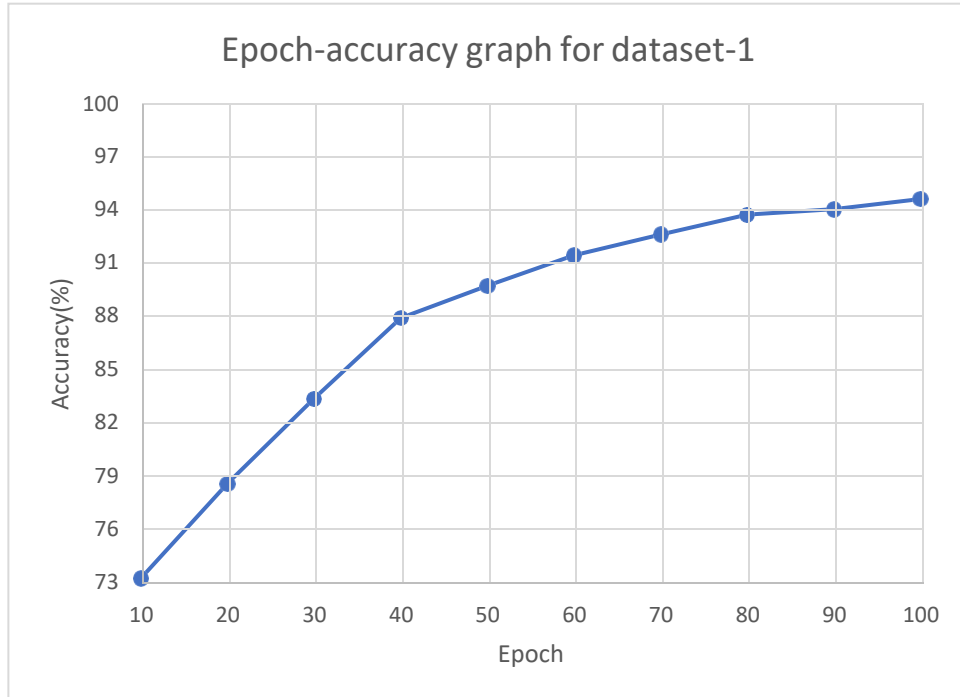
Figure 4.10: The epoch-accuracy graph for Dset-1
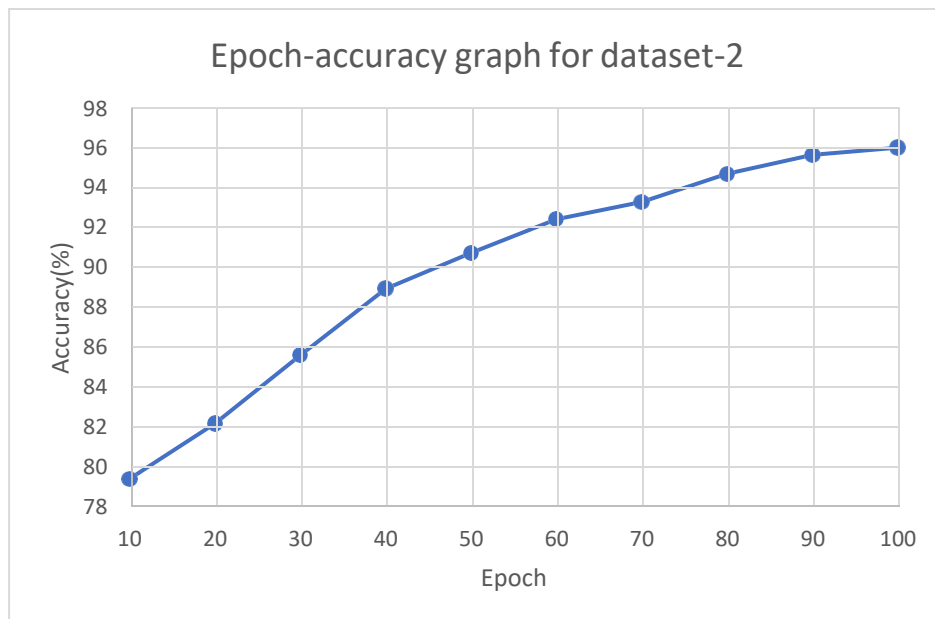
Figure 4.11: The epoch-accuracy graph for Dset-2

4.2 Summary

An effective CNN-SVM hybrid model is proposed for classification of BTND and MTND USG images in this chapter. The work has been evaluated on 1180 and 2616 public TDID and collected TNDs image datasets on *Google Colaboratory*. The proposed model is found to perform well even when the sample size of the dataset is less. It has shown an improvement of

3% to 5% on Dset-1 and 4% to 6% on Dset-2 in comparison with existing models reported in literature for the identification and classification of TNDs.

CHAPTER 5

AN OPTIMIZED CONVOLUTIONAL NEURAL NETWORK MODEL FOR THE IDENTIFICATION AND CLASSIFICATION OF THYROID NODULE

In DL, hyperparameter (hyp) optimization is problem of choosing a set of optimal parameters for a learning algorithm. It chooses the best parameter to control the learning process [118]. In this chapter, Grid Search Optimization (GSO) based CNN model is proposed for the identification and classification of TNDs. Several DL models like Alex-Net, Deep Neural Network (DNN), Res-Net-50 and Visual Geometry Group (VGG-16) are explored along with segmentation and boundary detection techniques. The proposed approach is tested on public TDID and collected datasets using GSO technique. The result shows that proposed GSO-CNN model outperforms from reported literature and improves the accuracy of the model.

5.1 Proposed Methodology

This section covers various phases involved for the working of the GSO-CNN model. The model works in five phases: (1) data collection, (2) pre-processing, (3) morphological, segmentation and boundary detection, (4) optimization and classification and (5) result analysis. Figure 5.1 shows the systematic flow of the proposed GSO-CNN model.
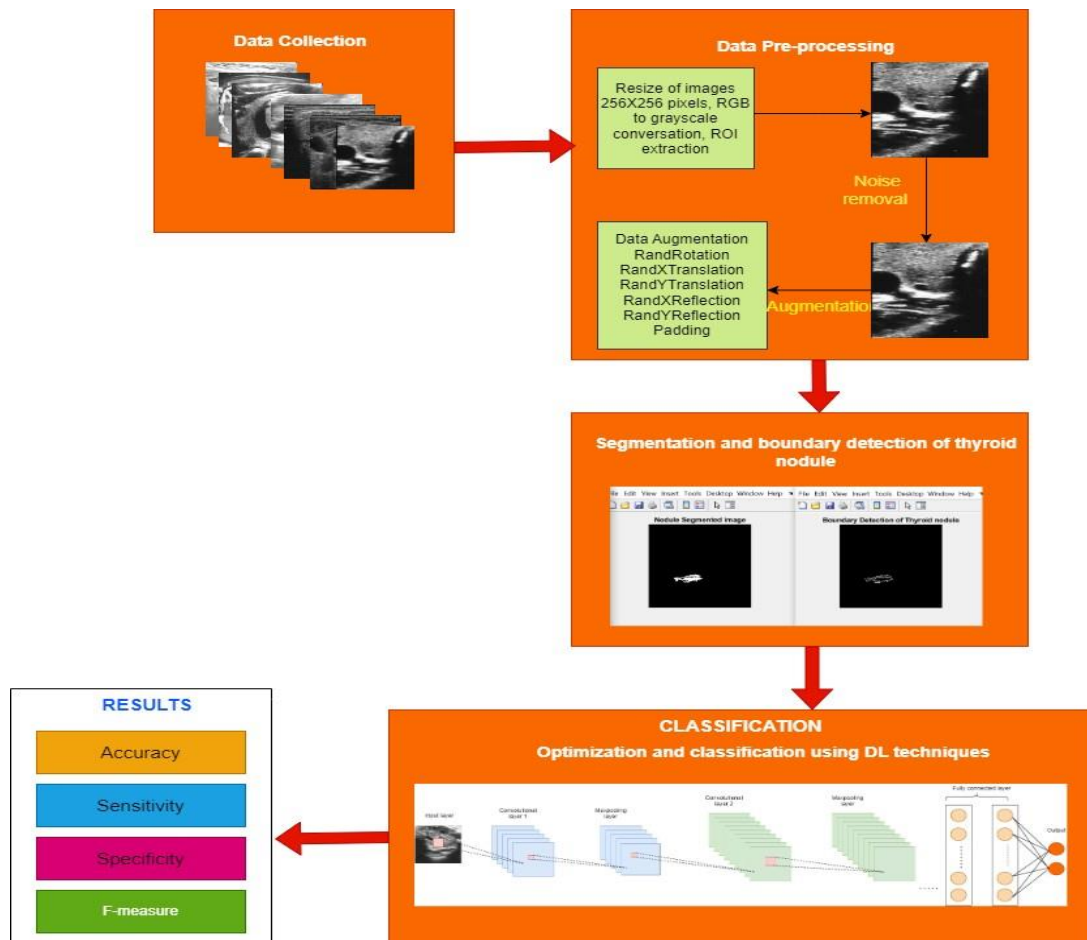
Figure 5.1: Systematic flow of the proposed GSO-CNN model

5.1.1 Data Collection

Public TDID and collected datasets are considered for the evaluation of the model as discussed in section **4.1.1**

5.1.2 Pre-processing

The various pre-processing steps involved in this work are image resizing, noise removal, RGB to grayscale conversion as discussed in section 3.2.2. The various data augmentation techniques involved in this work are RandRotation, RandXTranslation, RandYTranslation, RandXReflection, RandYReflection and Padding.

5.1.3 Morphological Operation, Segmentation and Boundary Detection

5.1.3.1 Morphological Operation

Morphological operation is applied on the image to extract out the exact region of TNDs with using basic operation [119]. Figure 5.2 shows the morphological operation.
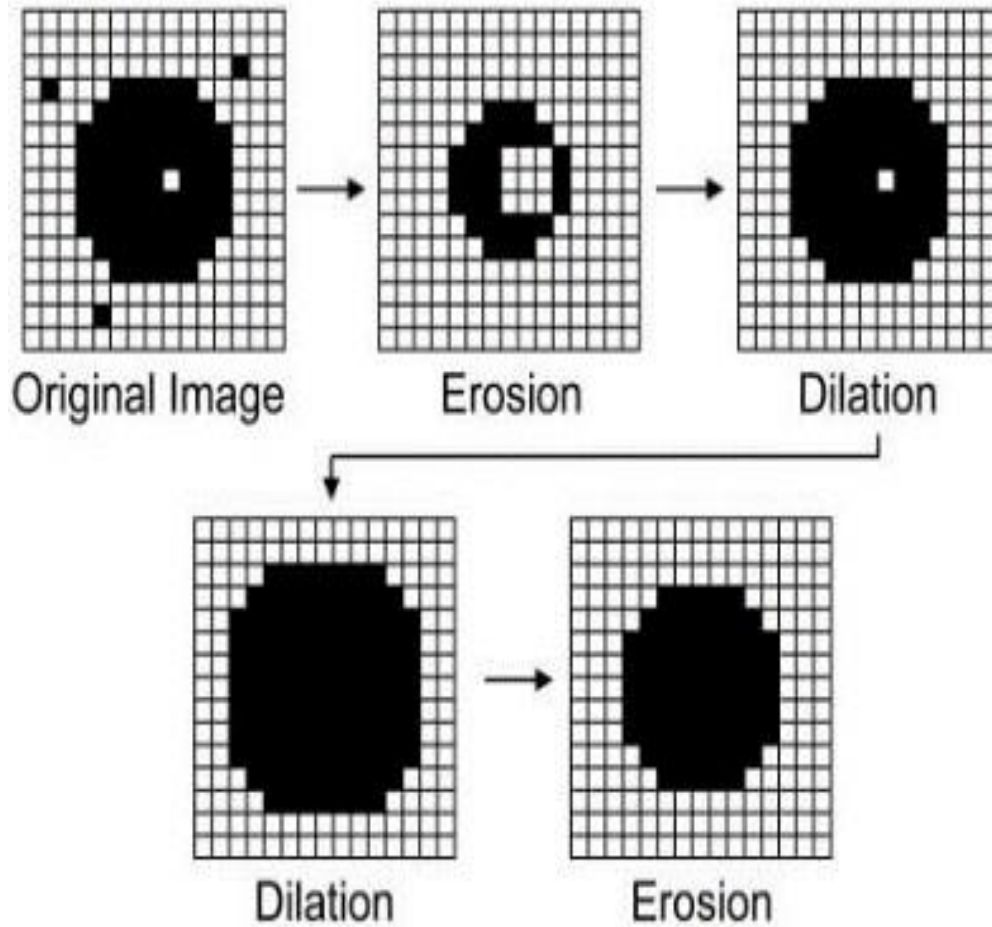
Figure 5.2: The morphological operation [120]

In this work, dilation and erosion operation are considered. The structure used in this work is "disk". The dilation and erosion are computed using equation 5.24 and 5.25:

$$I(dilate)S = \{I + S; for\ all\ pixels\ in\ I \in S\} \tag{5.24}$$

$$I(eroded)S = \{I(errored)S\}(eroded)S \tag{5.25}$$

The morphological gradient (G) function is computed using equation 5.26:

$$G = \{I(dilate)S - \{I(eroded)S\} \tag{5.26}$$

5.1.3.2 Segmentation

It is defined as the process of partitioning image into image segments formerly known as image objects [121]. It is mostly used to change the representation into more meaningful form for easy analysis [122]. Active Contour (AC) segmentation technique was first coined by "Kass" [123]. It is basically the curve in the image space whose deformation is based on energy minimization. Let x and y be the position of co-ordinates of an 2D image I(x,y), and curve be:

$$V(s) = (x(s), y(s)) \tag{5.27}$$

where $s \in [0,1]$

The energy function (E) is defined using equation 5.28 and 5.29:

$$E_{total} = \int_0^1 E(V(s))ds \tag{5.28}$$

$$E_{total} = \int_0^1 [E_{int} \quad (V(s)) + E_{exl} \quad (V(s))] \, ds \tag{5.29}$$

where E_{int}: internal & E_{ext}: external energy

To control the deformation and displacement, E_{int} and E_{ext} are converted into internal and external forces.

The E_{int} and E_{ext} energy component can be defined as:

$$E_{int}(V(s)) = [\frac{1}{2} \alpha(s)|V_s(s)|^2 + \frac{1}{2}\beta(s)|V_{ss}(s)|^2] \tag{5.30}$$

where α: weight factor, β(s): control factor

$$E_{int}(V(s)) = [\frac{1}{2} \alpha(s)|V_s(s)|^2 + \frac{1}{2}\beta(s)|V_{ss}(s)|^2] \tag{5.31}$$

where γ: weight factor, G_σ (x,y): 2D gaussian function, *:convolution operator, ∇: gradient operator, σ: standard deviation

At equation 5.32, the E_{int} and E_{ext} attain the minimum value. Hence goal is achieved.

$$F_{int} + F_{ext} = 0 \tag{5.32}$$

5.1.3.3 Boundary Detection

It works by finding the boundaries between the light and dark pixels in an input image [124]. It is computed using equation 5.33:

$$B(A) = A - (A \ominus B) \tag{5.33}$$

where A: Matrix of an image M x N, B(A): Boundary detection, $\ominus$: Erosion function, B: Structuring element

5.1.4 Optimization and Classification

Different variants of the CNN models are considered such as Res-Net-50, Alex-Net, VGG-16 and DNN for classification of TNDs. The working of CNN has been explained in section 4.1.3.1.

5.1.4.1 Res-Net-50

Res-Net-50 model is a residual deep learning network having 50 layers developed by He, Zhang [125]. Res-Net-50 attempts to address the problem of vanishing gradient problem that occur during back-propagation of CNN [126]. The network allows training of networks by constructing through modules called as residual model. Figure 5.3 shows the structure of Res-Net-50.
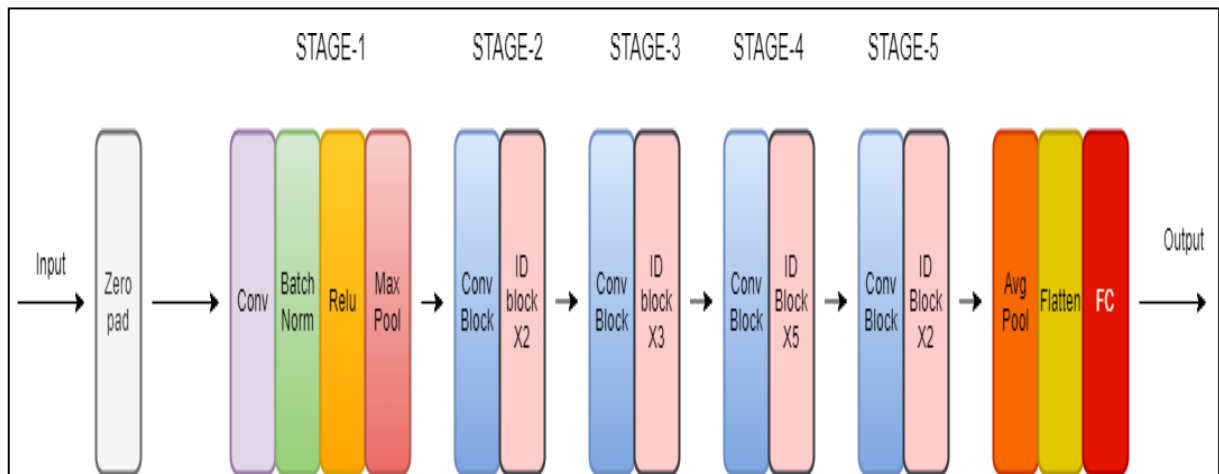
Figure 5.3: Structure of Res-Net-50[127]

5.1.4.2 Alex-Net

It was coined in 2012 and employed for generalized image classification for the first time [128]. In the Alex-Net, ReLU function is introduced to solve the problem of non-linearity and speed up of the network [129]. Alex-Net consists of five convolutional(conv.) layer, three fully connected layers and one output layer. There is a Local Response Normalization (LRN) layer that follows the first as well as the second convolutional layer [130]. Figure 5.4 shows the structure of Alex-Net.
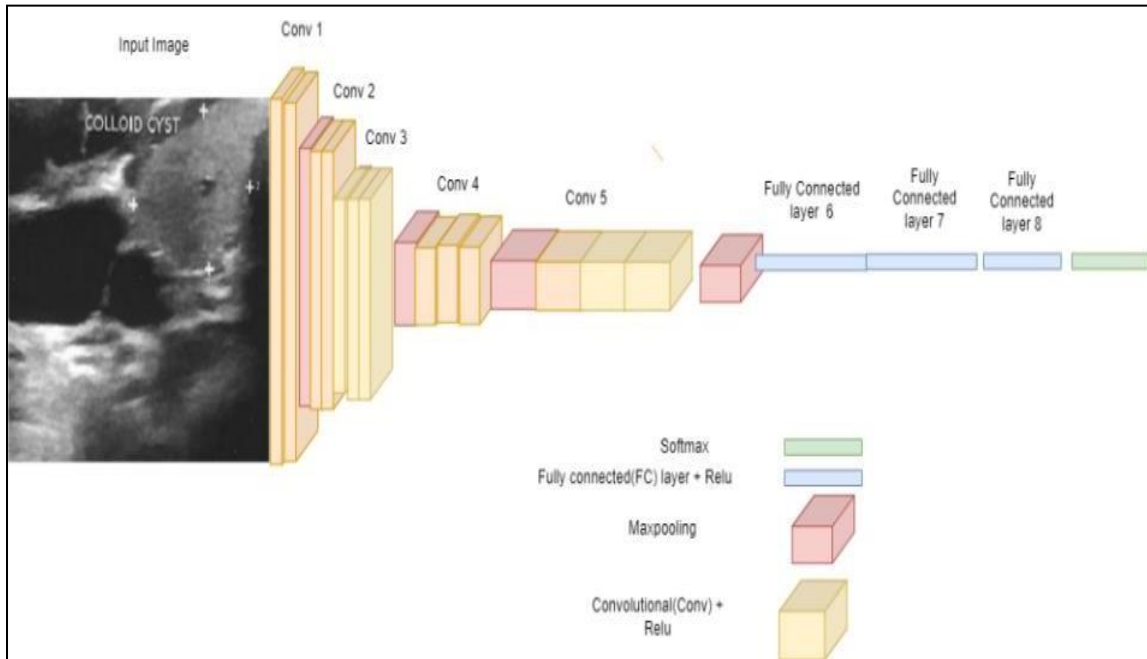
Figure 5.4: Structure of Alex-Net [131]

5.1.4.3 VGG-16

The idea was coined from the "University of Oxford" and trained on ImageNet dataset [132].
A traditional VGG-16 consists of multiple "3X3 kernel-sized filters" that help the model in
learning complex features by increasing depth of the network [133]. Figure 5.5 shows the
architecture of VGG-16.
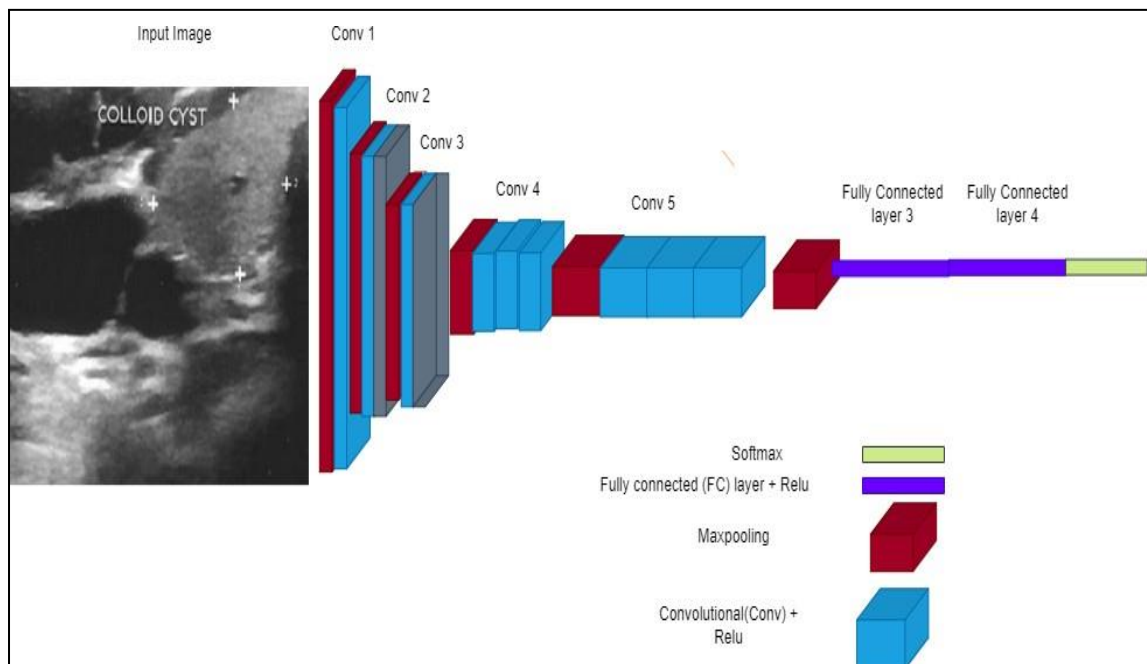
Figure 5.5: Structure of VGG-16 [134]

5.1.4.4 DNN

It is the improved versions of ANN with multiple layers [135]. The DNN is highly preferred over traditional ML algorithms like SVM, KNN and DT. These include extracting high level features thereby learning more complex patterns [136-137]. Due to the mentioned reasons, DNN is highly preferred image processing, computer vision, machine translation and Natural Language Processing (NLP) [138]. Figure 5.6 shows the structure of DNN.
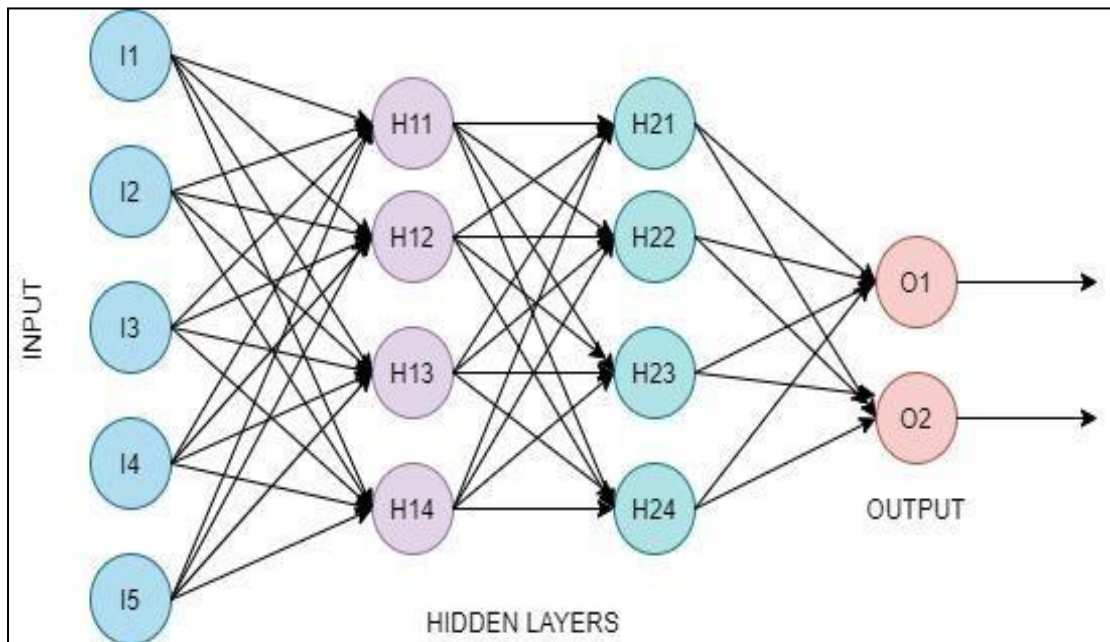
Figure 5.6: Structure of DNN [139]

5.1.4.5 Optimizing Using GSO Technique

Optimization of drop-out and learning rate factor using GSO technique is discussed in this section. Let the hyperparameters be $hyp_1,……..hyp_n$ of the DL model and $\alpha_1,…..\alpha_n$ be domains. The model is trained with hyp (DLtrain) on the training of TNDs images. The main aim behind hyp is to find the best parameter $hyp_1{}^*$, $hyp_2{}^*$. Figure 5.7 shows the proposed GSO-CNN model.
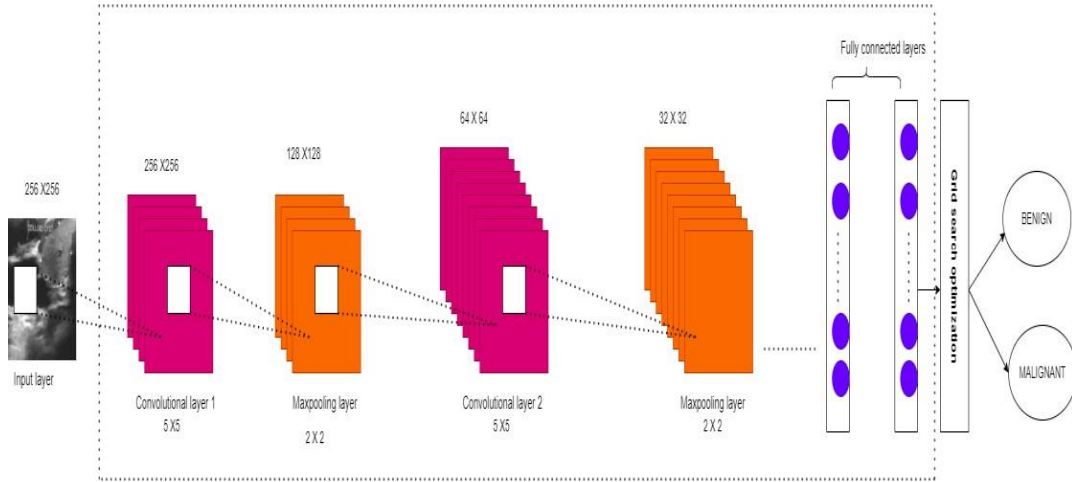
Figure 5.7: Proposed GSO-CNN model

5.1   Algorithm for optimization of CNN model using GSO technique

---
Algorithm 5.1: Optimization of CNN model using GSO technique

Input: hyp_1*
Output: hyp_1*, hyp_2*
      create deeplmodel ()
      ml.add(hyp_1*, values_of_drop-out _actor, optimization_algo)
      gridsearch= GriddSearchCV(par grid=par, grid,est=ml)
      result=gridsearchd.fit( )
      Print ("best_drop-out_factor, best_learnin_rate");
      Return hyp_1 *, hyp_2 *

5.2 Proposed GSO-CNN Algorithm for the identification and classification of TNDs

---
Algorithm: Classification using GSO-CNN model

Input: TNDs USG images
Output: Type of TNDs
BEGIN
1.   Upload sample images of TNDs.
2.   Use pre-processing step for the uniformity of the TNDs images.
3.   Use active contour segmentation technique.
4.   Apply B(A) to find boundary of the TNDs.
5.   Set the training and testing ratio of the model.
6.   Initialize the parameters of CNN
    -dropoutfactor
    - maxepoch
    - batchsize
    - learning rate
    - activation function
    - optimizer
7.   Use gd_technique to find the best hyp_1 * and hyp_2 *.

8.   Train the model
     Classify type of TNDs
END

5.1.5 Result Analysis

This section focuses on the various results obtained for the GSO-CNN model. In this work, datasets are renamed as follows: Dset-1: public TDID and Dset-2: collected dataset. Initially, the sample size of public and collected datasets were 295 and 654. After considering six different augmentation techniques (RandRotation, RandXTranslation, RandYTranslation, RandXReflection, RandYReflection and Padding), the new sample size of the datasets are 1770 and 3924 USG images. 8:2 ratio is set for GSO-CNN model for training and testing purpose. Table 5.1 shows the various parameters setting for GSO-CNN model for Dset -1 and Dset-2. Table 5.2 shows the comparison of the proposed GSO-CNN model with Alex-Net, Res-Net-50, VGG-16 and DNN based on with (CASE-1) and without segmentation and boundary detection techniques (CASE-2) on Dset -1 and Dset-2. From the table, it can be observed that the results obtained in CASE-2 are better than CASE-1. The proposed GSO-CNN, VGG-16, Alex-Net, and Res-Net-50 models have shown an improvement of 1% to 2% in CASE-2 with respect to performance parameters. Table 5.3 shows results of GSO obtained on dropout factor and learning rate parameters on proposed GSO-CNN, Alex-Net, Res-Net-50, VGG-16 and DNN models. The best results are obtained on 0.01 learning rate and 0.2 dropout factor. The best results obtained by the models on Dset -1 are 95.30%, 91.01%, 82.84%, 86.01%, 86.66% for GSO-CNN, DNN, Alex-Net, Res-Net-50 and VGG-16 models respectively. The models achieved 96.02%, 92.30%, 83.08%, 91.76% and 87.16% for GSO-CNN, DNN, Alex-Net, Res-Net-50 and VGG-16 models respectively on Dset-2. Table 5.4 shows the comparison of the GSO-CNN model and existing models on Dset -1 and Dset-2. From the table, it can be analyzed that the proposed GSO-CNN model has achieved better results in comparison with the existing models. The proposed GSO-CNN model achieved 95.30%, 96.66%, 97.20%, 94.87% on Dset -1 and 96.02%, 96.70%, 98.34%, 95% on Dset -2 on accuracy, sensitivity, F-measure and specificity parameters. Figure 5.8 shows the comparative analysis of the accuracy parameter with the models on Dset -1 and Dset-2. The results obtained on accuracy parameter of the GSO-CNN model have shown an increment of 3% to 4% on Dset -1 and Dest-2. The model has achieved an accuracy of 95.30% on Dset -1 and 96.02% on Dset -2. Figure 5.9 shows the comparative analysis of sensitivity, specificity and F-measure parameters with

existing models on Dset -1 and Dset-2. The model has achieved sensitivity of 96.66% and 96.70% on Dset -1 and Dset-2 & F-measure of 97.20% and 98.34% on Dset -1 and Dset-2. The GSO-CNN model has shown rise of 4 to 5% on sensitivity and 8% to 9% on F-measure parameters. However, the model has not achieved better results on specificity parameter. The model has achieved specificity of 94.87% on Dset -1 and 95% on Dset -2 which is lower than the results obtained by Song et al. (2019) with 96.2% and higher with Wang et al. (2018) model with 80%. Figure 5.10 and figure 5. 11 show the accuracy-epoch graph for Dset -1 and Dset-2 respectively.

Table 5.1: Parameter setting for GSO-CNN model for Dset -1 and Dset- 2

Parameters	Value
Batch size	15
Activation function	Softmax
Max-pooling	2X2
Drop-out factor	0.2
Max-epoch	10
Learning rate	0.01
Optimizer	SGDM

Table 5.2: Performance comparison of the GSO-CNN model with Alex-Net, Res-Net-50, VGG-16 and DNN on Dset -1 and Dset-2

Dset	Techniques	Models	Accuracy (%)	Specificity (%)	F-measure (%)	Sensitivity (%)
Dset -1	CASE 1 — Without segmentation and boundary detection techniques	**GSO-CNN model**	94.11	93.33	96.20	95.65
		DNN	90.90	89.85	89	92.63
		Alex-Net	82.98	80.98	83.96	83.96
		Res-Net-50	86.48	84.52	87.25	87.25
		VGG-16	85.71	83.90	86.40	86.40
Dset -2		**GSO-CNN model**	95.33	95	97.20	96.66
		DNN	91.81	90.78	92.14	92.63
		Alex-Net	82.28	81.92	82.60	83.51
		Res-Net-50	90.11	89.33	93.61	91.66
		VGG-16	86.63	84.88	87.25	87.25

Dset -1	**CASE 2**	**With segmentation and boundary detection techniques**	**GSO-CNN model**	95.30	94.87	97.20	96.66
			DNN	91.01	90.27	93.54	92.55
			Alex-Net	83.85	81.81	84.76	84.76
			Res-Net-50	87.91	86.58	88.55	89
			VGG-16	86.66	83.95	87.56	87.12
Dset -2			**GSO-CNN model**	96.02	95	98.34	97.02
			DNN	92.30	90.16	93.19	93.68
			Alex-Net	83.08	82.97	85.98	84.76
			Res-Net-50	91.76	90.66	92.14	92.63
			VGG-16	87.16	86.04	87.68	88.11

Table 5.3: Results of GSO technique obtained on dropout factor and learning rate parameters obtained on GSO-CNN model, Alex-Net, Res-Net-50, VGG-16 and DNN

Para-meters		**Learning rate**	**0.01**	0.04	0.07	0.09	0.1	0.05	0.08
		Dropout factor	**0.2**	0.02	0.06	0.09	0.1	0.04	0.08
Accuracy Dset-1 Models		**(GSO-CNN) Model**	**95.30**	80.90	85.16	89	76.06	82.32	87.19
		DNN	**91.01**	69	76.88	82.76	62.3	71.1	81.1
		Alex-Net	**82.84**	59.99	68.3	77.9	58	64	73.6
		Res-Net-50	**86.01**	62.7	64	78.41	54	69.6	74.29
		VGG-16	**86.66**	68.2	78.55	81.27	59	73.3	80.3
Accuracy Dset -2 Models		**(GSO-CNN) Model**	**96.02**	84.96	88.86	92.70	77.39	86.40	90.81
		DNN	**92.30**	65.2	79.27	88.9	59.5	72.2	85.1
		Alex-Net	**83.08**	64.44	73.23	78.9	57.11	69.9	75
		Res-Net-50	**91.76**	76	86	91	72.6	81.49	88.1
		VGG-16	**87.16**	64.7	75	81.9	60	71.34	79.81

Table 5.4: Comparison of the proposed GSO-CNN model and existing models on Dset -1 and Dset-2

Models	F-measure (%)	Accuracy (%)	Specificity (%)	Sensitivity (%)
(Wang et. al (2018))	-	80.91	80	81.82
(Nguyen et. al (2019))	-	90.88	-	-
(Song et. al (2019))	-	92.1	96.2	94.1
(Ajilisa et. al (2020))	89.43	89.93	-	92.76
(Nguyen et. al (2021))	-	92.05	-	-
Proposed (GSO-CNN) model on Dset -1	**97.20**	**95.30**	**94.87**	**96.66**
Proposed (GSO-CNN) model on Dset -2	**98.34**	**96.02**	**95**	**96.70**
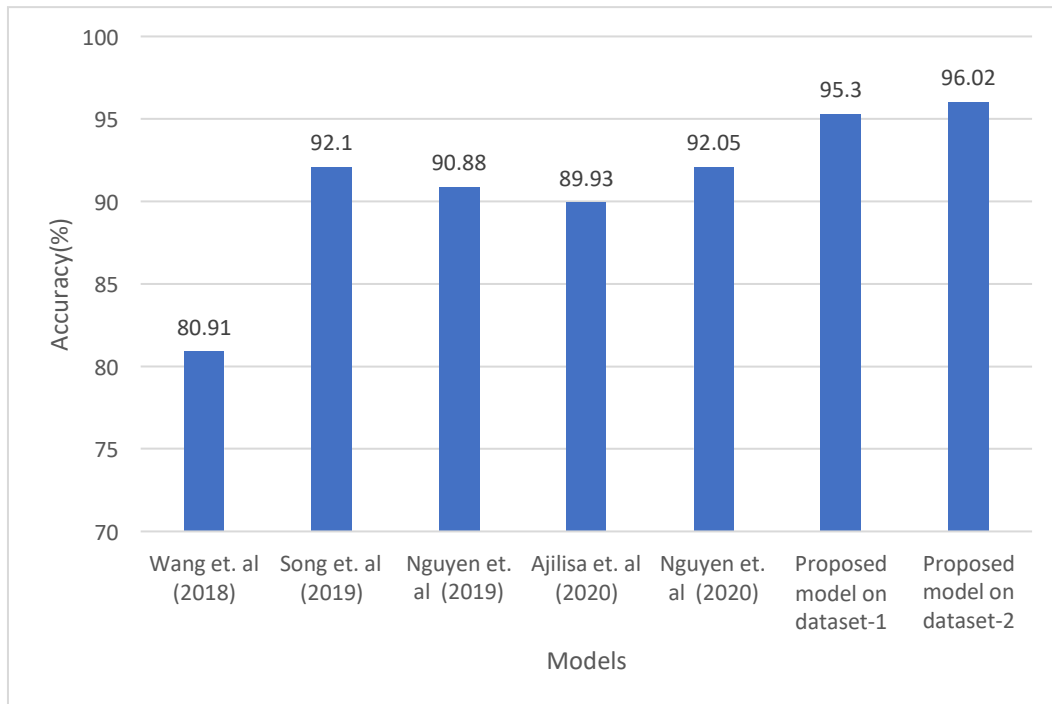
Figure 5.8: Comparative analysis of the accuracy parameter with models on Dset -1 and Dset-2
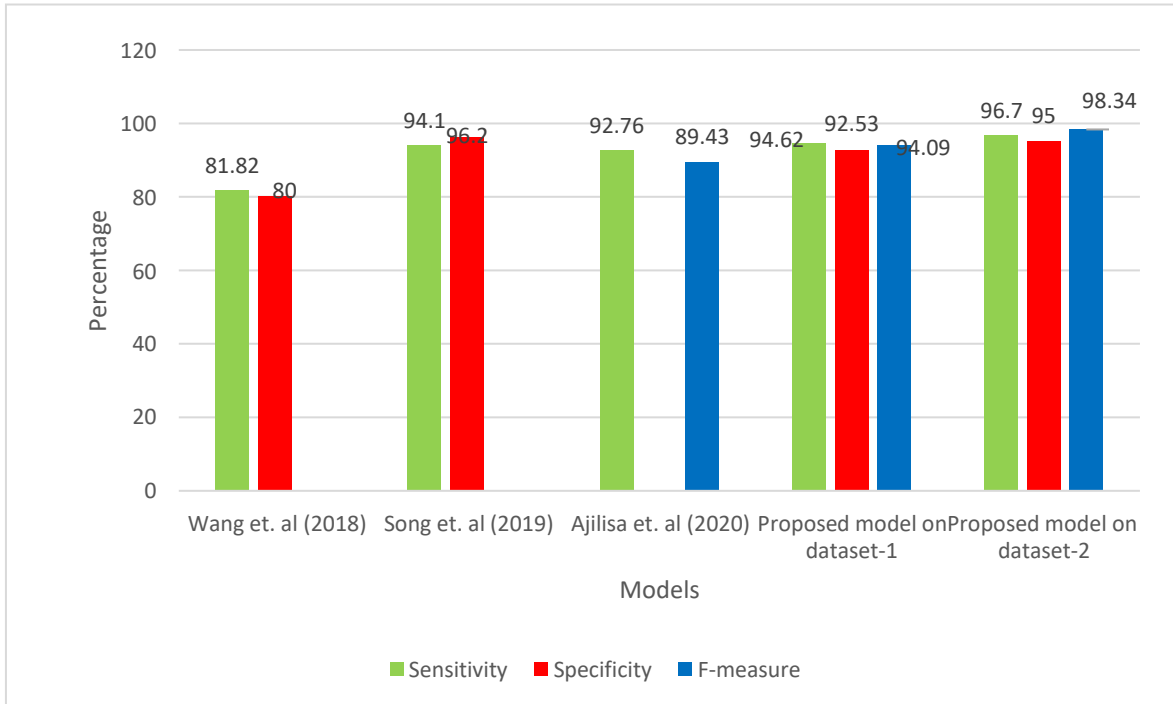
Figure 5.9: Comparative analysis of models based on sensitivity, f-measure and specificity on Dset -1 and Dset-2
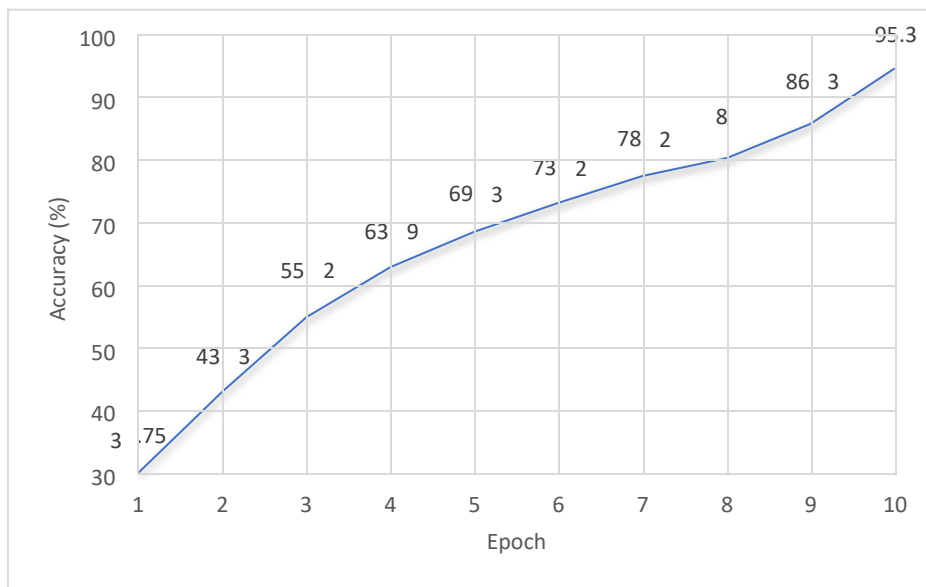
Figure 5.10: Accuracy-epoch graph for Dset -1
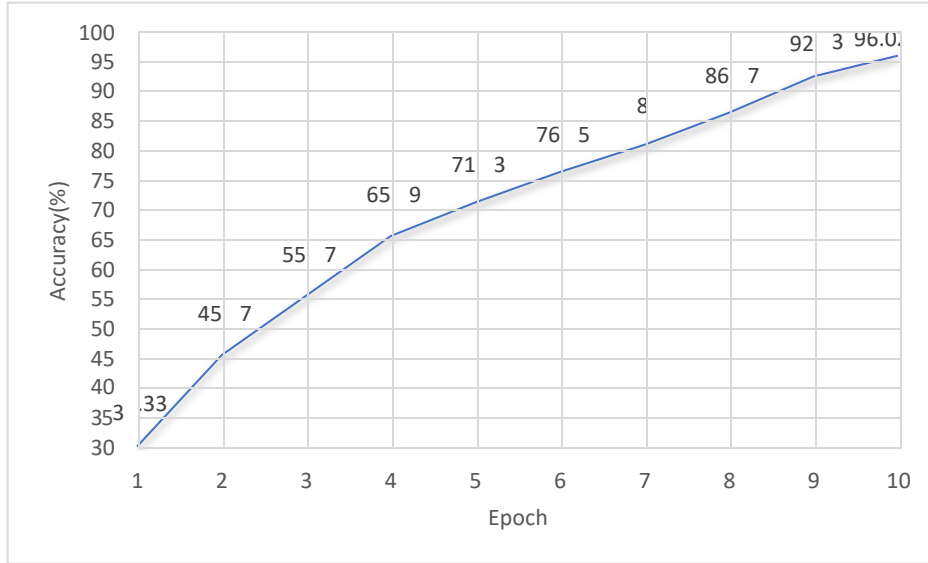
Figure 5.11: Accuracy-epoch graph for Dset -2

5.2 Summary

GSO-CNN model is proposed for the identification and classification of TNDs in this chapter. The model is compared with Res-Net-50, DNN, VGG-16, Alex-Net and various reported models. It is concluded from the results that the proposed GSO-CNN outperforms when compared with and without segmentation and boundary detection techniques. The GSO technique is used to optimize the drop-out factor and learning rate parameters to find the best results.

CHAPTER 6

AN IMPROVED DEEP-GAN MODEL FOR IDENTIFICATION AND CLASSIFICATION OF THYROID NODULE

Health care is conventionally regarded as essential determinant in promoting the general mental, physical, and social well-being of people around the world [140]. A reliable system forTNDs is necessary for early identification and classification of BTND and MTND to save effort, time and human life [141-145]. In this chapter, Deep- Generative Adversarial Network (Deep- GAN) based model is proposed for the early identification and classification of TNDs. GSO technique is used for tunning of the Deep-GAN (i.e., Alex-GAN and VGG-GAN) model by optimizing the optimizer, batch size and learning rate parameters.

6.1 Proposed Methodology

This section presents the proposed methodology adopted for Deep-GAN model. It works in four phases namely: (1) data collection and pre-processing, (2) data augmentation, (3) classification using Deep-GAN model and (4) result analysis. Figure 6.1 shows the systematicflow of the proposed Deep-GAN model.
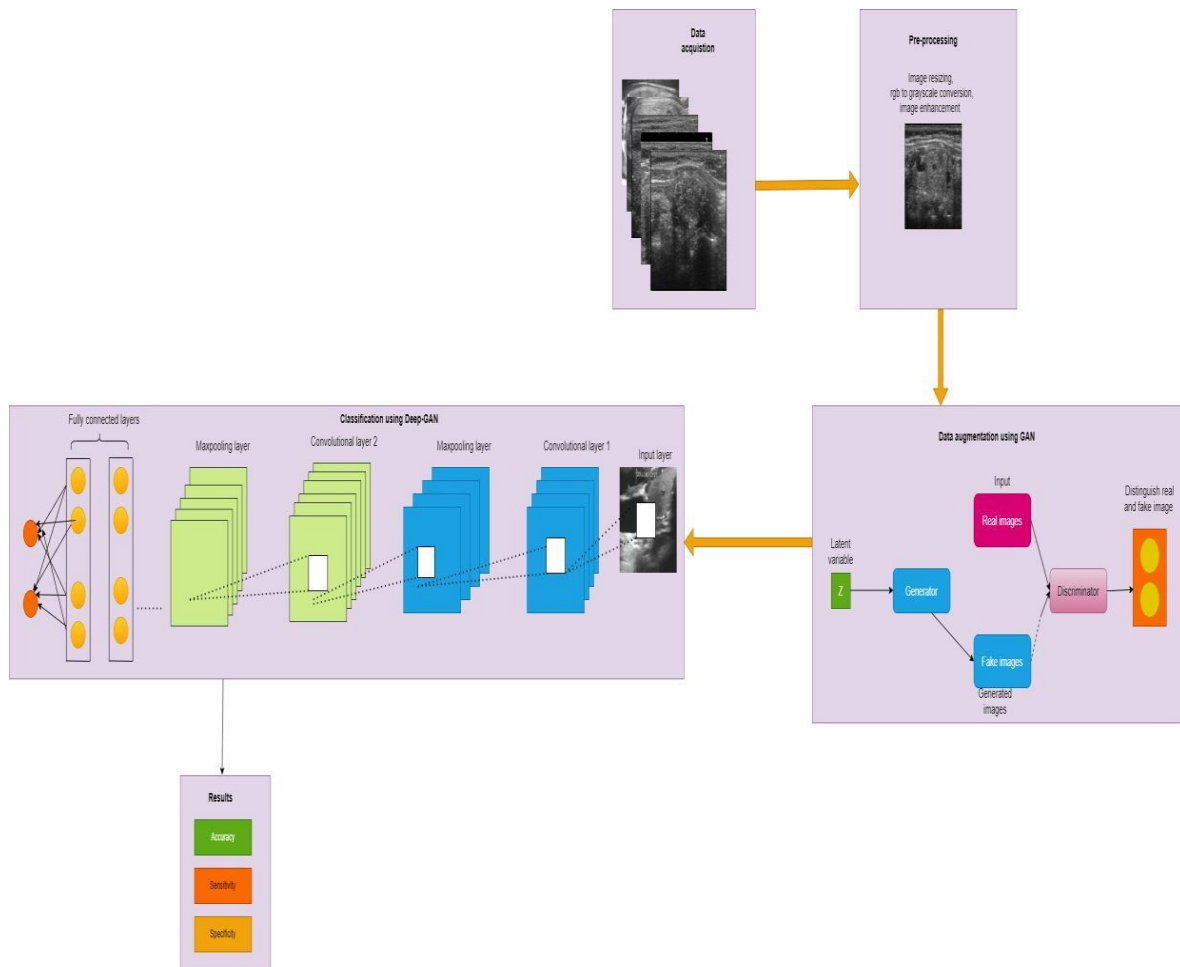
Figure 6.1: The systematic flow of Deep-GAN model

6.1.1 Data Collection and Pre-processing

This phase has been discussed in section 4.1.1

6.1.2 Data Augmentation

Data Augmentation (DA) plays an important role in medical image analysis for synthetically increasing the sample size by generating new data points from existing data. [146]. Here, GAN based DA technique is used to increase the sample size.[147]. In 2014, Ian Goodfellow introduced the adversial process to learn Generative Models (GM) [148]. The core idea of GANs is inspired by a two-player zero-sum minimax game between the Discriminator *(D)* and the Generator *(G)* [149]. Here, there are two players namely *(G)* and *(D)* who participates in this game and tries to win by defeating the other and vice-versa. The *D* tries to determine whether the sample belongs to fake or real distribution whereas *G* aims to deceive *D* by generating fake sample distribution. The *D* tries to produce probability that the sample is real sample. The value close to zero interpret that the sample is fake sample whereas the probability

(*P*) near to 0.5 indicates *D* is unable to differentiate fake or real sample [150]. Figure 6.2 shows the architecture of GAN.
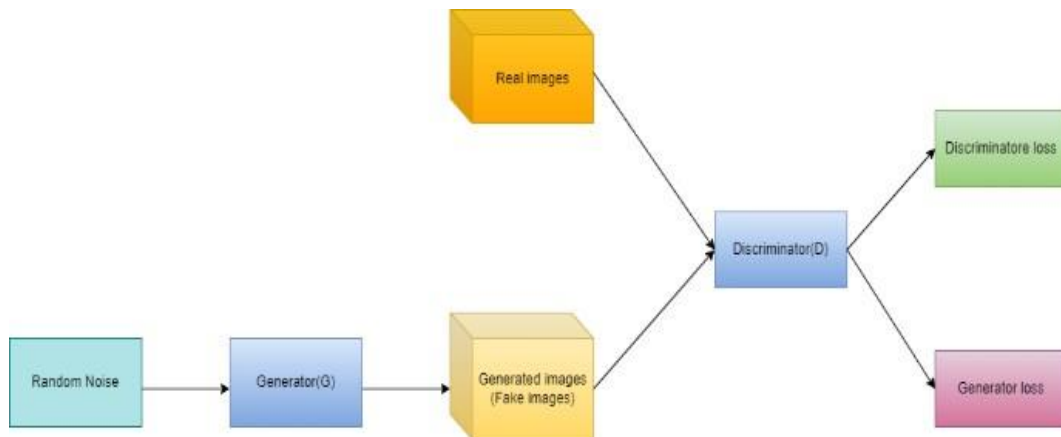
Figure 6.2 : Architecture of GAN[151]

6.1.3 Classification Using Deep-GAN

In this chapter, VGG-16 and Alex-Net model are considered for classification of TNDs. Some of the popular reasons for considering Alex-Net and VGG-16 are: (i) ReLU function is used in pre trained architectures as it has a proven record of increasing the training speed of the models in literature [152], (ii) Such pertained architectures reduce the over fitting problem by using drop-out factor, (iii) Alex-Net allows multi-GPU training, (iv) Alex-Net shows good accuracy on different proposed models despite having 8 layers[153], (v) VGG-16 network introduced the concept of grouping multiple convolutional layers with smaller kernel size to increases the performance of the model [154], and (vi) VGG-16 is a deeper model having 16 layers with increased capability to extract features from images[155]. Its architecture explanation is discussed in chapter 5 under subsection 5.1.4.2 and 5.1.4.3. Figure 6.3 shows the proposed Alex-GAN model and Figure 6.4 shows the proposed VGG-GAN model.
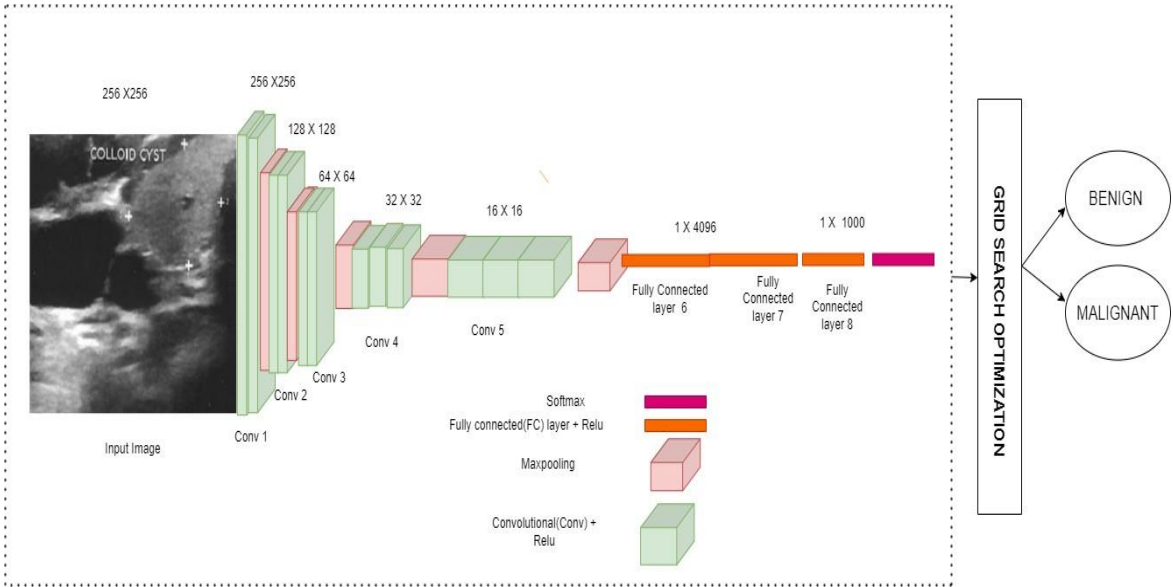
Figure 6.3: Proposed Alex-GAN model
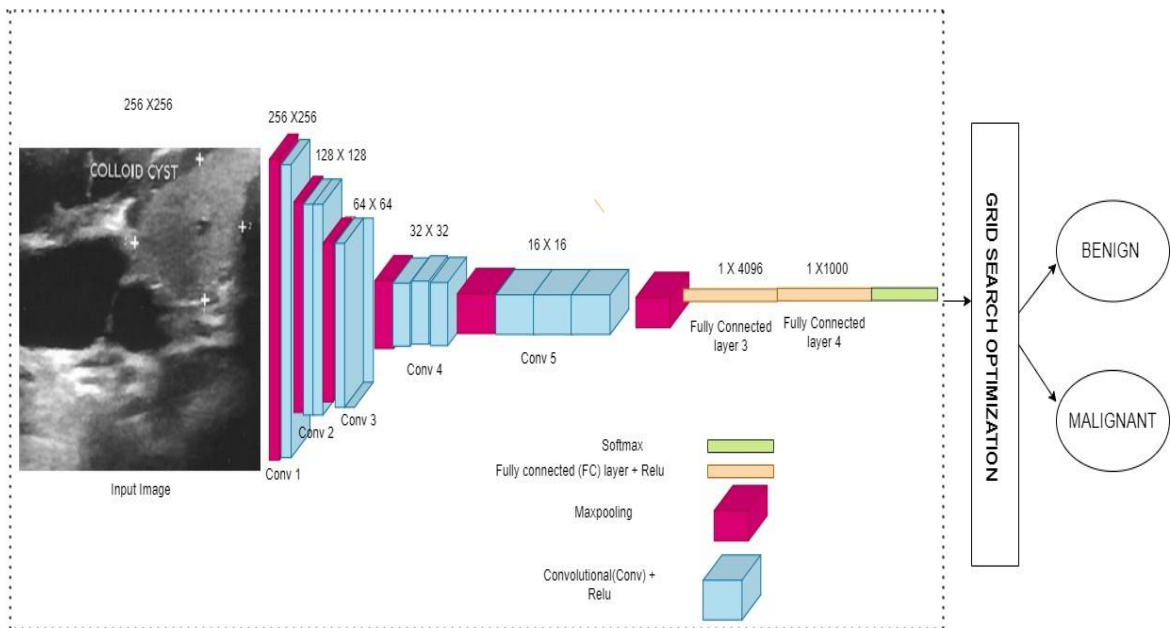
Figure 6.4: Proposed VGG-GAN model

6.1 Algorithm for classification of TNDs using Deep-GAN

Algorithm 6.1: Classification of TNDs using Deep-GAN
Input: Image dataset

Output: Type of TNDs
BEGIN
1.   Upload dataset.
2.   Perform pre-processing steps.

3.	Use GAN for data augmentation
4.	Divide train and test part of TNDs images
5.	Initialize the parameters of Deep-GAN model
	-dropoutfactor
	- maxepoch
	- batchsize
	- learning rate
	- activation function
	- optimizer
6.	Use GSO technique for optimization of Deep-GAN.
7.	Train the model
	Classify type of TNDs

END

6.1.4 Result Analysis

The section will focus on the results of the Deep-GAN model. GAN model is used to increase the sample size of the datasets for building and evaluating the Deep-GAN model. The public and collected datasets are divided into 8:2 ratio. The public dataset and collected datasets are renamed as Dset-1 and Dset-2. Table 6.1 shows the parameter settings of Deep-GAN on Dset-1 and Dset-2. Table 6.2 shows the grid search results over different values of hyperparameters set for the proposed Alex-GAN and VGG-GAN models. The hyper tuning of the following parameters like optimizer, batch size and learning rate is optimized using GSO technique. It can be concluded from table 6.2 that the proposed models perform best on Adam optimizer with learning rate of 0.001 and batch size of 35 on both datasets. Table 6.3 shows comparative performance comparison of VGG-16, Alex-Net, VGG-GAN and Alex-GAN models. Experiments are performed on Alex-Net and VGG-16 architectures CASE-1: without data augmentation and CASE 2: with GAN as augmentation i.e., Alex-GAN and VGG-GAN. Table 6.3 shows the results of VGG-16, Alex-Net, VGG-GAN and Alex-GAN models. The result obtained in CASE-1 shows that the obtained results were not good. Hence, CASE-2 is carried out with GAN to achieve better results. In CASE-1, Alex-Net has achieved (96%, 94.91%, 96.70%, 96.65%) and VGG-16 has achieved (93.60%, 90.32%,95.18%, 96.73%) in terms of accuracy, specificity, sensitivity and F-measure parameters. While in CASE-2, Alex-GAN model has achieved (97.03%, 95.83%, 97.70%, 98.26%) and VGG-GAN achieved (94.28%, 96.73%,90.32%, 96.7%) on both datasets in terms of considered parameters. Table 6.4 shows the performance comparison of the Deep- GAN model (i.e., Alex-GAN and VGG-GAN) with reported models used for classification of TNDs. The Alex-GAN model has shown performance

improvement of 2% to 4% with VGG-GAN and existing models. Figure 6.5 shows the generator network and figure 6.6 shows the discriminator network. Figure 6.7(a-b) shows the training of Alex-Net architecture whereas figure 6.8(a-d) shows the training of VGG-16 architecture. Figure 6.9 and 6.10 show the accuracy epoch graph of Alex-GAN model on Dset-1 and Dset-2. Figure 6.11 and 6.12 show the accuracy epoch graph of VGG-GAN model on Dset-1 and Dset-2.

Table 6.1: Parameter setting of Deep-GAN model on Dset-1 and Dset-2

Parameter	Epoch	Optimizer	Learning rate	Batch size	Stride	Pooling layer	Kernel size
Values	80	Adam	0.001	35	2	Max-pooling	3

Table 6.2: The grid search results over different values of hyperparameters set for Alex-GAN and VGG-GAN models

					Results			
Parameters					**Alex-GAN**		**VGG-GAN**	
					Dset-1	Dset-2	Dset-1	Dset-2
Sr. No	Epochs	Batch size	Optimizer	Learning rate	Accuracy	Accuracy	Accuracy	Accuracy
1	80	55	SGD	0.1	79.64	75.9	70.1	72.9
2	80	55	Adam	0.1	80.1	77.7	74.89	78.23
3	80	45	SGD	0.01	84.7	83.55	85.27	81.46
4	80	45	Adam	0.01	87.89	88.6	86	87.34
5	80	35	SGD	0.001	93.6	94.89	91.88	92.12
6	**80**	**35**	**Adam**	**0.001**	**96**	**97.03**	**93.60**	**94.28**
7	80	25	SGD	0.0001	91.3	92.6	92	93.4
8	80	25	Adam	0.0001	92.5	93.22	90.43	92
9	80	15	SGD	0.00001	86.20	88.89	84.5	85.7
10	80	15	Adam	0.00001	87.45	91.12	88.99	82

Table 6.3: Comparative performance comparison of VGG-16, Alex-Net, VGG-GAN and Alex-GAN models

Models	Dsets	Accuracy (%)	Sensitivity (%)	Specificity (%)	F-measure (%)
Alex-Net without data augmentation technique **(CASE-1)**	**Dset-1**	92.16	93.68	91.42	95.18
	Dset-2	94.89	95.69	91.11	95.69
VGG-16 without data augmentation technique **(CASE-1)**	**Dset-1**	92.40	94.68	91.35	93.19
	Dset-2	93.37	94.62	91.37	94.11

Alex-GAN (CASE-2)	Dset-1	96	96.70	94.91	95.65
	Dset-2	97.03	97.70	95.83	98.26
VGG-GAN (CASE-2)	Dset-1	93.60	96.73	90.32	95.18
	Dset-2	94.28	95.98	91.48	96.7

Table 6.4: Performance comparison of the Deep- GAN model (i.e., Alex-GAN and VGG-GAN) with existing models for classification of TNDs

Models	F-measure (%)	Accuracy (%)	Sensitivity (%)	Specificity (%)
(Wang et al. (2018))	-	80.91	81.82	80
(Nguyen et al. (2019))	-	90.88	-	-
(Song et al. (2019))	-	92.1	94.1	96.2
(Ajilisa et al. (2020))	89.43	89.93	92.76	-
(Hang et al. (2021))	-	95	-	-
(Nguyen et al. (2021))	-	92.05	-	-
Proposed model (Alex-GAN) on Dset-1	95.65	96	96.70	94.91
Proposed model (Alex-GAN) on Dset-2	98.26	97.03	97.70	95.83
Proposed model (VGG-GAN) on Dset-1	95.18	93.60	96.73	90.32
Proposed model (VGG-GAN) on Dset-2	96.7	94.28	95.98	91.48

```
Model: "generator"

Layer (type)                    Output Shape              Param #
=================================================================
dense_31 (Dense)                (None, 131072)            13238272

reshape_5 (Reshape)             (None, 32, 32, 128)       0

conv2d_transpose_15 (Conv2D     (None, 64, 64, 128)       262272
Transpose)

leaky_re_lu_33 (LeakyReLU)      (None, 64, 64, 128)       0

conv2d_transpose_16 (Conv2D     (None, 128, 128, 256)     524544
Transpose)

leaky_re_lu_34 (LeakyReLU)      (None, 128, 128, 256)     0

conv2d_transpose_17 (Conv2D     (None, 256, 256, 512)     2097664
Transpose)

leaky_re_lu_35 (LeakyReLU)      (None, 256, 256, 512)     0

conv2d_48 (Conv2D)              (None, 256, 256, 1)       12801

=================================================================
Total params: 16,135,553
Trainable params: 16,135,553
Non-trainable params: 0
```

Figure 6.5: Generator network

```
Model: "discriminator"

Layer (type)                    Output Shape              Param #
=================================================================
conv2d_45 (Conv2D)              (None, 128, 128, 64)      1088

leaky_re_lu_30 (LeakyReLU)      (None, 128, 128, 64)      0

conv2d_46 (Conv2D)              (None, 64, 64, 128)       131200

leaky_re_lu_31 (LeakyReLU)      (None, 64, 64, 128)       0

conv2d_47 (Conv2D)              (None, 32, 32, 128)       262272

leaky_re_lu_32 (LeakyReLU)      (None, 32, 32, 128)       0

flatten_10 (Flatten)            (None, 131072)            0

dropout_20 (Dropout)            (None, 131072)            0

dense_30 (Dense)                (None, 1)                 131073

=================================================================
Total params: 525,633
Trainable params: 525,633
Non-trainable params: 0
```

Figure 6.6: Discriminator network

```
Model: "sequential_5"

Layer (type)                    Output Shape              Param #
=================================================================
conv2d_49 (Conv2D)              (None, 64, 64, 96)        11712

batch_normalization_45 (Bat     (None, 64, 64, 96)        384
chNormalization)

activation_45 (Activation)      (None, 64, 64, 96)        0

max_pooling2d_15 (MaxPoolin     (None, 32, 32, 96)        0
g2D)

conv2d_50 (Conv2D)              (None, 32, 32, 256)       614656

batch_normalization_46 (Bat     (None, 32, 32, 256)       1024
chNormalization)

activation_46 (Activation)      (None, 32, 32, 256)       0

max_pooling2d_16 (MaxPoolin     (None, 16, 16, 256)       0
g2D)

conv2d_51 (Conv2D)              (None, 16, 16, 384)       885120
```

```
batch_normalization_48 (Bat     (None, 16, 16, 384)       1536
chNormalization)

activation_48 (Activation)      (None, 16, 16, 384)       0

conv2d_53 (Conv2D)              (None, 16, 16, 256)       884992

batch_normalization_49 (Bat     (None, 16, 16, 256)       1024
chNormalization)

activation_49 (Activation)      (None, 16, 16, 256)       0

max_pooling2d_17 (MaxPoolin     (None, 8, 8, 256)         0
g2D)

flatten_11 (Flatten)            (None, 16384)             0

dense_32 (Dense)                (None, 4096)              67112960

batch_normalization_50 (Bat     (None, 4096)              16384
chNormalization)

activation_50 (Activation)      (None, 4096)              0

dropout_21 (Dropout)            (None, 4096)              0
```

Figure 6.7a: part-1   **Figure 6.7b**:part-2
Figure 6.7(a-b): Training of Alex-Net architecture

```
Model: "generator"

Layer (type)                      Output Shape              Param #
=================================================================
dense_31 (Dense)                  (None, 131072)            13238272

reshape_5 (Reshape)               (None, 32, 32, 128)       0

conv2d_transpose_15 (Conv2D       (None, 64, 64, 128)       262272
Transpose)

leaky_re_lu_33 (LeakyReLU)        (None, 64, 64, 128)       0

conv2d_transpose_16 (Conv2D       (None, 128, 128, 256)     524544
Transpose)

leaky_re_lu_34 (LeakyReLU)        (None, 128, 128, 256)     0

conv2d_transpose_17 (Conv2D       (None, 256, 256, 512)     2097664
Transpose)

leaky_re_lu_35 (LeakyReLU)        (None, 256, 256, 512)     0

conv2d_48 (Conv2D)                (None, 256, 256, 1)       12801

=================================================================
Total params: 16,135,553
Trainable params: 16,135,553
Non-trainable params: 0
```

Figure 6.8a: Generator network

```
Model: "discriminator"

Layer (type)                      Output Shape              Param #
=================================================================
conv2d_45 (Conv2D)                (None, 128, 128, 64)      1088

leaky_re_lu_30 (LeakyReLU)        (None, 128, 128, 64)      0

conv2d_46 (Conv2D)                (None, 64, 64, 128)       131200

leaky_re_lu_31 (LeakyReLU)        (None, 64, 64, 128)       0

conv2d_47 (Conv2D)                (None, 32, 32, 128)       262272

leaky_re_lu_32 (LeakyReLU)        (None, 32, 32, 128)       0

flatten_10 (Flatten)              (None, 131072)            0

dropout_20 (Dropout)              (None, 131072)            0

dense_30 (Dense)                  (None, 1)                 131073

=================================================================
Total params: 525,633
Trainable params: 525,633
Non-trainable params: 0
```

Figure 6.8b: Discriminator network

```
conv2d_40 (Conv2D)                (None, 128, 128, 128)     73856

conv2d_41 (Conv2D)                (None, 128, 128, 128)     147584

max_pooling2d_11 (MaxPoolin       (None, 64, 64, 128)       0
g2D)

conv2d_42 (Conv2D)                (None, 64, 64, 256)       295168

conv2d_43 (Conv2D)                (None, 64, 64, 256)       590080

conv2d_44 (Conv2D)                (None, 64, 64, 256)       590080

max_pooling2d_12 (MaxPoolin       (None, 32, 32, 256)       0
g2D)

conv2d_45 (Conv2D)                (None, 32, 32, 512)       1180160

conv2d_46 (Conv2D)                (None, 32, 32, 512)       2359808

conv2d_47 (Conv2D)                (None, 32, 32, 512)       2359808

max_pooling2d_13 (MaxPoolin       (None, 16, 16, 512)       0
g2D)

conv2d_48 (Conv2D)                (None, 16, 16, 512)       2359808
```

```
max_pooling2d_13 (MaxPoolin       (None, 16, 16, 512)       0
g2D)

conv2d_48 (Conv2D)                (None, 16, 16, 512)       2359808

conv2d_49 (Conv2D)                (None, 16, 16, 512)       2359808

conv2d_50 (Conv2D)                (None, 16, 16, 512)       2359808

max_pooling2d_14 (MaxPoolin       (None, 8, 8, 512)         0
g2D)

flatten_5 (Flatten)               (None, 32768)             0

dense_12 (Dense)                  (None, 4096)              134221824

dense_13 (Dense)                  (None, 4096)              16781312

dense_14 (Dense)                  (None, 2)                 8194

=================================================================
Total params: 165,724,866
Trainable params: 165,724,866
Non-trainable params: 0
```

Figure 6.8c: part-1   **Figure 6.8d**: part-2
Figure 6.8(a-d): Training for VGG-16 architecture
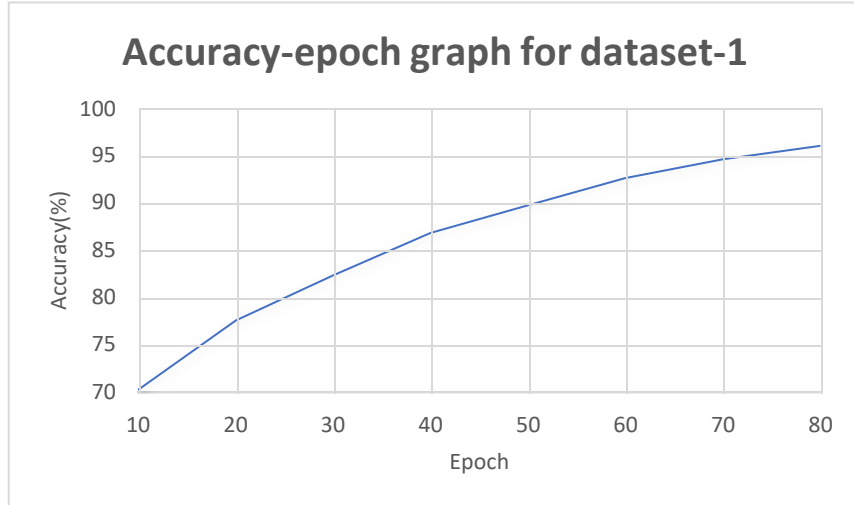
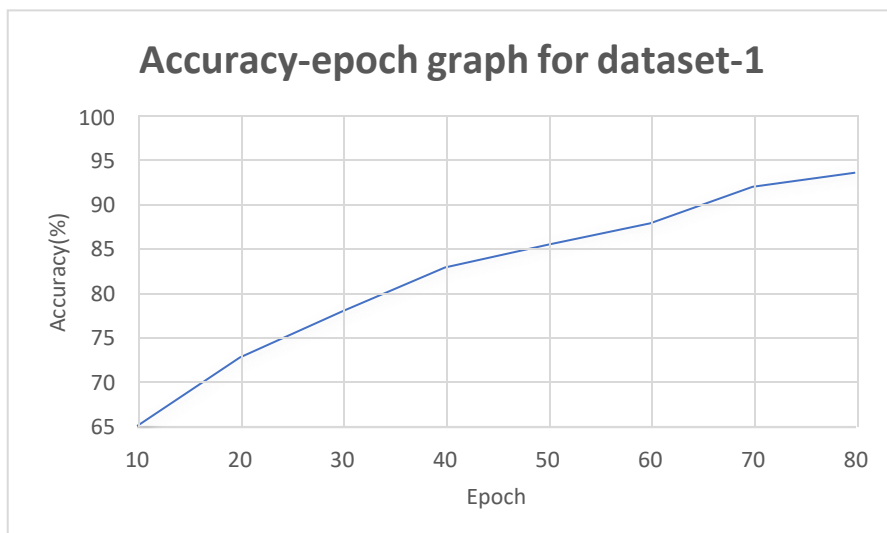**Figure 6.9:** The accuracy-epoch graph of Alex-GAN model on Dset-1
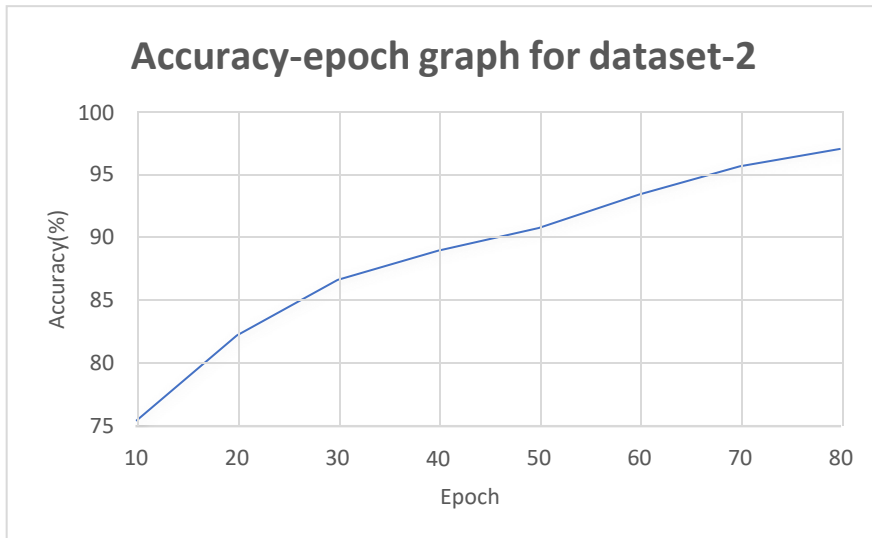
Figure 6.10: The accuracy-epoch graph of Alex-GAN model on Dset-2

Figure 6.11: The accuracy-epoch graph of VGG-GAN model on Dset-1
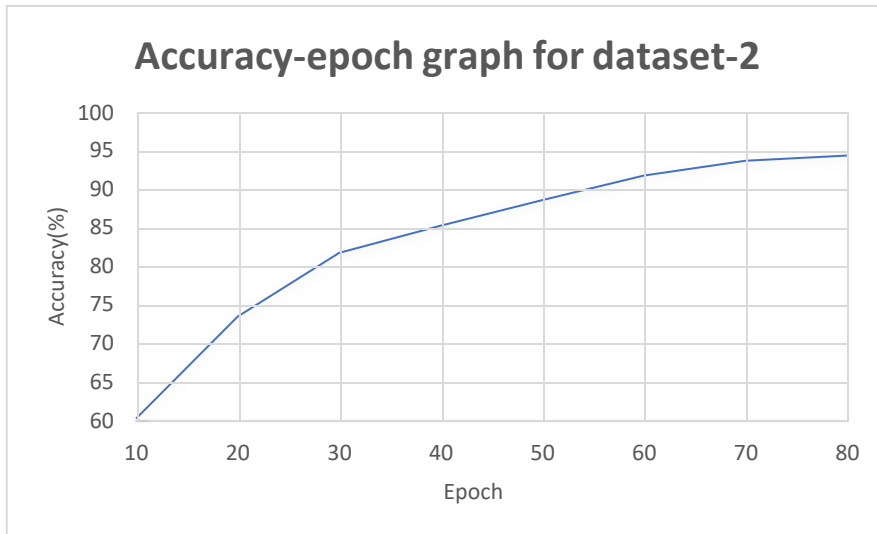
Figure 6.12: The accuracy-epoch graph of VGG-GAN model on Dset-2

6.2 Summary

The proposed Deep-GAN model has achieved promising results for the early identification and classification of TNDs. GSO technique is used for tunning of the Deep-GAN (i.e. Alex-GAN and VGG-GAN) model. The experimental results demonstrate that the proposed Alex-GAN performs better in comparison with VGG-GAN and other DL models reported in literature with an improvement of 2% to 4%. The developed models have been evaluated on TDID and findings are generalized by evaluating such models on collected dataset. The proposed model will help the radiologists for early identification and classification of TNDs in USG images.

CHAPTER 7

CONCLUSION AND FUTURE WORK

This chapter concludes research work written in the thesis. The major research contributions and future research directions are discussed as follows.

7.1 Major Research Contributions

The following are the major contributions of this research work.

- The proposed model has been evaluated on public TDID and collected dataset taken from Kriti Scanning Center, Prayagraj, Uttar Pradesh, India duly approved by NABH and Healthcare Providers. The duration of dataset collection was from July 2020 to March 2021.The goal behind using collected dataset is to generalize the results of the proposed models for the identification and classification of benign and malignant TNDs.

- Two hybrid models are proposed: (1) hybridization of two ML classifiers i.e., ANN-SVM hybrid model and (2) hybridization of DL and ML classifier i.e., CNN-SVM hybrid model. The experimental results for these models show that hybridization of DL and ML classifier outperforms in comparison with hybridization of two ML classifiers. The findings demonstrate that the proposed CNN-SVM hybrid model performs better as compared to the standalone classifier.

- A GSO-CNN model is proposed for the classification of TNDs in medical USG images. The variants of CNN models like Res-Net-50, DNN, Alex-Net and VGG-16 are explored for the classification of TNDs. The proposed model is optimized using GSO technique in terms of hyperparameters like optimizer, batch size and learning rate. The proposed GSO-CNN model experimental results are compared with Res-Net, DNN, Alex-Net, VGG-16 and other state-of-the-art models. The results shows that the proposed GSO-CNN model is competitive in comparison with the reported models in literature.

- Deep-GAN model is proposed to improve the accuracy for the identification and classification of TNDs. GSO technique is used for tunning of the Deep-GAN (i.e. Alex-GANand VGG-GAN) model by optimizing the optimizer, learning rate and batch size hyperparameters. The experimental results demonstrate that the proposed Alex-GAN performs better in

comparison with proposed VGG-GAN and other reported DL models in literature with an improvement of 2% to 4 %.

- The proposed (i) CNN-SVM hybrid model, (ii) GSO-CNN model and (iii) Deep -GAN models are evaluated in terms of accuracy, F-measure, specificity and sensitivity parameters on the public and collected datasets. Based on the performance evaluation of these proposed model among themselves, Deep-GAN model is ranked 1, GSO-CNN model as ranked 2 and CNN-SVM model is ranked 3 for the identification and classification of TNDs.

The proposed models can be used by the clinicians, doctors, researchers and practitioners for the diagnostic purpose. The proposed models will act as an early alarm for patients having TNDs.

7.2 Future Work

- Internet of Things (IOT) enabled healthcare application can be developed using DL techniques.
- Different types of optimization techniques can be explored to improve accuracy of model.
- A mobile based application can be designed for better feasibility to the doctors.
- Other kinds of diseases related to lung, kidneys etc. can be considered to further verify the universality of the proposed approaches.

REFERENCES

[1] Das, D., Banerjee, A., Jena, A. B., Duttaroy, A. K., & Pathak, S., "Essentiality, relevance, and efficacy of adjuvant/combinational therapy in the management of thyroid dysfunctions", *Biomedicine & Pharmacotherapy*, vol. 146, 2022.

[2] https://www.thyroid.org/professionals/ata-professional-guidelines

[3] Nilsson, Mikael, and Henrik Fagman, "Development of the thyroid gland", *Development*, vol. 144, pp. 2123-2140, 2017.

[4] Zhang, X., Malik, B., Young, C., Zhang, H., Larkin, D., Liao, X. H., & Arvan , P., "Maintaining the thyroid gland in mutant thyroglobulin-induced hypothyroidism requires thyroid cell proliferation that must continue in adulthood", *Journal of Biological Chemistry*, 2022.

[5] Darras, Veerle M., "Thyroid gland", *In Sturkie's Avian Physiology*, pp. 795-812, *Academic Press,* 2022.

[6] Sadeghi, D., Shoeibi, A., Ghassemi, N., Moridian, P., Khadem, A., Alizadehsani, R., ... & Acharya, U. R, "An overview of artificial intelligence techniques for diagnosis of Schizophrenia based on magnetic resonance imaging modalities: Methods, challenges, and future works", *Computers in Biology and Medicine*, 2022.

[7] Abbasian Ardakani, A., Reiazi, R., & Mohammadi, A., "A Clinical Decision Support System Using Ultrasound Textures and Radiologic Features to Distinguish Metastasis from Tumor-Free Cervical Lymph Nodes in Patients with Papillary Thyroid Carcinoma", *Journal of Ultrasound in Medicine,* vol. 37(11), pp. 2527-2535, 2018.

[8] Hegedus, L., Bianco, A. C., Jonklaas, J., Pearce, S. H., Weetman, A. P., & Perros, P., "Primary hypothyroidism and quality of life", *Nature Reviews Endocrinology*, vol. 18(4), pp. 230-242, 2022.

[9] Demet, M. M., Ozmen, B., Deveci, A., Boyvada, S., Adiguzel, H., & Aydemir, O, "Depression and anxiety in hyperthyroidism", *Archives of medical research*, vol. 33(6), pp. 552-556, 2002.

[10] Kwong, N., Medici, M., Angell, T. E., Liu, X., Marqusee, E., Cibas, E. S., ... & Alexander, E. K., "The influence of patient age on TND formation, multinodularity, and thyroid cancer risk", *The Journal of Clinical Endocrinology & Metabolism*, vol. 100(12), pp. 4434-4440, 2015.

[11] Richman, D. M., Benson, C. B., Doubilet, P. M., Wassner, A. J., Asch, E., Cherella, C. E., & Frates, M. C, "Assessment of American college of radiology thyroid imaging reporting and data system (TI-RADS) for pediatric thyroid nodules", *Radiology*, vol. 294(2), pp. 415-420.

[12] Ker, J., Wang, L., Rao, J., & Lim, T, "Deep learning applications in medical image analysis", *IEEE Access*, vol. 6, pp. 9375-9389, 2017.

[13] Yap, P. T., Zhang, Y., & Shen, D., "Multi-Tissue Decomposition of Diffusion MRI Signals via ℓ_{0} Sparse-Group Estimation", *IEEE Transactions on Image Processing*, vol. 25(9), pp. 4340-4353, 2016.

[14] Schmidhuber, J, "Deep learning in neural networks: An overview", *Neural networks,* vol. 61, pp. 85-117, 2015.

[15] Bengio, Y., "Learning deep architectures for AI", *Now Publishers Inc.*, 2009.

[16] Hinton, G. E., & Salakhutdinov, R. R, "Reducing the dimensionality of data with neural networks", *Science,* vol. 313(5786), pp. 504-507, 2006.

[17] Vincent, P., Larochelle, H., Lajoie, I., Bengio, Y., Manzagol, P. A., & Bottou, L, "Stacked denoising autoencoders: Learning useful representations in a deep network with a local denoising criterion", *Journal of machine learning research*, 2010.

[18] Nair, V., & Hinton, G. E, "Rectified linear units improve restricted boltzmann machines", *In Icml*, 2010.

[19] Srivastava, N., Hinton, G., Krizhevsky, A., Sutskever, I., & Salakhutdinov, R., "Dropout: a simple way to prevent neural networks from overfitting", *The journal of machine learning research*, vol. 15(1), pp. 1929-1958, 2014.

[20] Ioffe, S., & Szegedy, C, "Batch normalization: Accelerating deep network training by reducing internal covariate shift", *In International conference on machine learning*, pp. 448-456, 2015.

[21] Pedraza, L., Vargas, C., Narváez, F., Duran, O., Munoz, E., & Romero, E., "An open access thyroid ultrasound image database", *In 10th International Symposium on Medical Information Processing and Analysis,* vol. 9287, pp.188-193, SPIE, 2015.

[22] Quality Council of India, Accessed: 07- Sep. 2022, [Online], Available: https://www.nabh.co/frmViewCGHSRecommend.aspx?Type=Diagnostic%20Centre&cityID=94

[23] Guvenir, H. A., Acar, B., Demiroz, G., & Cekin, A, "A supervised machine learning algorithm for arrhythmia analysis", *In Computers in Cardiology*, pp. 433-436, IEEE, 1997.

[24] Gupta, V., Sachdeva, S., & Dohare, N, "Deep similarity learning for disease prediction", *Trends in Deep Learning Methodologies*, pp.183-206, 2021.

[25] Zhu, L. C., Ye, Y. L., Luo, W. H., Su, M., Wei, H. P., Zhang, X. B., & Zou, C. L, "A model to discriminate malignant from benign thyroid nodules using artificial neural network", *PLoS One*, vol. 8(12), 2013.

[26] Narayan, N. S., Marziliano, P., Kanagalingam, J., & Hobbs, C. G., "Speckle patch similarity for echogenicity-based multiorgan segmentation in ultrasound images of the thyroid gland", *IEEE journal of biomedical and health informatics*, vol. 21(1), pp.172-183, 2015.

[27] Song, G., Xue, F., & Zhang, C., "A model using texture features to differentiate the nature of thyroid nodules on sonography", *Journal of Ultrasound in Medicine*, vol. 34(10), pp. 1753-1760, 2015.

[28] Ardakani, A. A., Gharbali, A., & Mohammadi, A., "Application of texture analysis method for classification of benign and malignant thyroid nodules in ultrasound images", *Iranian journal of cancer prevention*, vol. 8(2), 2015.

[29] Nugroho, H. A., Nugroho, A., & Choridah, L., "Thyroid nodule segmentation using active contour bilateral filtering on ultrasound images", *In 2015 International Conference on Quality in Research (QiR)*, pp. 43-46, 2015.

[30] Song, G., Xue, F., & Zhang, C, "A model using texture features to differentiate the nature of thyroid nodules on sonography", *Journal of Ultrasound in Medicine*, vol. 34(10), pp. 1753-1760, 2015.

[31] Pan, Q., Zhang, Y., Zuo, M., Xiang, L., & Chen, D., "Improved ensemble classification method of thyroid disease based on random forest", *In 2016 8th International Conference on Information Technology in Medicine and Education (ITME)*, pp. 567-571, 2016.

[32] Alrubaidi, W. M., Peng, B., Yang, Y., & Chen, Q., "An interactive segmentation algorithm for thyroid nodules in ultrasound images", *In International Conference on Intelligent Computing*, pp. 107-115, Springer, Cham, 2016.

[33] Vanithamani, R., & Dhivya, R., "Thyroid Nodule Classification in Medical Ultrasound Images", *In International Conference on Soft Computing and Pattern Recognition*, pp. 509-514, Springer, Cham, 2016.

[34] Nugroho, H. A., Rahmawaty, M., Triyani, Y., & Ardiyanto, I., "Texture analysis for classification of thyroid ultrasound images", *In 2016 International Electronics Symposium (IES)*, pp. 476-480, 2016.

[35] Mustafa, N., Memon, R. A., Li, J. P., & Omer, M. Z., "A classification model for imbalanced medical data based on PCA and farther distance based synthetic minority oversampling technique", *Int. J. Adv. Comput. Sci. Appl*, vol.8(1), pp.61-67, 2017.

[36] Pasha, S. J., & Mohamed, E. S., "Ensemble gain ratio feature selection (EGFS) model with machine learning and data mining algorithms for disease risk prediction", *In 2020 International Conference on Inventive Computation Technologies (ICICT),* pp. 590-596, 2020.

[37] Jothi, J. A. A., & Rajam, V. M. A., "Automatic classification of thyroid histopathology images using multi-classifier system", *Multimedia Tools and Applications*, vol. 76(18), pp. 18711-18730, 2017.

[38] Jiang, Y., Deng, Z., Chen, J., Wu, H., Choi, K. S., & Wang, S, "Intelligent diagnostic methods for thyroid nodules", *Journal of Medical Imaging and Health Informatics*, vol. 7(8), pp. 1772-1779, 2017.

[39] Shankar, K., Lakshmanaprabu, S. K., Gupta, D., Maseleno, A., & De Albuquerque, V. H. C., "Optimal feature-based multi-kernel SVM approach for thyroid disease classification", *The Journal of Supercomputing*, vol. 76(2), pp. 1128-1143, 2020.

[40] Ma, X., Xi, B., Zhang, Y., Zhu, L., Sui, X., Tian, G., & Yang, J., "A Machine Learning-based Diagnosis of Thyroid Cancer Using Thyroid Nodules Ultrasound Images.", *Current Bioinformatics*, vol.15(4), pp. 349-358, 2020.

[41] Zheng, X., Lv, G., Du, G., Zhai, Z., Mo, J., & Lv, X., "Rapid and low-cost detection of thyroid dysfunction using Raman spectroscopy and an improved support vector machine", *IEEE Photonics Journal*, vol. 10(6), pp. 1-12, 2018.

[42] Dandan, L., Yakui, Z., Linyao, D., Xianli, Z., & Yi, S., "Texture analysis and classification of diffuse thyroid diseases based on ultrasound images*", In 2018 IEEE International Instrumentation and Measurement Technology Conference (I2MTC)*, pp. 1-6, 2018.

[43] Poudel, P., Illanes, A., Ataide, E. J., Esmaeili, N., Balakrishnan, S., & Friebe, M., "Thyroid ultrasound texture classification using autoregressive features in conjunction with machine learning approaches", *IEEE Access*, vol. 7, pp. 79354-79365, 2019.

[44] Prochazka, A., Gulati, S., Holinka, S., & Smutek, D., "Classification of thyroid nodules in ultrasound images using direction-independent features extracted by two-threshold binary decomposition", *Technology in cancer research & treatment*, vol. 18, 2019.

[45] Wu, Y., & Liu, P., "A Classification Algorithm of Ultrasonic Thyroid Standard Planes Using LBP and HOG Features", I*n 2019 IEEE 13th International Conference on Anti-*

counterfeiting, Security, and Identification (ASID), pp. 103-107, 2019.

[46] Colakoglu, B., Alis, D., & Yergin, M., "Diagnostic value of machine learning-based quantitative texture analysis in differentiating benign and malignant thyroid nodules", *Journal of oncology*, 2019.

[47] Zhang, B., Tian, J., Pei, S., Chen, Y., He, X., Dong, Y., & Zhang, S., "Machine learning–assisted system for thyroid nodule diagnosis", *Thyroid*, vol. 29(6), pp. 858-867, 2019.

[48] Kesarkar, X. A., & Kulhalli, K. V., "Thyroid Nodule Detection using Artificial Neural Network", *In 2021 International Conference on Artificial Intelligence and Smart Systems (ICAIS)*, pp. 11-15, 2021.

[49] Zhao, C. K., Ren, T. T., Yin, Y. F., Shi, H., Wang, H. X., Zhou, B. Y., ... & Xu, H. X., "A comparative analysis of two machine learning-based diagnostic patterns with thyroid imaging reporting and data system for thyroid nodules: diagnostic performance and unnecessary biopsy rate", *Thyroid*, vol. 31(3), pp. 470-481, 2021.

[50] Bengio, Y, "Learning deep architectures for AI", *Foundations and trends in Machine Learning*, vol. 2(1), pp. 1-127, 2009.

[51] Rusk, N, "Deep learning", *Nature Methods*, vol. 13(1), pp. 35-35, 2016.

[52] Lauzon, F. Q, "An introduction to deep learning" *In 2012 11th International Conference on Information Science, Signal Processing and their Applications (ISSPA)*, pp. 1438-1439, 2012.

[53] Voulodimos, A., Doulamis, N., Doulamis, A., & Protopapadakis, E, "Deep learning for computer vision: A brief review", *Computational intelligence and neuroscience*, 2018.

[54] Ronao, C. A., & Cho, S. B, "Human activity recognition with smartphone sensors using deep learning neural networks", *Expert systems with applications*, vol. 59, pp. 235-244, 2016.

[55] Du, W., & Sang, N., "An effective method for ultrasound thyroid nodules segmentation", *In 2015 International Symposium on Bioelectronics and Bioinformatics (ISBB)*, pp. 207-210, 2015.

[56] Acharya, U. R., Chowriappa, P., Fujita, H., Bhat, S., Dua, S., Koh, J. E., ... & Ng, K. H, "Thyroid lesion classification in 242 patient population using Gabor transform features from high resolution ultrasound images", *Knowledge-Based Systems*, vol. 107, pp. 235-245, 2016.

[57] Peng, W., Liu, C., Xia, S., Shao, D., Chen, Y., Liu, R., & Zhang, Z., "Thyroid nodule recognition in computed tomography using first order statistics", *Biomedical engineering*

online, vol.16(1), pp. 1-14, 2017.

[58] Zhu, Y., Fu, Z., & Fei, J., "An image augmentation method using convolutional network for thyroid nodule classification by transfer learning", *In 2017 3rd IEEE International Conference on Computer and Communications (ICCC)*, pp. 1819-1823, 2017.

[59] Song, W., Li, S., Liu, J., Qin, H., Zhang, B., Zhang, S., & Hao, A., "Multitask cascade convolution neural networks for automatic thyroid nodule detection and recognition", *IEEE journal of biomedical and health informatics*, vol. 23(3), pp. 1215-1224, 2018.

[60] Zhang, R., Liu, Q., Cui, H., Wang, X., Song, S., Huang, G., & Feng, D., "Thyroid classification via new multi-channel feature association and learning from multi-modality MRI images", *In 2018 IEEE 15th international symposium on biomedical imaging (ISBI 2018)*, pp. 277-280, 2018.

[61] Sundar, K. S., Rajamani, K. T., & Sai, S. S. S., "Exploring image classification of thyroid ultrasound images using deep learning", *In International Conference on ISMAC in Computational Vision and Bio-Engineering*, pp. 1635-1641, Springer, Cham, 2018.

[62] Wang, J., Li, S., Song, W., Qin, H., Zhang, B., & Hao, A., "Learning from weakly-labeled clinical data for automatic thyroid nodule classification in ultrasound images", *In 2018 25th IEEE International Conference on Image Processing (ICIP)*, pp. 3114-3118, 2018.

[63] Chen, D., Zhang, J., & Li, W., "Thyroid Nodule Classification Using Two Levels Attention-Based Bi-Directional LSTM with Ultrasound Reports", *In 2018 9th International Conference on Information Technology in Medicine and Education (ITME)*, pp. 309-312, 2018.

[64] Li, Z., Qin, J., Zhang, X., & Wan, Y., "A Hybrid Intelligent Framework for Thyroid Diagnosis", *In Cyberspace Data and Intelligence, and Cyber-Living, Syndrome, and Health*, pp. 441-451, Springer, Singapore, 2019.

[65] Ko, S. Y., Lee, J. H., Yoon, J. H., Na, H., Hong, E., Han, K., ... & Kwak, J. Y., "Deep convolutional neural network for the diagnosis of thyroid nodules on ultrasound", *Head & neck*, vol. 41(4), pp. 885-891, 2019.

[66] Wang, L., Yang, S., Yang, S., Zhao, C., Tian, G., Gao, Y., ... & Lu, Y., "Automatic thyroid nodule recognition and diagnosis in ultrasound imaging with the YOLOv2 neural network", *World journal of surgical oncology*, vol. 17(1), pp. 1-9, 2019.

[67] Liu, T., Guo, Q., Lian, C., Ren, X., Liang, S., Yu, J., ... & Shen, D., "Automated detection and classification of thyroid nodules in ultrasound images using clinical-knowledge-guided convolutional neural networks", *Medical image analysis*, vol. 58, 2019.

[68] Aboudi, N., Guetari, R., & Khlifa, N., "Multi-objectives optimization of features selection for the classification of thyroid nodules in ultrasound images", *IET Image Processing*, 2020.

[69] Guo, X., Zhao, H., & Tang, Z., "An Improved Deep Learning Approach for Thyroid Nodule Diagnosis", *In 2020 IEEE 17th International Symposium on Biomedical Imaging (ISBI)*, pp. 296-299, 2020.

[70] Ajilisa, O. A., Jagathyraj, V. P., & Sabu, M. K, "Computer-Aided Diagnosis of Thyroid Nodule from Ultrasound Images Using Transfer Learning from Deep Convolutional Neural Network Models", *In 2020 Advanced Computing and Communication Technologies for High Performance Applications (ACCTHPA),* pp. 237-241, 2020.

[71] Nguyen, D. T., Kang, J. K., Pham, T. D., Batchuluun, G., & Park, K. R., "Ultrasound image-based diagnosis of malignant thyroid nodule using artificial intelligence", *Sensors*, vol. 20(7), 2020.

[72] Vasile, C. M., Udriștoiu, A. L., Ghenea, A. E., Popescu, M., Gheonea, C., Niculescu, C. E., ... & Alexandru, D. O., "Intelligent Diagnosis of Thyroid Ultrasound Imaging Using an Ensemble of Deep Learning Methods", *Medicina*, vol. 57(4), 2021.

[73] Zhu, Y. C., AlZoubi, A., Jassim, S., Jiang, Q., Zhang, Y., Wang, Y. B., ... & Hongbo, D. U., "A generic deep learning framework to classify thyroid and breast lesions in ultrasound images", *Ultrasonics*, vol. 110, 2021.

[74] Yang, W., Dong, Y., Du, Q., Qiang, Y., Wu, K., Zhao, J., ... & Zia, M. B., "Integrate domain knowledge in training multi-task cascade deep learning model for benign–malignant thyroid nodule classification on ultrasound images", *Engineering Applications of Artificial Intelligence*, vol. 98, 2021.

[75] Dabowsa, N. I. A., Amaitik, N. M., Maatuk, A. M., & Aljawarneh, S. A., "A hybrid intelligent system for skin disease diagnosis", *In 2017 International Conference on Engineering and Technology (ICET)*, pp. 1-6, 2017.

[76] Liu, T., Xie, S., Zhang, Y., Yu, J., Niu, L., & Sun, W., "Feature selection and thyroid nodule classification using transfer learning", *In 2017 IEEE 14th International Symposium on Biomedical Imaging (ISBI 2017)*, pp. 1096-1099, 2017.

[77] Xia, J., Chen, H., Li, Q., Zhou, M., Chen, L., Cai, Z., ... & Zhou, H., "Ultrasound-based differentiation of malignant and benign thyroid Nodules: An extreme learning machine approach", *Computer methods and programs in biomedicine*, vol. 147, pp. 37-49, 2017.

[78] Nguyen, D. T., Pham, T. D., Batchuluun, G., Yoon, H. S., & Park, K. R., "Artificial

intelligence-based thyroid nodule classification using information from spatial and frequency domains", *Journal of clinical medicine*, vol. 8(11),2019.

[79] Qin, P., Wu, K., Hu, Y., Zeng, J., & Chai, X., "Diagnosis of benign and malignant thyroid nodules using combined conventional ultrasound and ultrasound elasticity imaging", *IEEE journal of biomedical and health informatics*, vol. 24(4), pp. 1028-1036, 2019.

[80] Xie, J., Guo, L., Zhao, C., Li, X., Luo, Y., & Jianwei, L., "A Hybrid Deep Learning and Handcrafted Features based Approach for Thyroid Nodule Classification in Ultrasound Images", *In Journal of Physics: Conference Series*, vol. 1693, 2020.

[81] Sun, H., Yu, F., & Xu, H., "Discriminating the Nature of Thyroid Nodules Using the Hybrid Method", *Mathematical Problems in Engineering*, 2020.

[82] Hang, Y, "Thyroid nodule classification in ultrasound images by fusion of conventional features and res-GAN deep features", *Journal of Healthcare Engineering,* 2021.

[83] Srivastava, R., Kumar, P., "A hybrid model for the identification and classification of thyroid nodules in medical ultrasound images", *International Journal of Modelling, Identification and Control (IJMIC)*, 2021.

[84] Kwak, J. Y., Han, K. H., Yoon, J. H., Moon, H. J., Son, E. J., Park, S. H., & Kim, E. K, "Thyroid imaging reporting and data system for US features of nodules: a step in establishing better stratification of cancer risk.", *Radiology*, vol. 260(3), pp. 892-899, 2011.

[85] Karanja, E. M., Masupe, S., & Jeffrey, M. G, "Analysis of internet of things malware using image texture features and machine learning techniques", *Internet of Things*, vol. 9, pp. 100-153, 2020.

[86] Garg, M., & Dhiman, G, "A novel content-based image retrieval approach for classification using GLCM features and texture fused LBP variants", *Neural Computing and Applications*, pp. 1-18, 2020.

[87] Chapelle, O., Haffner, P., & Vapnik, V. N, "Support vector machines for histogram-based image classification", *IEEE transactions on Neural Networks*, vol. 10(5), pp. 1055-1064, 1999.

[88] Keramidas, E. G., Maroulis, D., & Iakovidis, D. K, "TND: a thyroid nodule detection system for analysis of ultrasound images and videos", *Journal of medical systems*, vol. 36(3), pp. 1271-1281, 2012.

[89] Zhang, B., Tian, J., Pei, S., Chen, Y., He, X., Dong, Y., & Zhang, S, "Machine learning–assisted system for thyroid nodule diagnosis", *Thyroid,* vol. 29(6), pp. 858-867, 2019.

[90] Jothi, A. A. J., & Rajam, M. A, "Automatic classification of thyroid histopathology images using multi-classifier system", *Multimedia Tools and Applications*, vol. 76(18), pp. 18711-18730, 2017.

[91] Zhou, H., Zhang, J., Zhou, Y., Guo, X., & Ma, Y, "A feature selection algorithm of decision tree based on feature weight", *Expert Systems with Applications,* vol.164, 113842, 2021.

[92] Abiodun, O. I., Jantan, A., Omolara, A. E., Dada, K. V., Mohamed, N. A., & Arshad, H, "State-of-the-art in artificial neural network applications: A survey", *Heliyon*, vol. 4(11), e00938, 2018.

[93] A. Liaw, and M. Wiener, "Classification and regression by random Forest", *R news*, vol. 2, pp. 18-22, 2002.

[94] Gu, J., Wang, Z., Kuen, J., Ma, L., Shahroudy, A., Shuai, B., ... & Chen, T, "Recent advances in convolutional neural networks", *Pattern recognition*, vol. 77, pp. 354-377, 2018.

[95] Zhou, D. X, "Theory of deep convolutional neural networks: Down sampling", *Neural Networks*, vol. 124, pp. 319-327, 2020.

[96] Srivastava, R., Kumar, P, "A contemporary review on soft computing techniques for thyroid disorder identification and detection", *International Journal of Computer Applications in Technology (IJCAT)*, 2021.

[97] Kang, M., & Tian, J, "Machine Learning: Data Pre-processing. Prognostics and Health Management of Electronics: Fundamentals", *Machine Learning, and the Internet of Things*, pp. 111-130, 2018.

[98] Masoudi, S., Harmon, S. A., Mehralivand, S., Walker, S. M., Raviprakash, H., Bagci, U., ... & Turkbey, B, "Quick guide on radiology image pre-processing for deep learning applications in prostate cancer research", *Journal of Medical Imaging*, vol. 8(1), 010901, 2021.

[99] Qi, P. F., Meng, Q. H., & Zeng, M, "A CNN-based simplified data processing method for electronic noses", *In 2017 ISOCS/IEEE International Symposium on Olfaction and Electronic Nose (ISOEN),* pp. 1-3, IEEE, 2017.

[100] Pitaloka, D. A., Wulandari, A., Basaruddin, T., & Liliana, D. Y, "Enhancing CNN with preprocessing stage in automatic emotion recognition", *Procedia computer science*, vol.116, pp. 523-529, 2017.

[101] Vimal Kurup, R., Sowmya, V., & Soman, K. P, "Effect of data pre-processing on brain

tumor classification using capsulenet", *In International Conference on Intelligent Computing and Communication Technologies*, pp. 110-119, 2019.

[102] Haryanto, T., Wasito, I., & Suhartanto, H, "Convolutional Neural Network (CNN) for gland images classification", *In 2017 11th International Conference on Information & Communication Technology and System (ICTS),* pp. 55-60, IEEE, 2017.

[103] Rajan, S., Chenniappan, P., Devaraj, S., & Madian, N, "Novel deep learning model for facial expression recognition based on maximum boosted CNN and LSTM", *IET Image Processing*, vol. 14(7), pp. 1373-1381, 2020.

[104] Soomro, T. A., Afifi, A. J., Shah, A. A., Soomro, S., Baloch, G. A., Zheng, L., & Gao, J, "Impact of image enhancement technique on CNN model for retinal blood vessels segmentation", *IEEE Access*, vol. 7, pp. 158183-158197, 2019.

[105] Garg, G., Kumar, D., Sonker, Y., & Garg, R, "A Hybrid MLP-SVM Model for Classification using Spatial-Spectral Features on Hyper-Spectral Images", arXiv preprint arXiv:2101.00214, 2021.

[106] Guo, T., Dong, J., Li, H., & Gao, Y, "Simple convolutional neural network on image classification", *In 2017 IEEE 2nd International Conference on Big Data Analysis (ICBDA)*, pp. 721-724, IEEE, 2017.

[107] Han, D., Liu, Q., & Fan, W, "A new image classification method using CNN transfer learning and web data augmentation", *Expert Systems with Applications*, vol. 95, pp. 43-56, 2018.

[108] Lei, X., Pan, H., & Huang, X, "A dilated CNN model for image classification", *IEEE Access*, vol. 7, pp. 124087-124095, 2019.

[109] Li, Q., Cai, W., Wang, X., Zhou, Y., Feng, D. D., & Chen, M, "Medical image classification with convolutional neural network", *In 2014 13th international conference on control automation robotics & vision (ICARCV)*, pp. 844-848, IEEE, 2014.

[110] Sultana, F., Sufian, A., & Dutta, P, "Advancements in image classification using convolutional neural network", *In 2018 Fourth International Conference on Research in Computational Intelligence and Communication Networks (ICRCICN)*, pp. 122-129, IEEE, 2018.

[111] Jmour, N., Zayen, S., & Abdelkrim, A, "Convolutional neural networks for image classification*", In 2018 international conference on advanced systems and electric technologies (IC_ASET),* pp. 397-402, 2018.

[112] Li, W., Chen, C., Zhang, M., Li, H., & Du, Q, "Data augmentation for hyperspectral image

classification with deep CNN", *IEEE Geoscience and Remote Sensing Letters*, vol. 16(4), pp. 593-597, 2018.

[113] Alkhaleefah, M., & Wu, C. C, "A hybrid CNN and RBF-based SVM approach for breast cancer classification in mammograms" *In 2018 IEEE International Conference on Systems, Man, and Cybernetics (SMC)*, pp. 894-899, 2018.

[114] Sun, X., Liu, L., Li, C., Yin, J., Zhao, J., & Si, W, "Classification for remote sensing data with cimproved CNN-SVM method", *IEEE Access*, vol. 7, pp. 164507-164516, 2019.

[115] Rosasco, L., De Vito, E., Caponnetto, A., Piana, M., & Verri, A, "Are loss functions all the same?", *Neural computation*, vol. 16(5), pp. 1063-1076, 2004.

[116] Ilhan, U., & Ilhan, A, "Brain tumor segmentation based on a new threshold approach", *Procedia computer science*, vol.120, pp. 580-587, 2017.

[117] Yu, S., Jia, S., & Xu, C, "Convolutional neural networks for hyperspectral image classification", *Neurocomputing*, vol. 219, pp. 88-98, 2017.

[118] Priyadarshini, I., & Cotton, C, "A novel LSTM–CNN–grid search-based deep neural network for sentiment analysis", *The Journal of Supercomputing*, vol. 77(12), pp. 13911-13932, 2021.

[119] Louverdis, G., Vardavoulia, M. I., Andreadis, I., & Tsalides, P, "A new approach to morphological color image processing", *Pattern recognition*, vol. 35(8), pp. 1733-1741, 2002.

[120] Merzban, M. H., & Elbayoumi, M, "Efficient solution of Otsu multilevel image thresholding: A comparative study", *Expert Systems with Applications*, vol. 116, pp.299-309, 2019.

[121] Araujo, R. L., de Araujo, F. H., & Silva, R. R, "Automatic segmentation of melanoma skin cancer using transfer learning and fine-tuning", *Multimedia Systems*, vol. 28(4), pp. 1239-1250, 2022.

[122] Khan, M. Q., Hussain, A., Rehman, S. U., Khan, U., Maqsood, M., Mehmood, K., & Khan, M. A, "Classification of melanoma and nevus in digital images for diagnosis of skin cancer", *IEEE Access,* vol.7, pp. 90132-90144, 2019.

[123] Kass, M., Witkin, A., & Terzopoulos, D, "Snakes: Active contour models", *International journal of computer vision*, vol.1(4), pp. 321-331, 1988.

[124] Bovik, A. C, "Basic binary image processing. In The Essential Guide to Image Processing", *Academic Press*, pp. 69-96, 2009.

[125] He, K., Zhang, X., Ren, S., & Sun, J, "Deep residual learning for image recognition", *In*

Proceedings of the IEEE conference on computer vision and pattern recognition, pp. 770-778, 2016.

[126] Fulton, L. V., Dolezel, D., Harrop, J., Yan, Y., & Fulton, C. P, "Classification of Alzheimer's disease with and without imagery using gradient boosted machines and Res-Net-50", *Brain sciences*, vol.9(9), pp. 1-16, 2019.

[127] Yao, X., Wang, X., Wang, S. H., & Zhang, Y. D, "A comprehensive survey on convolutional neural network in medical image analysis", *Multimedia Tools and Applications*, pp. 1-45, 2020.

[128] Krizhevsky, A., Sutskever, I., & Hinton, G. E, "Imagenet classification with deep convolutional neural networks", *Communications of the ACM*, vol. 60(6), pp. 84-90, 2017.

[129] Simonyan, K., & Zisserman, A, "Very deep convolutional networks for large-scale image recognition", arXiv preprint arXiv:1409.1556, 2014.

[130] Liu, Y., Yin, B., Yu, J., & Wang, Z, "Image classification based on convolutional neural networks with cross-level strategy", *Multimedia Tools and Applications*, vol.76(8), pp. 11065-11079, 2017.

[131] Srivastava, S., Kumar, P., Chaudhry, V., & Singh, A, "Detection of ovarian cyst in ultrasound images using fine-tuned VGG-16 deep learning network", *SN Computer Science*, vol.1(2), pp.1-8, 2020.

[132] Hosny, K. M., Kassem, M. A., & Fouad, M. M, "Classification of skin lesions into seven classes using transfer learning with AlexNet", *Journal of digital imaging*, vol. 33(5), pp. 1325-1334, 2020.

[133] Islam, S., Khan, S. I. A., Abedin, M. M., Habibullah, K. M., & Das, A. K, "Bird species classification from an image using VGG-16 network", *In Proceedings of the 2019 7th international conference on computer and communications management*, pp. 38-42, 2019.

[134] Liu, X. Y., Fang, Y., Yang, L., Li, Z., & Walid, A, "High-performance tensor decompositions for compressing and accelerating deep neural networks", *In Tensors for Data Processing*, *Academic Press*, pp. 293-340, 2022.

[135] Rezaee, M., Zhang, Y., Mishra, R., Tong, F., & Tong, H, "Using a vgg-16 network for individual tree species detection with an object-based approach", *In 2018 10th IAPR Workshop on Pattern Recognition in Remote Sensing (PRRS)* pp. 1-7, 2018.

[136] Montavon, G., Samek, W., & Müller, K. R, "Methods for interpreting and understanding deep neural networks", *Digital signal processing*, vol. 73, pp. 1-15, 2018.

[137] Mahmood, A., Bennamoun, M., An, S., Sohel, F., Boussaid, F., Hovey, R., ... & Fisher, R.

B, "Deep learning for coral classification. *In Handbook of neural computation, Academic Press*, pp. 383-401, 2017.

[138] Bingham, E., Kaski, S., Laaksonen, J., & Lampinen, J, "Advances in independent component analysis and learning machines", *Academic Press*, 2015.

[139] Shams, S., Platania, R., Zhang, J., Kim, J., Lee, K., & Park, S. J, "Deep generative breast cancer screening and diagnosis", *In International Conference on Medical Image Computing and Computer-Assisted Intervention*, pp. 859-867, Springer, 2018.

[140] Lipkind, H. S., Vazquez-Benitez, G., DeSilva, M., Vesco, K. K., Ackerman-Banks, C., Zhu, J., ... & Kharbanda, E. O, "Receipt of COVID-19 vaccine during pregnancy and preterm or small-for-gestational-age at birth—Eight Integrated Health Care Organizations", *Morbidity and Mortality Weekly Report, United States*, December 15, 2020–July 22, 2021, vol. 71(1), 26, 2022.

[141] Mahajan, H. B., Rashid, A. S., Junnarkar, A. A., Uke, N., Deshpande, S. D., Futane, P. R., ... & Alhayani, B, "Integration of Healthcare 4.0 and blockchain into secure cloud-based electronic health records systems", *Applied Nanoscience*, vol.13(3), pp.2329-2342, 2023.

[142] Chengoden, R., Victor, N., Huynh-The, T., Yenduri, G., Jhaveri, R. H., Alazab, M., ... & Gadekallu, T. R, "Metaverse for healthcare: A survey on potential applications, challenges and future directions", *IEEE Access*, 2023.

[143] Dicuonzo, G., Donofrio, F., Fusco, A., & Shini, M, "Healthcare system: Moving forward with artificial intelligence", *Technovation*, vol. 120, 102510, 2023.

[144] Santana, I. R., Mason, A., Gutacker, N., Kasteridis, P., Santos, R., & Rice, N, "Need, demand, supply in health care: working definitions, and their implications for defining access", *Health Economics, Policy and Law*, vol. 18(1), pp. 1-13, 2023.

[145] Ali, O., Abdelbaki, W., Shrestha, A., Elbasi, E., Alryalat, M. A. A., & Dwivedi, Y. K, "A systematic literature review of artificial intelligence in the healthcare sector: Benefits, challenges, methodologies, and functionalities", *Journal of Innovation & Knowledge*, vol. 8(1), 100333, 2023.

[146] Rumelhart, D. E., Hinton, G. E., & Williams, R. J, "Learning representations by back-propagating errors", *Nature*, vol. 323(6088), pp. 533-536, 1986.

[147] Wang, D., Lu, Z., Xu, Y., Wang, Z., Santella, A., & Bao, Z, "Cellular structure image classification with small targeted training samples", *IEEE Access*, vol.7, pp. 148967-148974, 2019.

[148] Goodfellow, I., Pouget-Abadie, J., Mirza, M., Xu, B., Warde-Farley, D., Ozair, S., ... &

Bengio, Y, "Generative adversarial nets", *Advances in neural information processing systems*, vol. 27, 2014.

[149] Aggarwal, A., Mittal, M., & Battineni, G, "Generative adversarial network: An overview of theory and applications" International Journal of Information Management Data Insights, vol.1(1), 100004, 2021.

[150] Alqahtani, H., Kavakli-Thorne, M., & Kumar, G, "Applications of generative adversarial networks (gans): An updated review", *Archives of Computational Methods in Engineering*, vol.28(2), pp. 525-552, 2021.

[151] https://developers.google.com/machine-learning/gan/gan_structure

[152] Akbar, S. B., Thanupillai, K., & Sundararaj, S, "Combining the advantages of Alex-Net convolutional deep neural network optimized with anopheles search algorithm-based feature extraction and random forest classifier for COVID-19 classification", *Concurrency and Computation: Practice and Experience*, pp. 1-15, 2022.

[153] Rasheed, A., Ali, N., Zafar, B., Shabbir, A., Sajid, M., & Mahmood, M. T, "Handwritten Urdu characters and digits recognition using transfer learning and augmentation with AlexNet", *IEEE Access*, vol. 10, pp. 102629-102645, 2022.

[154] Hammad, I., & El-Sankary, K, "Impact of approximate multipliers on VGG deep learning network", *IEEE Access*, vol. 6, pp. 60438-60444, 2018.

[155] Jibhakate, P., Gole, S., Yeskar, P., Rangwani, N., Vyas, A., & Dhote, K, "Early Glaucoma Detection Using Machine Learning Algorithms of VGG-16 and Resnet-50", *In 2022 IEEE Region 10 Symposium (TENSYMP)*, pp. 1-5, 2022.

LIST OF PUBLICATIONS

Journal(s)

Published

1. **Srivastava, R.,** & Kumar, P., "Deep-GAN: an improved model for thyroid nodule identification and classification", *Neural Computing and Application*, Springer.

   Index: SCIE, Scopus, ACM digital library, **Impact factor:** 6

2. **Srivastava, R.,** & Kumar, P., "Optimizing CNN Based Model for Thyroid Nodule Classification Using Data Augmentation, Segmentation and Boundary Detection Techniques", *Multimedia Tools and Applications*, Springer.

   Index: SCIE, Scopus, ACM digital library, **Impact factor:** 3.6

3. **Srivastava, R.,** & Kumar, P., **"**A hybrid model for the identification and classification of benign and malignant thyroid nodules on medical USG image", *International Journal of Modelling, Identification and Control*, Inderscience., 2022.

   Index: ESCI, Scopus, ACM digital library

   DOI: 10.1504/IJMIC.2022.10051644

4. **Srivastava, R.,** & Kumar, P., **"**A contemporary review on soft computing techniques for thyroid identification and detection", *International Journal of Computer Applications in Technology (IJCAT),* Inderscience, 2022.

   Index: ESCI, Scopus, ACM digital library

   DOI: 10.1504/IJCAT.2022.10051647

5. **Srivastava, R.,** & Kumar, P., "GSO-CNN based model for the identification and classification of thyroid nodule in medical USG images", *Network Modeling Analysis in Health Informatics and Bioinformatics (NHIB),* Springer, 2022.

   Index: ESCI, Scopus, ACM digital library

   DOI: 10.1007/s13721-022-00388-w

6. **Srivastava, R.,** & Kumar, P., "A CNN-SVM hybrid model for the classification of thyroid nodules in medical ultrasound images"**,** *International Journal of Grid and Utility Computing (IJGUC)*, Inderscience, 2022.

   Index: ESCI, Scopus, ACM digital library

7. **Srivastava, R.,** & Kumar, P., "Performance comparison of various machine learning algorithms for the identification and classification of thyroid nodules", *International Journal of Grid and Utility Computing (IJGUC)*, Inderscience.

[**Index: ESCI, Scopus**, ACM digital library]

Communicated

1. **Srivastava, R.,** & Kumar, P., "Alex-GAN based synthetic ultrasound images augmentation model for increasing the performance of thyroid nodules classification", *Multimedia Tools and Applications.*

[**Submitted**] [**Index: SCIE, Scopus,** ACM digital library, **Impact factor:3.6**]

Conference(s)

1. **Srivastava, R.,** & Kumar, P, "BL_SMOTE ensemble method for prediction of thyroid disease on imbalanced classification problem", *In Proceedings of Second International Conference on Computing, Communications, and Cyber-Security*, pp. 731-741, Springer, Singapore.

[**Index: Scopus,** DBLP, Google Scholar, EI-Compendex, SCImago]

DOI: https://doi.org/10.1007/978-981-16-0733-2_52

2. **Srivastava, R.,** & Kumar, P, "A novel model for novel model for the identification and classification of thyroid nodules using deep neural network", *4th International Conference on Machine Intelligence and Signal Processing (MISP2022)*, NIT Raipur, Springer, 12-14 March 2022.

[**Index: Scopus,** DBLP, Google Scholar, EI-Compendex, SCImago]

JAYPEE UNIVERSITY OF INFORMATION TECHNOLOGY, WAKNAGHAT
PLAGIARISM VERIFICATION REPORT

Date: 17/12/22

Type of Document (Tick): **PhD Thesis** | M.Tech Dissertation/ Report | B.Tech Project Report | Paper

Name: Rajshree Srivastava Department: CSE Enrolment No 196204

Contact No. 8146629176 E-mail. rajshree.srivastava27@gmail.com

Name of the Supervisor: Dr. Pardeep Kumar

Title of the Thesis/Dissertation/Project Report/Paper (In Capital letters):

EARLY IDENTIFICATION AND CLASSIFICATION OF THYROID NODULE IN MEDICAL ULTRASOUND IMAGES

Complete Thesis/Report Pages Detail:
- Total No. of Pages = 112
- Total No. of Preliminary pages = 20
- Total No. of pages accommodate bibliography/references = 15

Rajshree
(Signature of Student)

FOR DEPARTMENT USE

We have checked the thesis/report as per norms and found **Similarity Index** at ....10....(%). Therefore, we are forwarding the complete thesis/report for final plagiarism check. The plagiarism verification report may be handed over to the candidate.

Pardeep Kumar
19/12/2022
(Signature of Guide/Supervisor)

Vivek sund
19/12/22
Signature of HOD

FOR LRC USE

The above document was scanned for plagiarism check. The outcome of the same is reported below:

Copy Received on	Excluded	Similarity Index (%)	Generated Plagiarism Report Details (Title, Abstract & Chapters)	
19th/DEC/2022	• All Preliminary Pages • Bibliography/Images/Quotes • 14 Words String	09%	Word Counts	13,583
Report Generated on			Character Counts	69,953
19th/DEC/2022		**Submission ID**	Total Pages Scanned	77
		1984287348	File Size	3.07M

Checked by
19/12/2022
Name & Signature

signature
19/12/2022
Librarian

Please send your complete thesis/report in (PDF) with Title Page, Abstract and Chapters in (Word File) through the supervisor at plagcheck.juit@gmail.com